UNIVERSITY OF LIVERPOOL

Charge Transport across Phospholipid Bilayer Membranes via Functionalised Gold Nanoparticles

Thesis submitted in accordance with the requirements of the University of Liverpool for the degree of Doctor in Philosophy by

Stephen Philip Danks

September 2019

Abstract

The University of Liverpool

Doctor of Philosophy

Charge Transfer across Phospholipid Bilayer Membranes via Functionalised Gold Nanoparticles

Stephen Philip Danks

Charge transfer across phospholipid bilayer membranes is an integral process for all biological species. The aim of this project was to mimic this process using functionalised gold nanoparticles.

Two distinct platforms were developed to allow the study of the phospholipid membranes electrochemically. These were characterised using cyclic voltammetry and potential measurements. Each platform was tested using the model ionophore gramicidin. Using the first platform, a membrane formed across an aperture, it was shown that gramicidin channels are blocked by divalent ions. The second platform used a droplet-based system, and Nernst-Donnan behaviour was confirmed in the presence of an electrochemical gradient of protons across the membrane.

Mercapto-carborane functionalised gold nanoparticles, which had been identified as potential ion-carriers in previous research, were examined using various metal-chlorides. These were found to be ion-selective ionophores that could themselves partition across the membrane and generate an electrochemical potential.

12-Crown-4 functionalised gold nanoparticles were also shown to act as charge transporters. Focusing on H^+ transport, these particles demonstrated two separate mechanisms of charge transfer that were dependent on the surrounding H^+ concentration. At low H^+ concentrations, the particles appeared to act as membrane-penetrating poly-anions. At high H^+ concentrations, they appeared to become hydrophobic and facilitate proton transfer across the membrane.

Ion and H^+ transport across synthetic phospholipid bilayer membranes have been demonstrated separately using two varieties of functionalised gold nanoparticles. This project reinforces and extends the conviction that metallic nanoparticles can be developed and used as artificial ionophores.

Acknowledgements

First and foremost, I would like to thank Prof. Mathias Brust for not only providing the opportunity to study for a PhD but also his support throughout the entirety of it. His passion for science was a constant catalyst for thoughts and ideas which meant the research was always interesting.

A huge thank you to everyone involved with the Brust group during my time with them, with special thanks to Dr Dan F. Bradley, Dr Casper Kunstmann and Dr Marcin Grzelczak whose mentoring and support helped throughout the project and kept me motivated during the tougher times. Without their expertise and assistance, this project would not have progressed as far as it has.

To my friends, thank you for keeping my mental state healthy during a tumultuous few years, with special thanks to Dr Mike Davidson, Dr Alex Hill, Dr Mike Craven and Mr Daniel Parsons. The gaming sessions were especially fun and would always reset my state of mind.

Last but certainly not least, thank you to my family. They were always just a phone call away, whether it was an emergency or just the need for a relaxing chat. Thank you especially to my parents, who provided unequivocal emotional support and no amount of recognition will do the help they have given me justice.

Contents

Abbreviations

ADP – Adenosine Diphosphate

ATP – Adenosine Triphosphate

AuNP – Gold Nanoparticle

Carb-AuNPs – Mercapto-carborane functionalised gold nanoparticles (2-3 nm)

C.E. – Counter Electrode

Crown-AuNPs – 12-crown-4 functionalised gold nanoparticles (2-3 nm)

CV – Cyclic Voltammogram

D.I.B. – Droplet Interface Bilayer

D.L.P. – Dynamic Light Projection

D.L.S. – Dynamic Light Scattering

F.F.F. – Fused Filament Fabrication

P_i – Inorganic Phosphate Group

P.L.B. – Planar Lipid Bilayer

R.E. – Reference Electrode

S.L.A. – Stereo-Lithography Apparatus

S.P.R. – Surface Plasmon Resonance

UV-Vis – Ultraviolet-Visible

W.E. – Working Electrode

Chapter 1 – Introduction

1.1 – Thesis Objective and Outline

1.1.1 – Objective

Biological processes have evolved over time to be highly efficient and selective, properties that are sought-after by scientists from all disciplines. Attempting to mimic these processes has often led to significant advancements in the fundamental understanding of each process, leading to technological breakthroughs in many fields of research. Charge transport across phospholipid bilayer membranes is one such process: performing major roles in cell communication and bio-energy production.

The objective of the research presented in this thesis was to establish a platform to study phospholipid membranes electrochemically and then to introduce functionalised gold nanoparticles (AuNPs) to facilitate charge transport across the membrane. By showing that metallic nanoparticles, which are not seen in nature, are capable of mimicking biological processes, it would lead to an increase in the avenues available for present and future research. In addition, developing the understanding of AuNP–membrane interactions would be beneficial for many areas of research, with particular importance in the medicinal and pharmaceutical industries.

1.1.2 – Outline

Chapter 1: This chapter presents the necessary background information to place the thesis into context within the surrounding literature. The phospholipid membrane and its functions are described, where charge transfer through the membrane, both natural and artificial, in biological

systems is presented. AuNPs and their interactions with the membrane are outlined, and the experimental techniques used to characterise the AuNPs are also briefly explained.

Chapter 2: Experimental methods are described in this chapter, along with a record of all chemicals and equipment used in the thesis. The methods include the preparation of both the 2-3 nm mercapto-carborane-AuNPs and 2-3 nm 12-crown-4-CH_2-SH-AuNPs, as well as the procedures to form the bilayer membranes. The two-electrode system is also described.

Chapter 3: This chapter focuses on the testing of the electrochemical platforms that are used to study the bilayer membranes. The Ag/AgCl ink wire electrodes are tested against commercial reference electrodes. The two methods used for creating cell membranes that can be analysed electrochemically are discussed and the design of both of the electrochemical cells are provided. Electrochemical studies of both the aperture and droplet interface bilayer (D.I.B) membranes are presented, with and without gramicidin, a model channel ionophore.

Chapter 4: This chapter is focused on the analysis of AuNPs functionalised with a mercapto-carborane ligand. Results from potential step experiments on different membrane environments are discussed. Estimations of the charges of the AuNPs using zero-current potential data in various ionic solutions are included.

Chapter 5: The analysis of the second functionalised AuNP is presented in this chapter, where 12-crown-4-CH_2-SH is used as the ligand to create a potential H^+ transporter. CVs of the membrane with different H^+ concentrations and AuNP concentrations are presented. ζ-potential measurements and UV-Vis spectra are used to theorise the mechanism of charge transport across the membrane.

Chapter 6: The final chapter of this thesis. A summary of the research is described, proposals for future work based on this research are presented, and the final conclusions are stated.

1.2 – Charge Transport in Biology

1.2.1 – The Phospholipid Bilayer Membrane

All animal, plant and bacterial cells have a biological membrane that compartmentalizes the cell and gives structural stability[1]. Cell membranes are primarily composed of phospholipids; amphiphilic molecules that form a boundary separating the cell from the environment. Each phospholipid has a hydrophilic phosphate "head" group connected to two hydrophobic lipid "tails". They self-assemble to form a bilayer that is 4 nm thick[2–4], with the hydrophobic tails positioning themselves together to create a hydrophobic, insulative region (Figure 1. 1).

For eukaryotic cells (animal and plant), the cell membrane is not the only phospholipid bilayer. Organelles in the cell are bound by their own phospholipid membrane, separating them from the cytosol. While this allows functional specialisation, it also causes some complications. Many processes that take place in cells require reactants that are not synthesised in every cell. These reactants (e.g. insulin[5]) may be produced by specialised cells elsewhere in the body, and so they must be able to pass through membranes to reach their intended destination. Many of these reactants are either too large or are too charged to be able to diffuse through the phospholipid bilayer un-mediated and so require a separate route. For the molecules that are too large

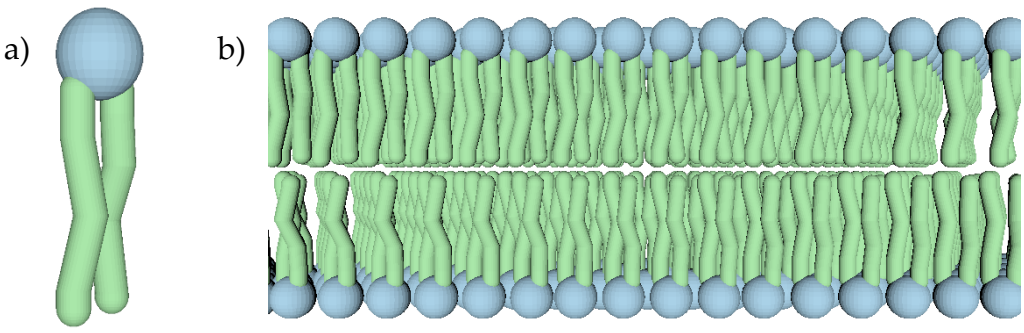

Figure 1. 1 – (a) Representation of a phospholipid, with the phosphate "head" group in blue and the lipid "tails" in green. (b) The phospholipids self-assembled as a bilayer.

(uncharged or charged), the most prevalent method of membrane transport is endo-/exocytosis, where the cell membrane fuses with phospholipid vesicles that contain the molecules and releases the contents into or out of the cell, thereby preventing the need to traverse through the phospholipid bilayer itself. For smaller, charged molecules such as metal ions, specialised proteins are required to facilitate their transport.

1.2.2 – Biological Processes involving Charge Transport across Membranes

1.2.2.1 – ATP Production

Transport of charge across the cell membrane is essential to multiple physiological processes. One such process is the production of adenosine triphosphate (ATP), the main energy-storage molecule in animal and plant biology. This involves a complex system of reactions that transport both electrons and ions – in this case, protons – through the phospholipid membrane[6].

The enzyme ATP-synthase is found in the mitochondrial inner membrane where it combines adenosine-diphosphate (ADP) and a phosphate group (P_i) to form ATP. This process is thermodynamically unfavourable and so, to achieve phosphorylation, the enzyme couples the process with transporting a proton through the membrane, down an electrochemical concentration gradient. As the proton diffuses through the enzyme, it causes a conformational change in the protein which forces the ADP and P_i together, and they are positioned to allow the formation of a bond between them. The entropic energy gained from the proton diffusing down the electrochemical gradient is then converted into the chemical energy necessary to form the bond and ATP is produced.

Photosynthesis also produces ATP in a similar manner, where a proton electrochemical gradient across the thylakoid membrane is maintained by an electron transport chain. The necessary energy to support this does not come from chemical energy but is instead initiated by photon absorption.

1.2.2.2 – Action Potentials

The nervous system communicates using electrical signals known as action potentials that travel along and between neurons. Ion transport across the phospholipid membrane of the neurons is essential to their function. At rest, the neural membrane is negatively polarised inside the cell. There are higher concentrations of K^+ in the cell than outside it and vice versa for Na^+, however, since the membrane is more permeable to K^+, this creates a negative potential inside. This electrochemical gradient is maintained through an active process whereby three Na^+ ions are pumped outside and two K^+ ions are pumped inside the cell.

When a sensory neuron is stimulated and reaches a threshold potential, voltage-gated Na^+ channels in the membrane open and there is an influx of Na^+ into the cell causing local depolarisation of the membrane. Nearby sodium channels that are affected also open, propagating the action potential. When the membrane is completely depolarised, the Na^+ channels close and voltage-gated K^+ channels open, allowing K^+ to diffuse down the electrochemical gradient, repolarising the membrane. A refractory period where the sodium channels cannot re-open immediately ensures the action potential travels through the nerve in one direction.

When the action potential reaches the synapse, voltage-gated Ca^{2+} channels open which cause vesicles of neurotransmitters to fuse with the membrane, releasing them via exocytosis. These neurotransmitters then bind to receptors

on another nerve cell, triggering another action potential if enough receptors are stimulated.

1.2.3 – Ion Transport Mechanisms

ATP-synthase and the ion channels responsible for the propagation of action potentials are types of specialised proteins – ionophores – that allow ions to travel through the otherwise impermeable cell membrane. Transport can be either an active or passive process depending on the ionophore in question. There are two main classes of ionophores: channel-forming ionophores and carrier ionophores (Figure 1. 2).

Channel ionophores are proteins that span the entire membrane and form a hydrophilic pore through which the ions can diffuse. They have a hydrophobic outer casing which allows them to insert themselves into the membrane and create a hydrophilic channel. Channel ionophores can be subdivided into more specialised mechanisms. Voltage- and ligand- gated channel proteins are specialised types of ionophore which undergo conformational changes depending on the membrane potential or whether a

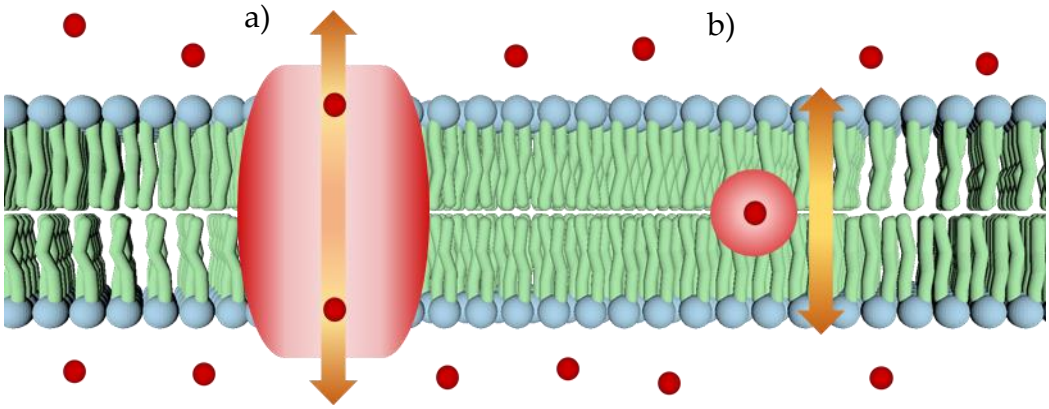

Figure 1. 2 – Schematic illustrating the two main ion transport mechanisms seen in biology. (a) Channel proteins (red and white "cylinder") insert into the membrane and allow ions (small red circles) to diffuse through. (b) Carrier ionophores (large red and white circle) complex and shuttle an ion across the hydrophobic region.

ligand is present, respectively. These conformational changes then dictate whether the transport pathway is open or closed. These types of ionophore are highly important in the nervous system described above.

Carrier ionophores are able to complex ions and freely diffuse in the hydrophobic region of the membrane. They shuttle the bound ions across the membrane and generally have a cyclic structure, with a hydrophilic cavity in the centre to bind the transported ions. The charge of the ions is masked by the carrier ionophore's hydrophobic outer casing.

There are a multitude of different ionophores, and some have the ability to transport multiple ions at the same time. These can be classified into two families of ionophores. Symporters are ionophores that transport multiple ions in the same direction across the membrane, whereas antiporters transport ions in opposite directions. Symporters can be either channel or carrier ionophores, however only channel ionophores can be antiporters.

1.2.3.1 – Gramicidin: A Model Channel Ionophore

Gramicidin, or gramicidin D, is an antibiotic agent effective against gram-negative and most gram-positive bacteria, with the exception being the *Bacillus* genus which produces it naturally. It is a mixture of three linear pentadecapeptides that fold into helices when in the cell membrane[7,8]. To form ion channels that span the whole membrane, two of the helices must dimerise, forming a channel ~28 Å in length with a pore diameter of ~4 Å[9].

Gramicidin channels transport H_2O and monovalent cations including H^+, alkali metals and NH_4^+ through the membrane passively. Each monomer has two cation binding sites, a strong binding site at the channel entrance, and a weaker site towards the centre. A maximum of six H_2O molecules can occupy

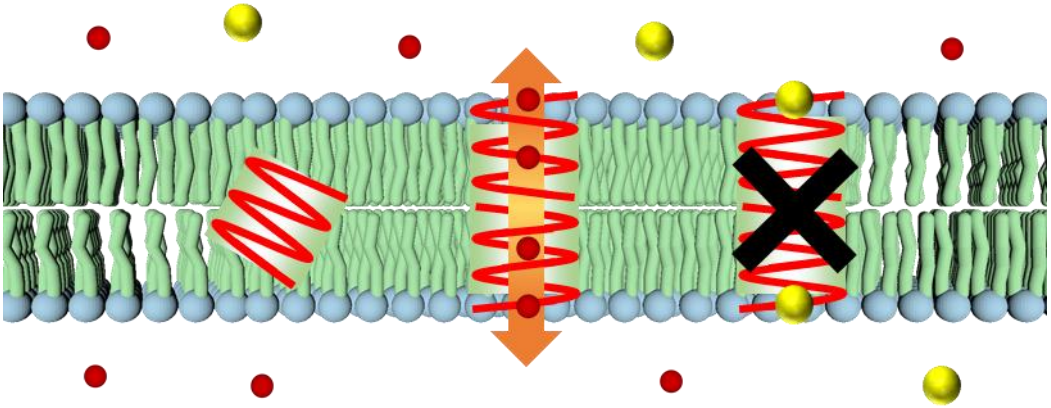

Figure 1. 3 – Gramicidin ion-transport mechanism. Gramicidin (red helices) are lipid-soluble proteins that dimerise to form a channel through the membrane, allowing monovalent cations (red spheres) to diffuse through. Multivalent cations (yellow spheres) bind too strongly at the entrance and block the channel.

the channel at one time, in a single file formation[10]. These must be displaced when an ion is transported through the channel[11,12]. The channel is specific for monovalent cations; multivalent cations such as Ca^{2+} bind irreversibly at the strong binding site in the channel entrance, blocking the pore[13] (Figure 1. 3).

The conductance through the channel is affected by the salt concentration and the complexing cation. At higher concentrations of monovalent cations (> 1 M), all four binding sites in the gramicidin dimer become occupied. This

Table 1. 1 – Ionic and hydrated radii, and hydration enthalpy for the alkali-metals as well as Mg^{2+} and Cl^-.

Ion	Ionic Radii (pm)	Hydrated Ionic Radii (pm)	Hydration Enthalpy (kJ mol^{-1})
Li^+	76	382	-519
Na^+	102	358	-409
K^+	138	331	-322
Rb^+	152	329	-293
Cs^+	167	329	-264
Mg^{2+}	72	428	-1921
Cl^-	181	332	-381

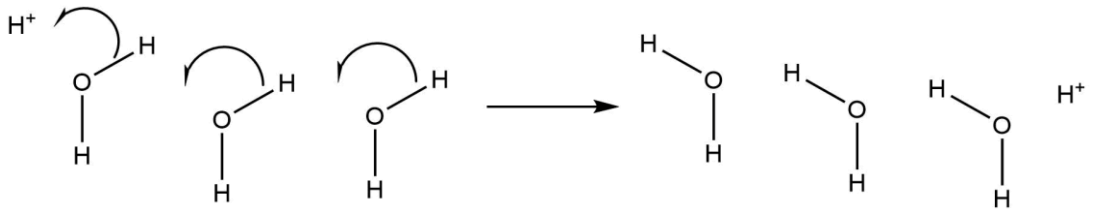

Figure 1. 4 – Grotthuss mechanism of proton diffusion. H^+ "hops" across space through a series of electron transfer steps.

hinders transportation as, the cations now must be displaced, rather than H_2O [14]. To transport a cation through the gramicidin channel, the surrounding hydration shell must be removed. Energy required to remove the hydration shell of an ion is the inverse of its hydration enthalpy, of which values for select ions can be found in Table 1. 1[15–17]. The lower the amount of energy required to do this, the higher the likelihood of a cation transporting through the channel, leading to the conductance of the channel for alkali-metals following the series $Cs^+ > Rb^+ > K^+ > Na^+ > Li^+$. Complementary anions are excluded from diffusing through the pore due to electrostatic repulsion but can affect the conductance of the channel. The anions are able to stabilise the cation-binding site at the entrance to the channel, promoting conductance through the channel[18].

H^+ transport produces the highest conductance; the transport of H^+ follows the Grotthuss mechanism, where H^+ "hops" across a chain of H_2O rather than diffusing through the solution[19] (Figure 1. 4) which removes the need to displace the H_2O molecules in the channel.

1.2.3.2 – Valinomycin: A Model Carrier Ionophore

A model ionophore of the carrier variety is Valinomycin; a cyclic dodecadepsipeptide which can dissolve in both aqueous and organic solvents (Figure 1. 5). It can, therefore, move through the cell cytosol and across phospholipid membranes with ease. It is highly toxic due to its ability to disturb electrochemical concentration gradients across membranes. However, it is often used as a model ionophore in cell membrane research[20–22].

The carbonyl oxygen lone pairs situated around the ring of the molecule act as ligands that surround and complex cations. The size of the cavity formed is ~1.33 Å, and this results in valinomycin being highly selective. It is two thousand times more likely to bind with K^+ over Na^+. K^+ is able to bind to six of the carbonyl oxygens from valinomycin when the ionophore folds into the correct conformation. For Na^+, the ion is too small (1.02 Å) and can only co-ordinate to four of the carbonyl oxygens located around the ring. As such, the complex formed between Na^+ and valinomycin is much more unstable compared to the complex with K^+.

Valinomycin transports ions through the phospholipid bilayer by complexing a cation at the membrane-water interface which causes the complex to become

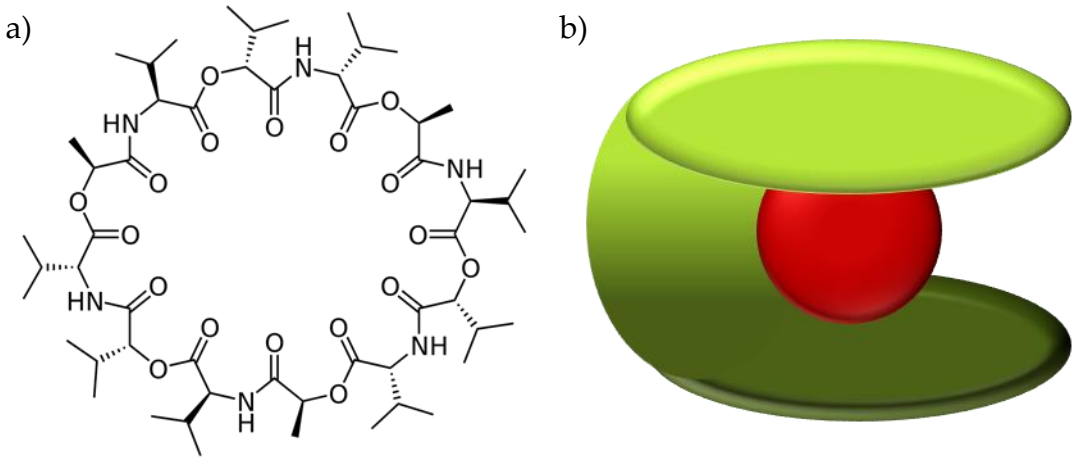

Figure 1. 5 – (a) Chemical structure of Valinomycin. (b) Valinomycin (green) folds around a cation (red) to form the host-guest complex. The folded structure resembles a tennis ball seam.

positively charged. This then forms an ion pair by coupling to a counter-anion which can then diffuse through the membrane and release the two ions on the other side of the membrane[23]. As with gramicidin above, it is maybe surprising that the transport mechanisms of these cation-specific ionophores show dependence on the anion counter ions.

1.2.4 – Electron Transport

Electron transport through the cell membrane is primarily accomplished through redox molecules diffusing between electron acceptors and donors on either side of the membrane[24]. In ATP production, the acceptors/ donors are the cytochrome complexes, and the redox molecule is ubiquinone, also known as co-enzyme Q10. Ubiquinone is reduced to semi-ubiquinone at Complex I, and further reduced to ubiquinol at Complex II[25]. It is then oxidised at cytochrome III back to ubiquinone (Figure 1. 6). Protons are pumped through the membrane up their electrochemical gradient at Complexes I and III. These steps are highly important in maintaining the proton gradient across the mitochondrial inner membrane which ATP-synthase then uses in the phosphorylation of ADP to ATP, as mentioned in Section 1.2.2.1.

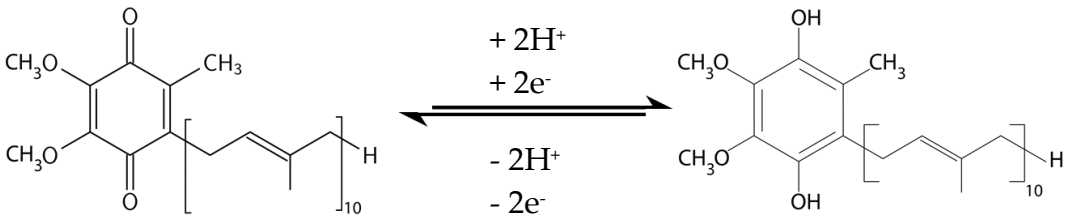

Ubiquinone Ubiquinol

Figure 1. 6 – The redox reaction involving ubiquinone and ubiquinol.

1.3 – Artificial Charge Transport

1.3.1 – Artificial Ionophores

Defective biological ionophores caused by gene mutations give rise to multiple diseases such as cystic fibrosis, which is caused by impaired Ca^{2+} channels[26]. Artificial ion channels and carriers provide a possible treatment route for such diseases. Host-guest chemistry has come to the fore in recent years, leading to complex structures formed via self-assembly. This chemistry is analogous to natural ionophores and many host-guest systems, including pillararenes, calixarenes, cyclo-dextrins and porphyrins have been used to transport ions across membranes[27–31].

1.3.1.1 – Artificial Channels

Artificial channel ionophores have been studied as potential therapeutic molecules[32]. The first artificial ion channel synthesised was similar to gramicidin, a β-helix folding peptide that created a pathway through which ions could diffuse[33]. Cylindrical tubes became the standard motif for many artificial ion channel studies[32] and have been made from many different materials[34]. Peptides and carbohydrates have since been shown to function as ion channels using this design[35].

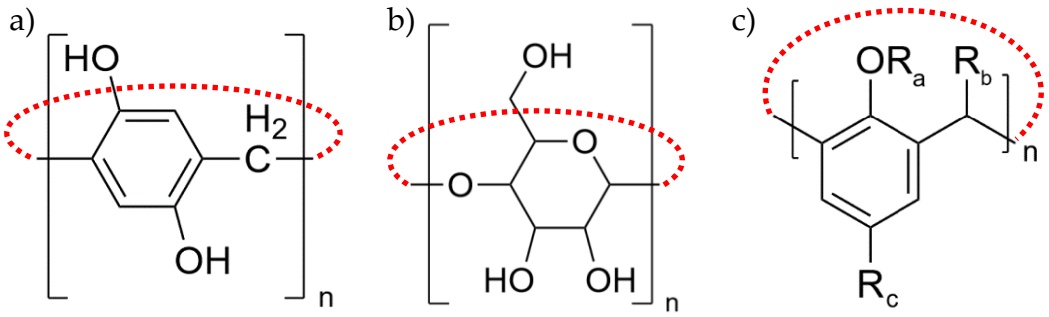

Figure 1. 7 – Structures showing the repeat units that form the macrocycles of (a) pillararene, (b) cyclodextrin, and (c) calixarene (R_a, R_b, and R_c are functional groups).

Pillararenes are an example of this type of design. These are molecules that form a macrocycle of repeat hydroquinone monomers (Figure 1. 7a). They not only act as ionophores[36–38], but are able to complex whole drug molecules and act as drug delivery agents[39–41]. Ion selectivity of pillararene channels is dependent on the size of the pore, which can be controlled based on the monomer number in the macrocycle (n = 5 to 16 have been synthesised successfully[42]). Recent work has shown that pillararenes able to selectively transport ions based on their size, where they have been coupled to another artificial channel molecule, a cyclodextrin, to selectively transport K^+ ions across a membrane[43].

Cyclodextrins have also been used as stand-alone ionophores and were the first example of an artificial ion channel[44]. They are also macro-cyclic structures like pillararenes; however, they are instead formed from glucose molecules joined together through glycosidic bonds (Figure 1. 7b). They are able to transport cations[35,45] or anions[46] depending on the functional groups present. Similarly to pillararenes, the diameter of the nanopore formed in the membrane is dependent on the number of monomers in the macrocycle, and they are classed as α-, β-, or γ- cyclodextrins corresponding to 6, 7, and 8 monomers respectively[47].

Calixarenes are another class of macrocyclic molecules that are comprised of phenol derivatives that have a large amount of customisable functional groups (Figure 1. 7c). They have been modified to selectively transport Li^+ and K^+ cations[48–50] as well as Cl^- anions[51–53]. These have been seen to have great ability as sensors, as well as ionophores, that can selectively detect nM concentrations of Cs^+ amidst other cations in solution[54].

Channels can also be formed by the self-assembly of multiple molecules – either by creating molecular "barrels" or by stacking cyclic compounds on top

of each other[55] (Figure 1. 8). Some simulations suggest that pores could be formed by Janus NPs, particles with double functionalities self-assembling in the membrane much like the barrel formation – with the hydrophobic regions associating with the lipid-tail section of the membrane, and the hydrophilic regions self-assembling to form a pore[56].

DNA-based synthesis of nanoscale structures with controllable characteristics has become more prominent in the area of ionophore research[55,57–59]. Complex structures can be designed and built, and they have recently been used to create ion channels that are controlled by light[60]. These structures can be relatively large, with some known examples reaching 20 nm in at least one dimension, and they are more akin to enzymes rather than simple membrane-spanning channel ionophores as they can have multiple regions that have distinct functions[55].

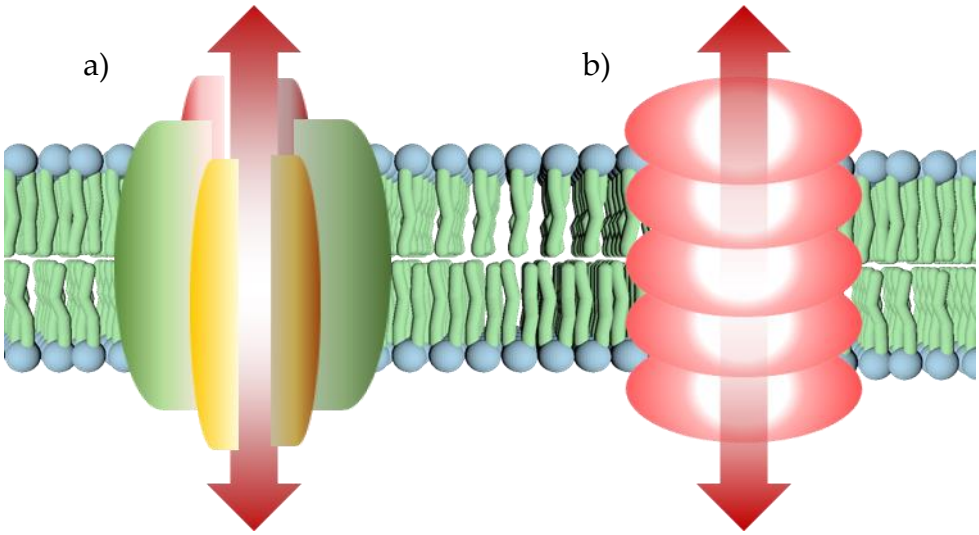

Figure 1. 8 – Molecules can self-assemble in the membrane to create (a) "barrels" and (b) ring stacking in the membrane to form pathways through which ions can diffuse.

1.3.1.2 – Artificial Carriers

Carriers such as crown ethers are able to transport single ions across a membrane, analogous to valinomycin. Crown ethers are ring structures (Figure 1. 9) made from repeating -CH_2-CH_2-O-groups that are able to form complexes with cations[61]. Their nomenclature comes from their 3D structure, with the covalent bonds between the carbon and oxygens resembling a crown due to the gauche effect. Crown ethers are named using a numerical system, for example, 12-crown-4. The first number relates to the total number of atoms in the ring system, with the last number representing the number of oxygen atoms in the ring system. Each crown ether shows ion selectivity based on the size of the ion compared to the binding site[62,63]. They have been used to transport cations through liquid and lipid membranes[64–66]. Aza-crowns are similar to crown ethers where one or more of the oxygen atoms in the ring are replaced by nitrogen. These can be used to form cryptands[67], such as [2,2,2]-cryptand, where another ether linkage is added to form a more "caged" structure. These form more stable complexes with the complementary ions compared to crown ethers due to the increased number of co-ordinating ligands, as the nitrogen atoms are also able to interact with complexing ions. The [2,2,2]- prefix refers to the number of oxygen atoms in each of the ether

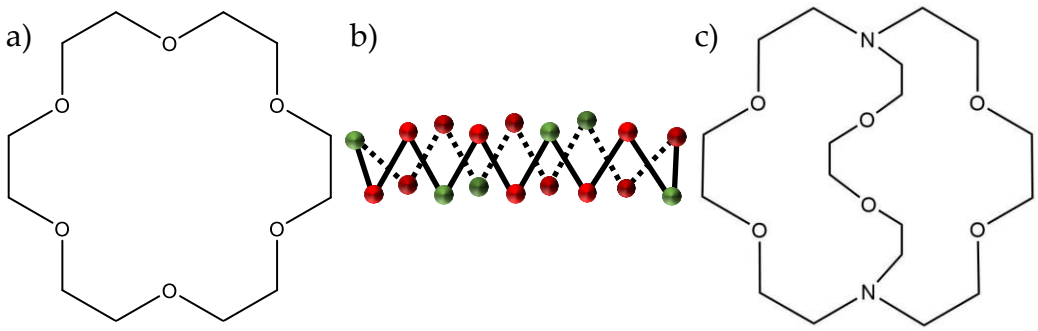

Figure 1. 9 – (a) Structure of 18-Crown-6. (b) A ball and stick model of 18-Crown-6 (carbon atoms are red and oxygen atoms are green, hydrogen omitted for clarity) showing the crown like structure that their nomenclature is derived from. (c). Structure of [2,2,2]-cryptand.

chains connecting the two nitrogen atoms. By functionalising the aza-crown ethers on the nitrogen with anion-binding sites, ionophores that can carry both cations and anions at the same time have been synthesised[68].

Modifications on existing natural ionophores including cereulide, another cyclic depsipeptide similar to valinomycin, have been synthesised that drastically alter the properties of the ionophores[69]. Cereulide is known to be more toxic than valinomycin, in terms of disturbing concentration gradients in cells[70], and it also greatly decreases the secretion of insulin into the bloodstream from β-cells[23]. The synthetically modified version of cereulide, however, functions as an antiporter, rather than a normal carrier ionophore, and reduces the effect on the disturbance of the electrochemical gradient and also promotes the secretion of insulin into the blood.

In much the same way as some anti-venoms are based on the venom that they counteract, using known toxins to create potential drug molecules that have the reverse properties could be a promising direction for future research.

1.3.2 – Artificial Electron Transport

Artificial electron transport has been attempted using covalently linked electron-donors and acceptors. Only a few procedures have been able to induce electron transport, and most use complex organic molecules based on ubiquinone[71]. Modified quinone-derivatives have been bonded to a porphyrin group that situates the molecule in the membrane. The electron transport was then coupled to active Ca^{2+} transport across the membrane[72]. Non-quinone-based electron transport is less well-known, where 1-methoxy-N-methylphenazinium has also been used as a catalyst for transporting electrons between redox couples either side of a membrane[71]. Fullerenes are another set of molecules that have successfully shown electron transport capabilities

when tethered to a porphyrin group[73,74]. Electrons can transfer into the large conjugated π-system that is delocalised over the whole molecule.

Porphyrins have also been used to mediate electron transport across membranes. Synthetic porphyrins, such as tetra-phenylporphyrin (Figure 1. 10), are molecules that are membrane soluble that can be reduced or oxidised, but they are also capable of forming complexes with cations in the centre of the porphyrin ring[75]. They have been seen to transport electrons across the membrane from ethylene-diamine-tetraacetic acid on one side of the membrane to methyl-viologen on the other. This can be enhanced through light, as the porphyrin group can absorb photons to become more reactive[76].

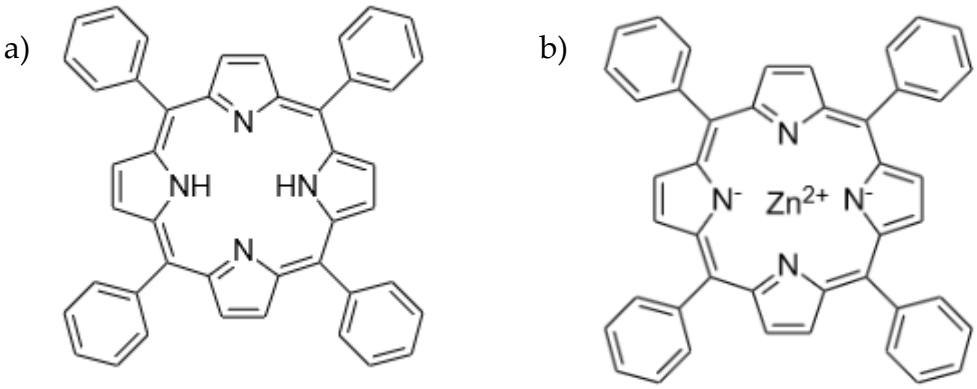

Figure 1. 10 – Structure of (a) tetra-phenylporphyrin. In the reduced form, the four nitrogen atoms in the centre of the porphyrin ring can co-ordinate to metal ions such as Zn^{2+} seen in (b) zinc tetra-phenylporphyrin

1.4 – AuNPs as Potential Artificial Ionophores

Most research into ion and electron transporters involves synthetic organic molecules with similar features to their natural analogues, and little work has been completed using other potential substrates such as metallic NPs. However, the use of AuNPs in biological systems has become of much interest, especially in the pharmaceutical industry[77–79]. Metallic wires are the most well-known method for transporting electrons/electricity in everyday life, however, the metallic state is not seen in biological systems and only rarely in the natural environment. Metallic NPs may also be able to offer a new route for electron transfer in biological systems.

1.4.1 – The Structure of AuNPs

Nanoparticles are structures that are usually classified as being between 1 and 100 nm in size in at least two dimensions[80]. They are primarily of interest due to their high surface area to volume ratio and as a result of this, the higher number of surface atoms compared to interior atoms. Surface atoms, especially those found on the edges of planes and vertices, are much more reactive compared to interior atoms due to an incomplete electronic configuration. The increased number of high-energy sites and small size leads to significant differences in chemical and physical properties when comparing a nanoparticle to its bulk equivalent. Whereas bulk Au is well known for its unreactive nature, this is not the case for AuNPs. They are increasingly being studied for many different uses including catalysis[81] and spectroscopic analysis[82].

Due to their increased area of high-energy surface atoms, the AuNPs are prone to aggregation. To prevent the AuNPs from aggregating, it is necessary to stabilise them. There are three predominant methods in which to stabilise

NPs to prevent them from aggregating: charge stabilisation[83], ligand stabilisation[84], and encapsulation[84,85] (Figure 1. 11).

Charge stabilisation occurs when the AuNPs are prevented from converging close enough to aggregate due to charged species of the same polarity being electrostatically repulsed by each other. This type of stabilisation allows the formation of stable AuNPs that are dispersible in polar solvents. The charge can be due to charged species that are bound to directly to the AuNP surface, such as citrate molecules used in the Turkevich method, or on ligands that are attached to the AuNPs, described below, with charged end-groups.

Ligand stabilisation involves covering the AuNPs in ligands, molecules that chemically bond to the surface of the NP core. The layer of ligands around the core creates a shell that sterically hinders the aggregation of the AuNPs into bulk Au. This type of stabilisation is predominantly used for producing AuNPs that are soluble in a-polar solvents as it is the method of producing mobile uncharged stable AuNPs. This method is particularly useful for AuNPs as it can take advantage of the strong Au-S bond[86]. Many ligands can be used to create a self-assembled monolayer on the surface of AuNPs as long as a thiol group is present on the molecule, as the Au-S bond readily replaces other ligands on the AuNP surface[87].

Encapsulation is the locking of the AuNPs in a solid matrix or a polymer gel. The surrounding medium prevents the AuNPs from being able to diffuse and encounter other nanoparticles, and so aggregation does not occur. However, the phospholipid membrane is not a rigid structure, behaving much like a fluid where molecules are able to diffuse and move around relatively freely. Consequently, AuNPs that rely on this type of stabilisation will be unsuitable in this experimental environment, and so AuNPs that are stabilised by encapsulation will not be discussed further.

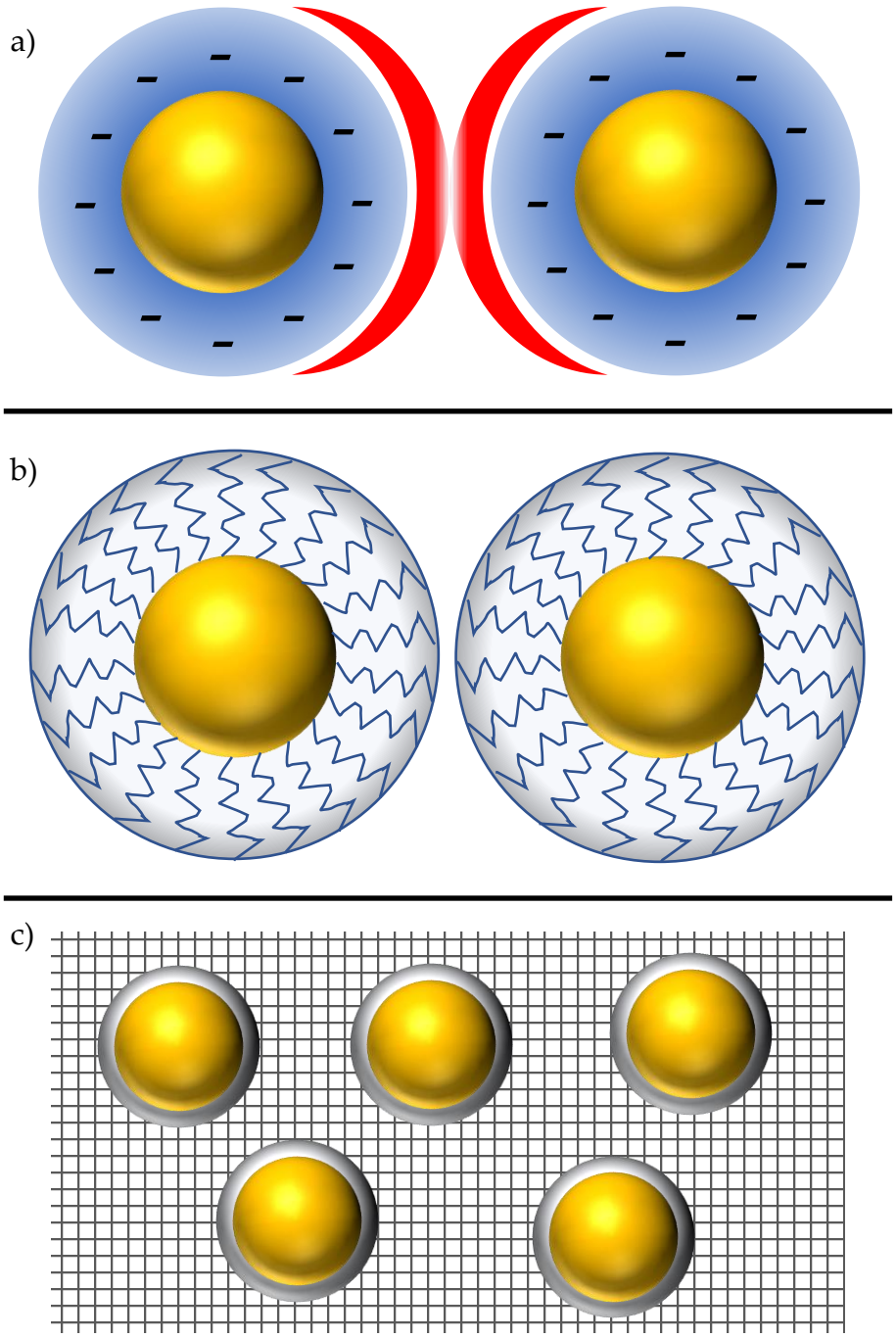

Figure 1. 11 – The three main methods of nanoparticle stabilisation. (a) Charge stabilisation. (b) Ligand stabilisation (c) Encapsulation

1.4.2 – Controlling AuNP Properties

Size[88,89], shape[90,91], and surface charge/hydrophobicity[92,93] are all factors that affect the interaction of the AuNPs with the cell membrane. Controlling these factors is necessary for the design of AuNPs with potential ionophoric properties.

Extensive research has been carried out in preparing monodisperse AuNPs of controlled core size and a variety of different preparative methods are used depending on the desired size. The Turkevich method produces charge-stabilised AuNPs by the reduction of Au^{3+} in the presence of sodium citrate in a heated aqueous solution[94,95]. The size can be controlled by varying the citrate concentration, and the sequence of additions. A more recent method allows the preparation of monodisperse citrate-stabilised 3–13 nm diameter AuNPs by growing the AuNPs in stages[96]. The Brust-Schiffrin method can be used to create small 1-3 nm diameter AuNPs stabilised via thiolate ligands, and can be used to produce organic-dispersible AuNPs[97].

The shape of the AuNPs can also be controlled. The methods already discussed can all produce spherical particles but it is also possible to create a number of shapes including cubes[98,99], rods[100,101] and stars[102–104]. Rods and stars show enhanced resonance and Raman scattering and have the potential to be employed in sensors and cancer treatments. They have also been shown to act as drug vectors when functionalised with thiolated phospholipid ligands[105].

The strong Au-thiol bond allows a large potential library of ligands that can be used to stabilise the AuNPs. The hydrophobicity of AuNPs is highly dependent on the surface functionalisation and so ligand-stabilised AuNPs adopt the prominent characteristics of the ligand that is bound to them. Using large organic molecules as ligands will produce hydrophobic particles, whereas polar/charged ligands will produce more hydrophilic AuNPs[106,107].

The use of ligands that are able to change their properties depending on the solutions in which they are dispersed, such as NPs functionalised with modified crown-ether ligands have been studied, showing controllable solubility based on the concentration of ions in the surrounding solvent[108].

The current understanding of AuNPs and the control of the properties, both physical and chemical, has led to the large scope in uses of AuNPs, from therapeutic cancer treatments[109] and drug delivery systems[77], and as sensors[110]. By applying the insights revealed in past research, the design of AuNPs that can facilitate the transfer of charge across biological membranes should be achievable.

1.4.3 – Cellular Uptake and Membrane Interactions

The barrier of the cell membrane provides a major obstacle for all potential drug molecules. For a drug to be effective, it must reach its intended target in the body. For some, these are receptor proteins on the outside of the cell, and so the drug molecules do not need to traverse through the membrane. For others, however, their targets are inside the cell and they must be able to enter. Drugs that can do so unaided are unperturbed, but for those that cannot, a delivery system is often needed. AuNPs are well known to facilitate drug delivery via mediated endo- and exocytosis[111], but little is known about their ionophoric activity. As well as testing AuNPs as potential ionic/electronic transporters, identifying toxic aspects of potential therapeutic AuNPs can be accomplished by analysing their interactions with cell membranes.

The interactions of AuNPs with cell membranes are dependent on many factors[91,112–114]. Large AuNPs (>10 nm diameter) enter cells via receptor-mediated endocytosis[115]. They are not able to permeate through the membrane un-mediated. Proteins adhere to the surface of the AuNPs which then activate receptors in the cell membrane to trigger transportation and this

has been seen to be dependent on the size and shape of the AuNP. The maximum uptake of AuNPs via endo-/exocytosis occurs for spherically-shaped AuNPs of 50 nm diameter[115]. Rod-shaped AuNPs are not as easily transported as those with spherical geometries. This is hypothesised to be because of increased membrane contact reducing receptor activity and reduced protein adherence due to particle preparative differences.

Conversely, smaller AuNPs (<10 nm diameter) have the ability to passively insert themselves into the membrane. Many simulation studies on particle-membrane interactions suggest that the AuNPs with diameters ranging from 1 to 5 nm are able to interact with the membrane directly[116]. Whilst hydrophilic particles are able to penetrate the membrane, hydrophobic AuNPs do not pass through but instead remain inside the membrane; the lipid tails on the phospholipids encapsulating the nanoparticles.

These studies also seem to suggest that cationic AuNPs have a much higher propensity to penetrate a membrane compared to anionic variants. The bilayer phospholipid head groups are negatively charged, and cationic AuNPs are more attracted to the membrane than anionic AuNPs. They are, however, more likely to cause disruptions and holes in the membrane[117–119].

The AuNPs used in this thesis are 2 nm core diameter, spherical AuNPs. Using this size AuNP would hopefully increase the probability that the particles would interact with the membrane and not disrupt the bilayer structure, as they would be a similar diameter to the width of the bilayer membrane (Figure 1. 12).

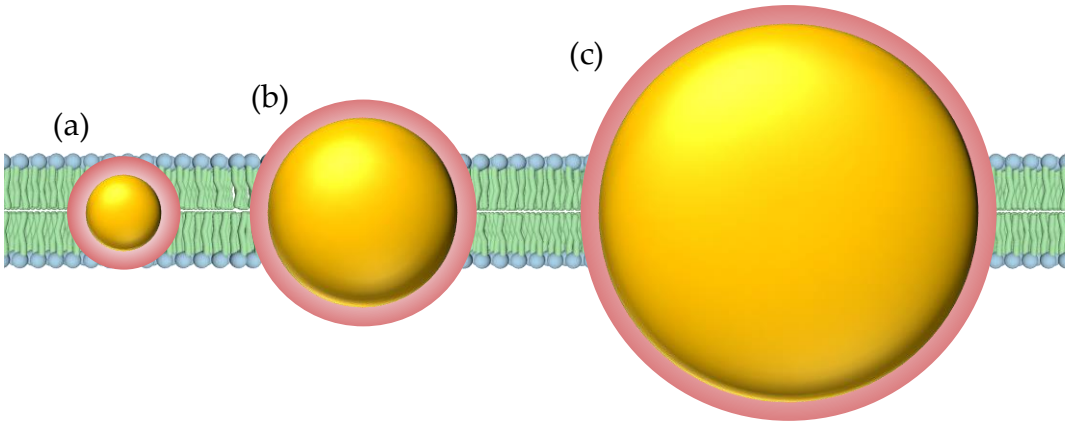

Figure 1. 12 – Various core sizes of AuNPs (gold circles) with a ligand shell (red surround) compared to the phospholipid bilayer: (a) 2 nm diameter (b) 5 nm diameter (c) 10 nm diameter. Larger AuNPs interact with the aqueous phase as well as the hydrophobic bilayer. For the purposes of creating an AuNP ionophore, 2 nm sized AuNPs were thought to be more appropriate.

1.5 – Electrochemical Interrogation of Cell Membranes

There are a multitude of techniques to study cell membranes, depending on research intent. Electrochemical measurements require the membrane to be between two current-bearing electrodes. Considering the dimensions of cells and the thickness of the membrane, this can pose substantial mechanical challenges.

1.5.1 – Patch Clamp Apparatus

To study the cell membrane amidst the whole-cell environment, specialist equipment known as a patch-clamp apparatus is necessary. A micropipette with an electrode contained within is manoeuvred into contact with the membrane surface, and negative pressure is applied to create a "giga-seal" between the pipette and the membrane[120] (Figure 1. 13). It can then be studied by placing the other electrode in the cell solution. The membrane can be detached from the cell to allow the analysis of specific proteins or processes individually. This method can also be used for single-channel recordings; the

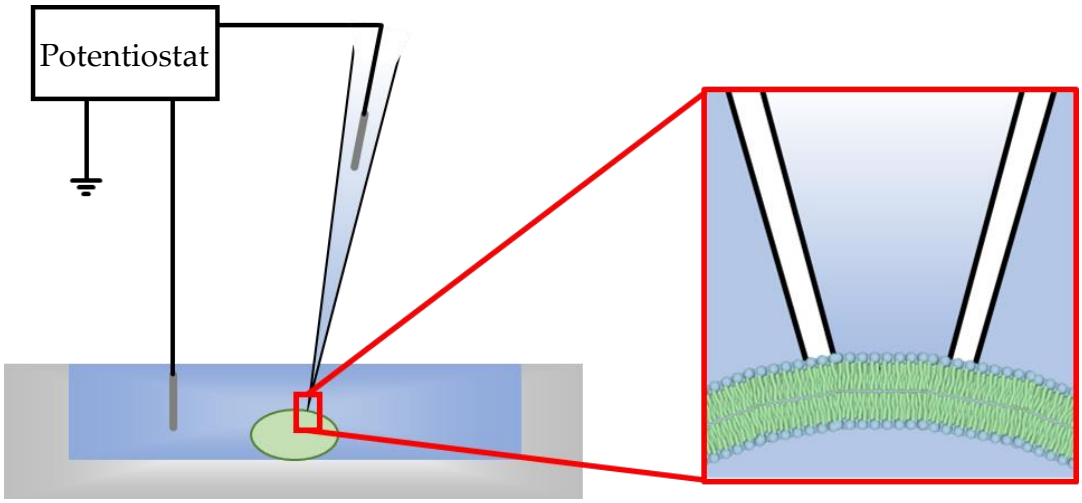

Figure 1. 13 – Diagram of a Patch-Clamp apparatus experiment. An electrode-fitted pipette is manoeuvred so that it is in contact with the membrane of a biological cell (green oval, see red insert). The second electrode is placed in the medium containing the cell. This makes it possible to analyse the entire cell, rather than just a phospholipid membrane.

high resistance of the membranes formed allows the recording of low currents with minimal noise.

1.5.2 – Free Standing Planar Lipid Bilayers

If "whole-cell" analysis or single-channel recordings are not required, planar lipid bilayers (P.L.B.s), sometimes referred to as black lipid membranes, represent a more accessible approach to studying membrane interactions. This method does not require the use of actual cells, it uses reconstituted phospholipids, such as asolectin[52,121] – a mixture of different phosphatidyl-choline molecules, to form the bilayers.

1.5.2.1 – Aperture Membranes

The first P.L.B.s that were produced were formed in apertures separating two electrolyte chambers (Figure 1. 14), introduced by Mueller *et al*[122] in the 1960s. The first published method required raising two aqueous solutions, each with a monolayer of lipids at the water-air/organic interface. The monolayers are brought into contact by the consecutive raising of the water level on each side of the aperture until the monolayers fold onto each other through the aperture to form the bilayer membrane. The aperture is usually formed by perforating

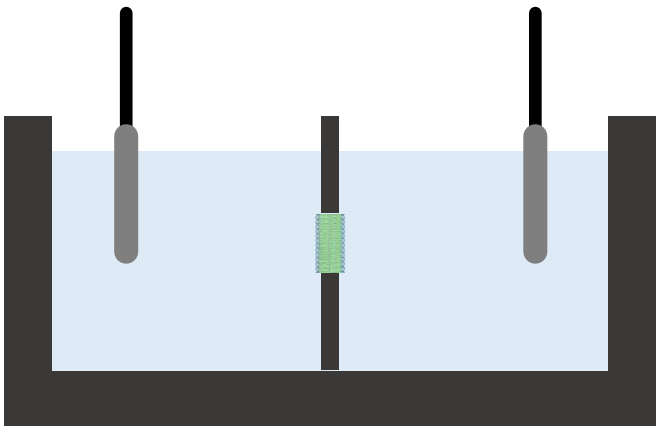

Figure 1. 14 – An aperture-style membrane experimental set-up. Two electrodes (silver bars) are placed in chambers that are connected through a small aperture. A membrane can then be formed in this aperture to allow electrochemical studies on the membrane.

a Teflon sheet, usually with a sharpened needle or a heated wire[123]. These P.L.B.s were used for the majority of early electrical analysis on cell membranes[123–125]. It is possible to form solvent-free membranes using this method. The surface monolayers can be formed using volatile organic solvents such as ethanol which evaporate leaving only the lipid monolayer. Using different lipid solutions on either side of the aperture allows the creation of asymmetric membranes which are more analogous to biological membranes. It is possible to make these both vertically, as Montal and Mueller first reported, but also horizontally between an upper and a lower electrolyte[126].

Another method, known as "painting", requires the filling of the two chambers with electrolyte so that the aperture is completely immersed[127]. An organic-lipid solution is then pipetted onto the aperture and a membrane forms as the organic solvent begins to spread out.

1.5.2.2 – Droplet Interface Bilayers

A different method for bilayer formation involves using aqueous droplets suspended in organic media known as droplet interface bilayers (D.I.B.s)[128,129].

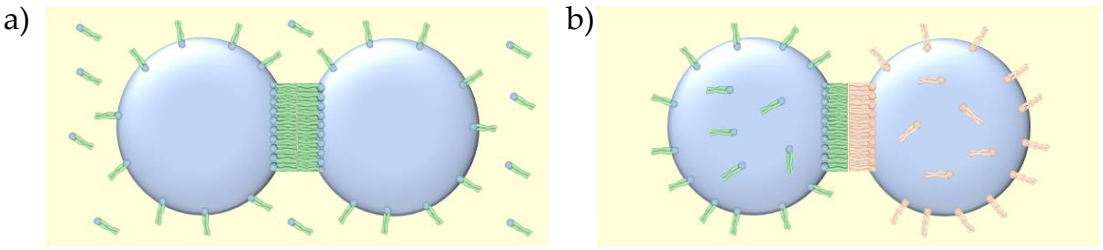

Figure 1. 15 – (a) Lipid out D.I.B. system: the lipids (green and blue sticks) are dissolved in the organic phase (yellow background) and a monolayer of lipids form around each of the two aqueous droplets (blue spheres). These droplets can then be brought into contact to create the bilayer membrane. (b) Lipid in D.I.B. system: The lipids are dissolved in the aqueous phase instead of the organic phase, creating the possibility to change the lipid in each droplet to create asymmetric membranes, with the different type of lipid shown in orange.

The droplets can be suspended on wire-electrodes held by micromanipulators. Once the lipids form a monolayer surrounding the droplets, they can be manoeuvred into contact, forming the membrane. The lipids that form the bilayer can be dissolved in either the organic phase (lipid out) or in the aqueous phase (lipid in). The D.I.B. lipid-in technique also allows the formation of asymmetric membranes using different lipids in each droplet[130] (Figure 1. 15).

Large multi-droplet networks can be achieved relatively easily using this technique where individual droplets can be placed into or removed from the network[131,132]. This allows high throughput analysis of membrane systems and multi-membrane investigations[133].

The main concerns with D.I.B. membranes are that solvent-free membranes are difficult to achieve and it also difficult to add analytes to the droplets. However, if additions are not necessary, the D.I.B. method provides a simple and reliable method of forming P.L.B.s.

1.5.3 – Supported/Tethered Planar Lipid Bilayers

First described by McConnell *et al*[134], P.L.B.s can be assembled directly on hydrophilic surfaces. Primarily used for current/conductance measurements, the structural support provided by the solid surfaces means the membranes are typically more stable than other formation methods[95]. They are created by

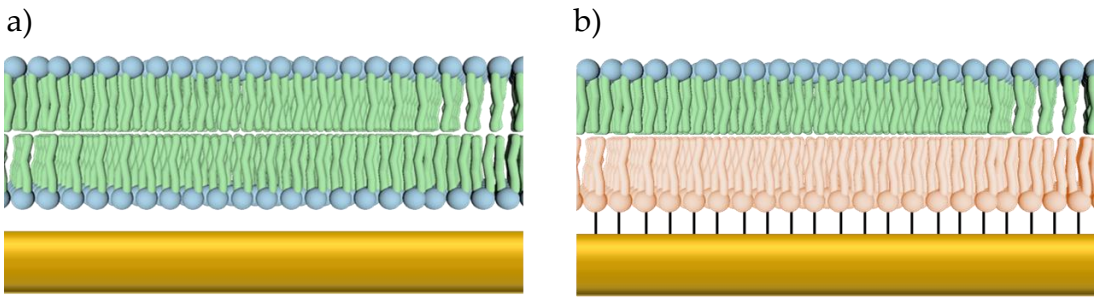

Figure 1. 16 – (a) A supported bilayer membrane on an Au support. (b) A tethered bilayer membrane– showcasing the possibility of asymmetric membrane formation.

either successive deposition of Langmuir-Blodgett monolayers onto the support, or by accumulating vesicles or micelles of lipids on the support, which rupture and form the bilayer.

A tethered-P.L.B. is produced much like a supported-P.L.B., but a monolayer of a thiol-functionalised phospholipid is chemically attached to the surface of a gold electrode before the monolayer deposition or vesicle/micelle fusion occurs, physically attaching the bilayer to the support[135,136]. This method can again produce asymmetric membranes by using different lipids for each stage if necessary or preferred (Figure 1. 16).

1.5.4 – Electrical Properties of Bilayer Membranes

Cell membranes have highly insulating properties and are usually characterised electrochemically by their resistance and capacitance[2,137,138]. The cell membrane can be seen as a resistor and capacitor in parallel (Figure 1. 17). Without ionophores present, the membrane has a high electrical resistance usually in the region of 10^7 - 10^9 Ωcm^2 [123,138]. The capacitance can range from 0.3-1 $\mu F cm^{-2}$ depending on the method of membrane formation and organic solvent used. When creating membranes with an organic solvent present, the solvent itself can affect the capacitance. Solvent-free membranes have a higher capacitance compared to those prepared with organic solvent molecules

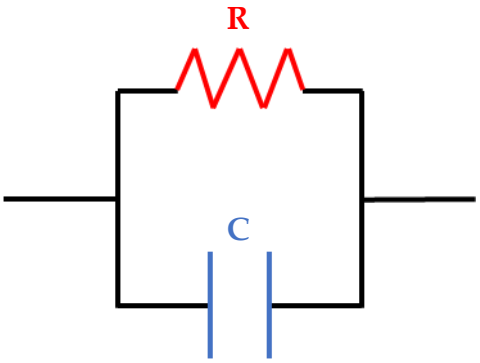

Figure 1. 17 – Basic diagram of a cell membrane as an electronic circuit component: a resistor (red) and a capacitor (blue) in parallel

present[139]. This is possibly due to fewer defects and solvent-spacing in the lipid assembly.

1.6 – Analytical Techniques

1.6.1 – Cyclic Voltammetry

Cyclic voltammograms (CVs) are often used when analysing the effect of time and potential on the current. The potential of an electrode is scanned back and forth between two potentials whilst measuring the current. The current data can be presented as both a function of potential and a function of time (Figure 1. 18). CVs can be run a single time or allowed to continuously cycle between the maximum and minimum potentials. The membrane resistance (or the inverse/reciprocal, conductance) and capacitance can be calculated from the resultant voltammograms.

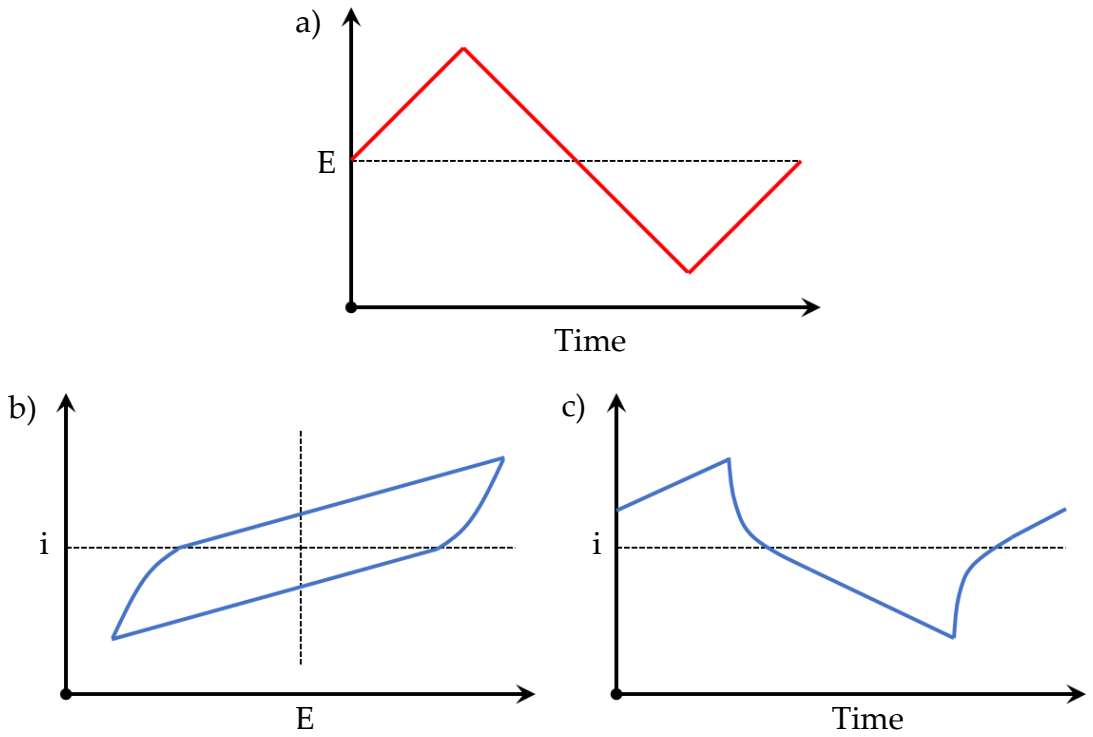

Figure 1. 18 – (a) Potential (red) waveform for a standard cyclic voltammogram seen in this thesis. (b) An example of current measured through a membrane as a function of applied potential. (c) The same current but as a function of time.

For cyclic voltammetry measurements, the voltage is swept back and forth over a potential range over time and C = Q/V can be written as:

$$C = \frac{\frac{dQ}{dt}}{\frac{dV}{dt}} \quad \text{(Eq. 1)}$$

Where C is the capacitance (F), Q is the charge (coulombs, C), t is time (s) and V is the applied potential (V). This can also be re-written as:

$$C = \frac{I_c}{\nu} \quad \text{(Eq. 2)}$$

Where I_c is the capacitive current (A) and ν is the scan rate (Vs^{-1}) of the CV. I_c is calculated using:

$$I_C = \frac{I_F - I_B}{2} \quad \text{(Eq. 3)}$$

Where I_F (A) is the average current of the forward sweep (from negative to positive potential) and I_B (A) is the average current of the backwards sweep (from positive to negative).

After the capacitive charging completes, i.e. when the membranes behave as a resistor, the resistance can be calculated using Ohms Law:

$$V = IR \quad \text{(Eq. 4)}$$

Where V is the voltage (V), I is the current (A) and R is the resistance (Ω).

1.6.2 – Potential Step Measurements

In a potential step, the current response is measured when the potential is instantaneously stepped from one value to another (Figure 1. 19a). This can be used to again calculate the two significant physical properties of the membrane: resistance and capacitance. The membrane acts as a resistor and capacitor in parallel and so, when a constant potential is applied, a current will pass through both the resistive and capacitive components until the capacitive component is completely charged. After this point, the current will flow through the resistor only and the resistance can be calculated using Ohm's Law (Eq. 4) (Figure 1. 19b).

Having calculated the resistance, it is then possible to calculate the capacitance by analysing the capacitive-charging region. For a potential step under non-faradaic conditions, the capacitive current charging follows:

$$i_t = \frac{E_{step}}{R} e^{\left(-\frac{t}{R\,C}\right)} \qquad \text{(Eq. 5)}$$

Where i_t is the current (A) at time t (s) after the potential step has occurred (where t = 0 is when the step occurs), E_{step} is the difference in potential (V)

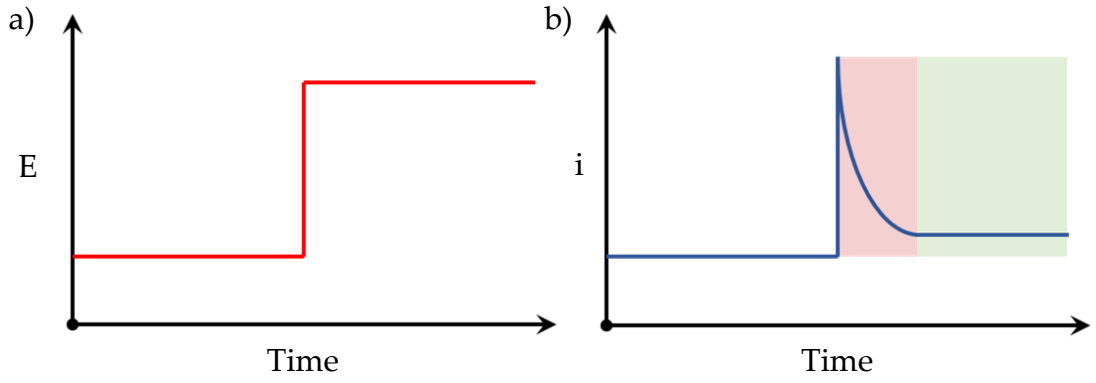

Figure 1. 19 – (a) Potential waveform (red) for a potential step experiment. (b) Current trace (blue) against time for a potential step experiment. The capacitive current region is the red background, and the resistive current region is in green.

before and after the step occurs, R is the resistance (Ω) and C is the capacitance of the membrane (F).

Potential steps can completely separate the capacitive currents from the resistive currents, which simplifies both capacitance calculations when identifying and verifying membrane formation, and the analysis of potential ionophores and their effect on the conductance of the membrane.

1.6.2.1 – Symmetric Stepping

In the experiments undertaken, there are two classes of experiments utilizing potential steps. The first is a symmetrical stepping class where the potential is periodically stepped between two potentials (Figure 1. 20).

This type of measurement is best used to identify changes in membrane conductance over time. This can then be used to see the effect on the resistance/capacitance of the membrane arising from the additions of an analyte, for instance, the addition of AuNPs. This however comes with the caveat that any change in conductance must occur at the potential that is applied. This may not be the case for systems that are only active above or below certain potential values, such as a voltage-gated ionophores.

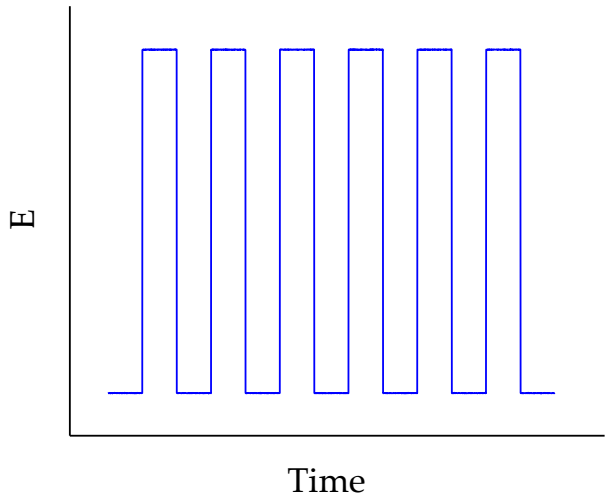

Figure 1. 20 – Potential trace of a "symmetric stepping" measurement. The applied potential is alternatingly stepped between two values.

1.6.2.2 – Progressive Stepping

The second class of potential step experiments used is progressive stepping. Rather than repeatedly switching between two potentials, the magnitude of the potential step is increased after each step (Figure 1. 21). This gives the opportunity to monitor how the membrane responds at various applied potentials without the continuous sweeping of potential as seen in cyclic voltammetry.

This type of experiment can be used to identify whether an ionophore is voltage-gated or not, by comparing the currents when the ionophore is and is not present. The average current values at each potential can be plotted against potential, and an I vs E graph can be produced. If the I vs E graph shows a linear dependence, then the ability of the molecule to act as an ionophore is not dependent on the applied voltage, and so the ionophore would not be voltage-gated. If the ionophore was voltage-gated, it would be expected that no change in current would be seen, compared to the base membrane, whilst the applied potential was below the voltage needed to activate the ionophore, but an increase in current once the threshold is passed.

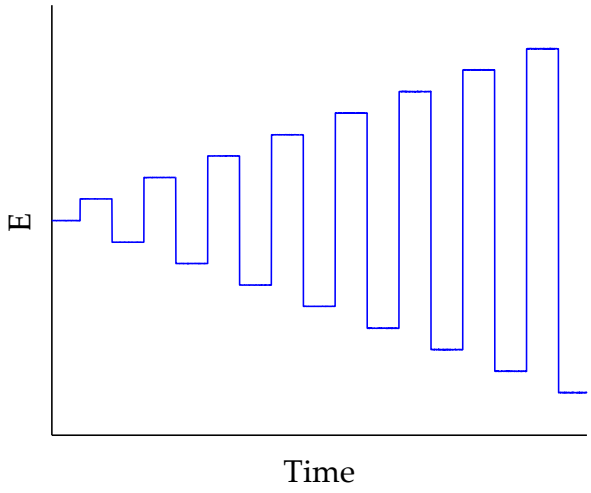

Figure 1. 21 – Potential trace for a "progressive stepping" measurement. The magnitude of the potential step is continuously increased after each successive step.

1.6.3 – Zero-Current Potential Measurements

At rest, the membrane has the ability to hold an electrochemical potential. This potential will occur when the charge transport through the membrane is equal in both directions, i.e. when the current measured is zero. This potential will be referred to as the "zero-current potential" throughout this thesis, as the "resting membrane potential" refers specifically to the potential of a neuron at rest. By controlling the electrical circuit so that no current flows through the system, the zero-current potential can be measured.

When no charge carriers that can diffuse through the membrane are present, this zero-current potential should be zero. When membrane-permeable charge carriers are present, the potential will depend on the concentrations of those charge carriers on both the right-hand side (R.H.S) and left-hand side (L.H.S) of the membrane, following the Nernst-Donnan equation:

$$\Phi = \frac{RT}{zF} ln\left(\frac{[x]_{R.H.S.}}{[x]_{L.H.S.}}\right) \quad \text{(Eq. 6)}$$

Where Φ is the membrane zero-current potential (V), R the universal gas constant (8.3145 J mol^{-1} K^{-1}), T the temperature (K), z the charge on ion x, F the Faraday constant (96485 C mol^{-1}), and $\frac{[x]_{R.H.S.}}{[x]_{L.H.S.}}$ the concentration ratio of ion x across the membrane.

When there are multiple ions in the electrolyte that are able to pass through the membrane, the zero-current potential can identify the relative permeabilities of those different ions. This is described in greater detail in Chapter 4.

1.6.4 – Zeta Potential

The charge of functionalised AuNPs in the context of attempting to understand membrane interactions is significant. Cationic, anionic and uncharged particles interact differently. Identifying their distinct charge can be experimentally difficult for colloidal particles, and it is often more appropriate to categorise them using electrochemical zeta potentials (ζ-potential).

The ζ-potential of a particle is the electrochemical potential at the slipping plane – where solvent molecules are no longer constrained by the particle's electrostatic influence (Figure 1. 22). This boundary represents the outer perimeter of the AuNP and will govern most molecular interactions. Consequently, in some situations, it is a more pertinent value than the

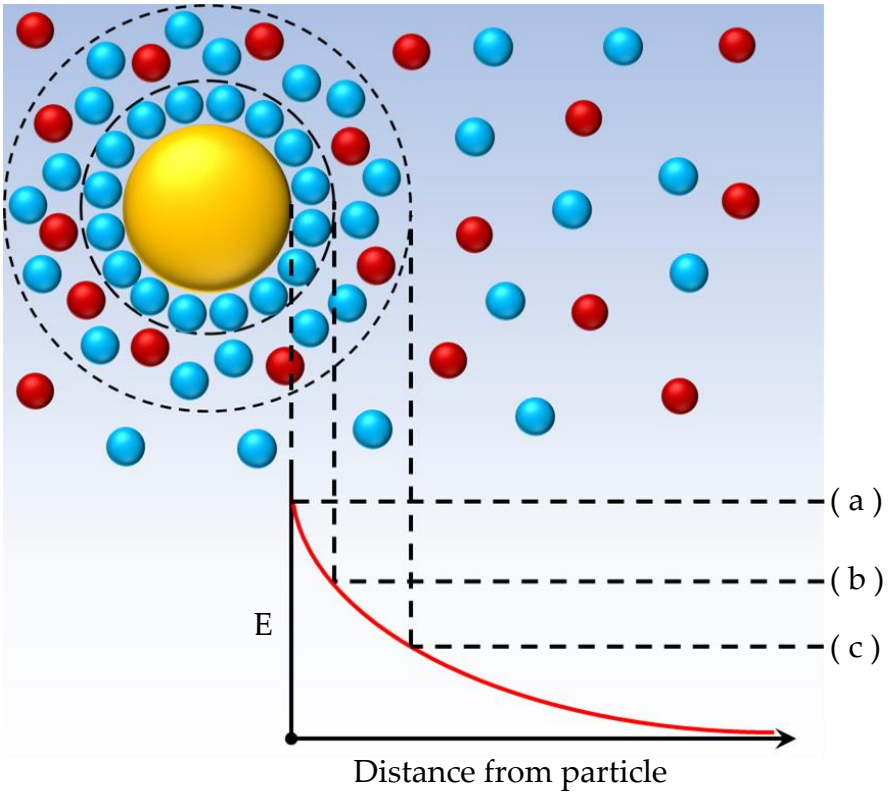

Figure 1. 22 – Diagram showing the change in potential as a function of the distance from the surface of a charged particle (gold circle) where (a) is the potential at the particle surface (b) is the stern potential and (c) is the ζ-potential at the slipping plane.

potential at the particle surface. The ζ-potential of a particle in a solution can be calculated using the Henry equation.

$$\mu_e = \frac{2\varepsilon_0\varepsilon_r\zeta}{3\eta}F(\kappa a) \qquad \text{(Eq. 7)}$$

Where μ_e is the electrophoretic mobility of the particle ($m^2\ s^{-1}\ V^{-1}$), ε_0 the vacuum permittivity constant ($C^2\ N^{-1}\ m^{-1}$), ε_r the dielectric constant of the solution, ζ is the ζ-potential (V), η the dynamic viscosity of the solution (Pa s), and $F(\kappa a)$ the Henry function which relates the radius of the particle, a (m), to the inverse Debye length, κ (m^{-1}).

The electrophoretic mobility can be measured using dynamic light scattering (D.L.S.). A laser is directed through the colloid and a directional electric field is applied to the colloidal solution. The AuNPs will diffuse according to their ζ-potential. When an AuNP passes through the laser, the incident light will be scattered. The frequency of the scattered light will be shifted compared to a reference beam, and μ_e can be calculated from that shift[140].

1.6.5 – UV-Vis Spectroscopy

Ultraviolet-visible (UV-Vis) spectroscopy is an experimental technique that uses electromagnetic wavelengths in the near-UV/visible spectrum. It characterises the colour of an analyte by measuring the absorbance or reflectance of a sample.

The colour of AuNP solutions can be used to characterise their size and shape. Delocalised electrons in the metallic core of the AuNP form an "electron cloud" that can resonate with specific electromagnetic wavelengths in a phenomenon known as surface plasmon resonance (S.P.R.). The ratio between the absorbance at the S.P.R. peak wavelength and the wavelength at 450 nm, is dependent on the size of the AuNPs and can be used to characterise them[141]. AuNPs of ~2-3 nm diameter do not feature an S.P.R peak in the spectrum and, since the AuNPs used in this thesis are ~2-3 nm in diameter, the UV-Vis

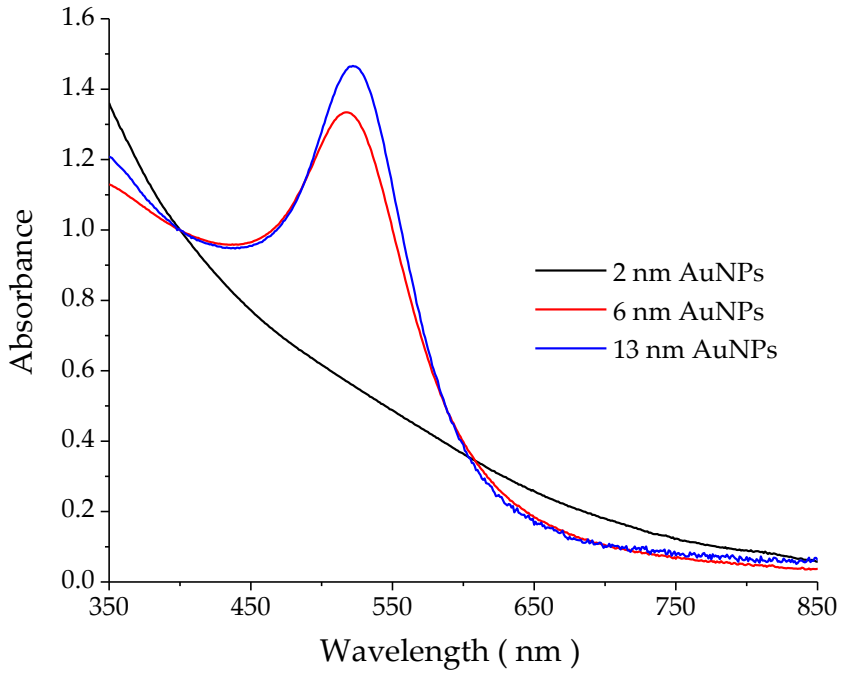

Figure 1. 23 – UV-Vis spectra for spherical AuNPs of different diameters, with the absorbance normalised to the value at 400 nm wavelength. The lack of an SPR peak is characteristic of AuNPs of <3 nm diameter

spectra can be used to confirm that the desired size of AuNPs has been prepared (Figure 1. 23).

The UV-Vis spectra were used to calculate the concentration of the AuNPs using an ε value calculated from a calibration curve, using known 2-3 nm AuNPs that had been sized using transmission electron microscopy[142], following the Beer-Lambert law:

$$A = \varepsilon c l \qquad \text{(Eq. 8)}$$

Where A is the absorbance, ε is the extinction coefficient of the analyte (mol^{-1} dm^3 cm^{-1}), c is the analyte concentration (mol dm^{-3}) and l is the incident light path length (cm).

1.6.6 – 3D Printing

First established during the 1980s, 3D printing has recently become a highly effective manufacturing process, used predominantly in prototyping, jewellery and dentistry. However, it has started to attract attention from scientists, especially in the microfluidic field[143–145]. The most prominent branch of additive manufacturing, it is the macroscopic version of bottom-up assembly whereby small molecules are joined together to form a larger structure. The two main techniques that consumer 3D printers currently operate by are fused filament fabrication (F.F.F.) and stereo-lithographic apparatus (S.L.A.).

F.F.F. printers create the 3D objects by passing heated thermoplastic fibres through a print head in consecutive layers. The plastic solidifies a short time after it exits the print head, allowing for a 3D structure to be built. The X- and Y-axis resolution of the structures is determined by the nozzle diameter, and the scanning speed of the print head controls the Z-axis resolution. Although

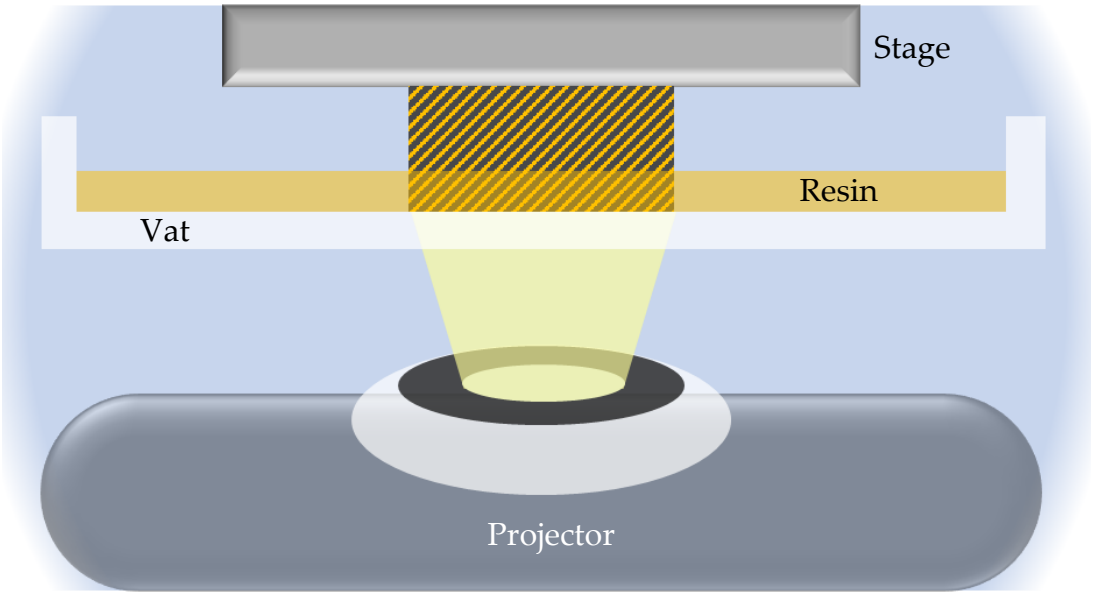

Figure 1. 24 – D.L.P. print schematic. A 3D structure (yellow and black-lined rectangle) is produced using a projector that cures the resin. The stage moves after each layer.

thermoplastics are the most commonly used material in F.F.F. printers, it is possible to use other materials such as concrete.

S.L.A. printers produce 3D structures by curing photopolymer resins with UV light in sequential layers. A stage is lowered onto the surface of a vat containing the resin and the laser cures the resin so that it binds to the stage. The stage is then raised and repositioned to allow for the next layer to be cured. The laser focus determines the X/Y resolution, and the exposure time/intensity of the light (and the accuracy of the Z-axis motor) determines the Z-axis resolution. The structures produced can range from opaque to transparent, completely solid to rubber-like consistencies depending on the precursor resins used. Dynamic light projection (D.L.P.) printers are closely related to S.L.A. printers where the entire layer image is projected onto the resin at the same time (Figure 1. 24), rather than drawn using a laser. This reduces printing time but can result in lower resolutions.

The current maximum resolution of S.L.A./D.L.P. printers is much higher than that of F.F.F. printers, with some printers able to achieve 6 μm X/Y-axis and 5 μm Z-axis resolution. However, this comes at a cost both financially and in

usability. S.L.A./D.L.P. printers produce much more waste and require solvents such as isopropanol and ethanol to clean and maintain the hardware. These is little waste when using F.F.F printers and they do not require the use of organic solvents during post-print processing. There are other 3D printing methods that are used for more specialised requirements or materials.

1.7 – Summary

The processes that occur at the phospholipid bilayer membranes of cells are an intrinsic part of how the body functions. Many of these processes involve the transport of ions and electrons through the hydrophobic layer of the membrane, which is facilitated by specialized proteins known as ionophores. These can range from small cyclic carriers such as valinomycin that can diffuse across the membrane, to large enzymes that span the entire membrane such as ATP-synthase. Trying to mimic these ionophores using synthetic analogues is a leading field of interest both theoretically and practically, with many ionophores being of medicinal and pharmaceutical importance. A possible new route for artificial ionophores is explored in this report, using functionalised AuNPs that use supramolecular interactions to for complexes with ions, with a novel property that the metallic core of the AuNPs may be able to additionally facilitate electron transfer.

Chapter 2 – Experimental Set-up and Methods

In this section, the details of the experimental set up and of the experiments themselves will be presented, along with information regarding the software and equipment used. Notes on the fabrication of the 3D-printed electrochemical cells and the ink-wire electrodes used in them are also included.

2.1 – Chemicals Used

All aqueous solutions were made using Milli-Q ultra-pure "type-1" water that was produced in the lab using a Millipore Milli-Q Plus Water Purification System. Methanol, ethanol, diethyl ether, toluene, and n-decane were bought from Sigma Aldrich.

All metal-salts were purchased from Sigma Aldrich: hydrogen tetrachloroaurate (III) trihydrate ($HAuCl_4.3H_2O$), lithium chloride (LiCl), sodium chloride (NaCl), potassium chloride (KCl), rubidium chloride (RbCl), caesium chloride (CsCl), magnesium chloride hexahydrate ($MgCl_2.6H_2O$), calcium chloride ($CaCl_2$), hexamine-ruthenium (II) chloride ($[Ru(NH_3)_6]Cl_2$), hexamine-ruthenium (III) chloride ($[Ru(NH_3)_6]Cl_3$) and sodium borohydride ($NaBH_4$).

Asolectin from soybean (the phospholipid mixture used throughout the project), Gramicidin D, hydrochloric acid (HCl, 37% wt), and agarose powder were also bought from Sigma Aldrich.

The mercapto-carborane ligand was synthesised by the Teixidor group at the Institut de Ciència de Materials de Barcelona using the literature method[146], and then given to the Brust Group. The 12-crown-4-CH_2-SH ligand was bought from Pro-Chimia.

The Ag/AgCl ink for reference electrodes (2 mℓ), and Ag/AgCl reference electrodes that were used for comparison were bought from ALS Co. (English supplier: IJ Cambria Scientific). The Ag wire (0.5 mm diameter) was bought from Sigma-Aldrich.

2.1.1 – Metal-Chloride Solutions

Stock solutions of metal-chloride solutions were made in volumetric flasks by dissolving a known mass of salt, measured using a 4-decimal place weighing balance, in Milli-Q water.

Stock solutions (~1 M) of LiCl, NaCl, KCl, RbCl, CsCl and $MgCl_2$ were all prepared in the above fashion. These were then used in the preparation of all analyte solutions.

2.1.2 – HCl Solutions

Three HCl stock solutions of different concentrations were made using the 37% HCl solution via dilution with Milli-Q water. The three solutions prepared were a pH -0.5 solution (~3.2 M HCl), a pH 0.5 solution (~ 0.32 M HCl), and a pH 1.5 (~0.032 M HCl) solution. The pH of each solution was measured using a ThermoFisher Orion 9810BN Micro pH electrode, connected to a ThermoFisher Orion Star A211 pH meter.

The analyte solutions were then prepared using an appropriate stock solution for the desired pH, e.g. pH3 analyte solutions were made via dilution of the pH 1.5 stock solution. The pH of the prepared analyte solutions was measured prior to experimentation. If the measured pH of any analyte solution differed from that expected (> ±0.05 pH units), the stock solutions were remade, and the analyte solutions were then re-prepared using the new stock solutions.

2.1.3 – Lipid Solutions

Lipid solutions were prepared at the start of each week where asolectin (0.1 g) was dissolved in n-decane (4 mℓ) in glass vial. These were kept in a fridge at 4 °C until required.

2.2 – Membrane Preparation

The 3D printer used to fabricate the cells was a Kudo3D Titan 2 HR D.L.P printer, bought from the manufacturer, as was the photopolymer resin used for the aperture cells: Kudo3D 3DSR Titan DX black resin, which produced opaque, black cells. The resin used for the D.I.B. cells was the 3D-Materials 3DM-ABS resin, bought from the manufacturer, which produced translucent, orange cells.

2.2.1 – Cell 3D Printing Procedure

All cell designs were created using the graphical modelling software Blender. The 3D models (.stl files) were then "sliced" into 2D images (.png files) using the open-source program SLAcer. These images were then used to 3D print the cells. The software used to 3D print the cells was the Kudo3D printing software supplied with the printer.

The printing stage was lowered until it was 2 cm above the resin vat surface. The resin was then poured into the vat so that the stage printing surface was fully immersed in the resin. This was done slowly from the side to prevent air bubbles being trapped across the printing surface which would cause areas of the resin to cure incorrectly. The stage was then lowered until the vat and the stage were in contact with each other, and the printing was started.

Once the printing had finished, the cells were removed from the stage and cleaned using isopropanol until the residual, unreacted resin had been removed, at which point they were left to dry until they were required

The aperture cells were replaced every week, whereas the D.I.B. cells were prepared daily. This was because the aperture cells could be cleaned out and the electrode gels for both electrodes could be kept hydrated throughout the week. This was not possible for the D.I.B. cells as only one of the electrodes was incorporated into the device. To make sure each pair of electrodes were as similar as possible, both were re-made for each device, rather than remaking only the suspended electrode.

2.2.2 – Ink-Wire Ag/AgCl Electrode Preparation

To prepare the ink-wire Ag/AgCl electrodes, Ag wire (0.5 mm diameter) was cut to the required length (~4 cm) and Ag/AgCl ink was then applied to the area of the wire that would be exposed to the analyte solutions. The wires were then heated in an oven at 120 °C for 5 minutes to dry the ink and bind it to the wire, in accordance with the instruction manual. After this, the electrodes were ready to be used. New electrodes were prepared every time a cell was prepared for use.

2.2.3 – Conductive Agarose Gel Preparation

Conductive agarose gels were used to prevent the analyte solutions from coming into direct contact with the Ag/AgCl electrodes. This was done to reduce the risk of any unwanted reaction between the Ag/AgCl electrodes and the AuNPs or H^+ ions in the analyte solutions.

The conductive gels were made by dissolving agarose powder (1 g) and NaCl (5.84 g) in Milli-Q water (93.16 g) in a glass beaker on a hot plate whilst stirring to make a 0.1 M NaCl gel with a 1% w/w agarose content. When the agarose

powder and NaCl had fully dissolved, the solution was decanted into glass vials and stored in a fridge at 4 °C until needed.

2.2.4 – Aperture Membrane Formation

The method used to form the bilayer membrane in the aperture electrochemical cells was similar to the method used by Montal and Mueller[123]. The printed cell was first prepared by securing the electrodes to the device using superglue, making sure that the glue did not come into contact with the ink-covered region of the electrodes, then surrounding each of the two electrodes with a conductive agarose gel (see above, Section 2.1.4) (Figure 2. 1a).

The analyte solutions (200 μℓ) were then added to each reservoir so that the bottom of the cell was completely immersed, but the aqueous level was below the aperture. Asolectin dissolved in n-decane (50 μℓ, 25 mg asolectin per 1 mℓ n-decane) was added on top of each of the analyte solutions and left for 15 minutes so that a monolayer of phospholipids self-assembled at the aqueous-organic interface on each side of the cell (Figure 2. 1b).

With more additions of the electrolyte (50 μℓ per addition), the monolayer level was raised until the lipid in decane solution was going through the aperture (Figure 2. 1c). Once the lipid-in-decane solution had reached the aperture, smaller additions of the electrolyte (20 μℓ per addition) were added, alternating between each side. This was done with care to prevent accidental increases in water pressure or mechanical forces caused during the addition process which could cause the analyte to flow through the aperture which would require the process to be restarted after having thoroughly cleaned out the device. Once both monolayers had been raised to cover the aperture, membrane formation occurs (Figure 2. 1d).

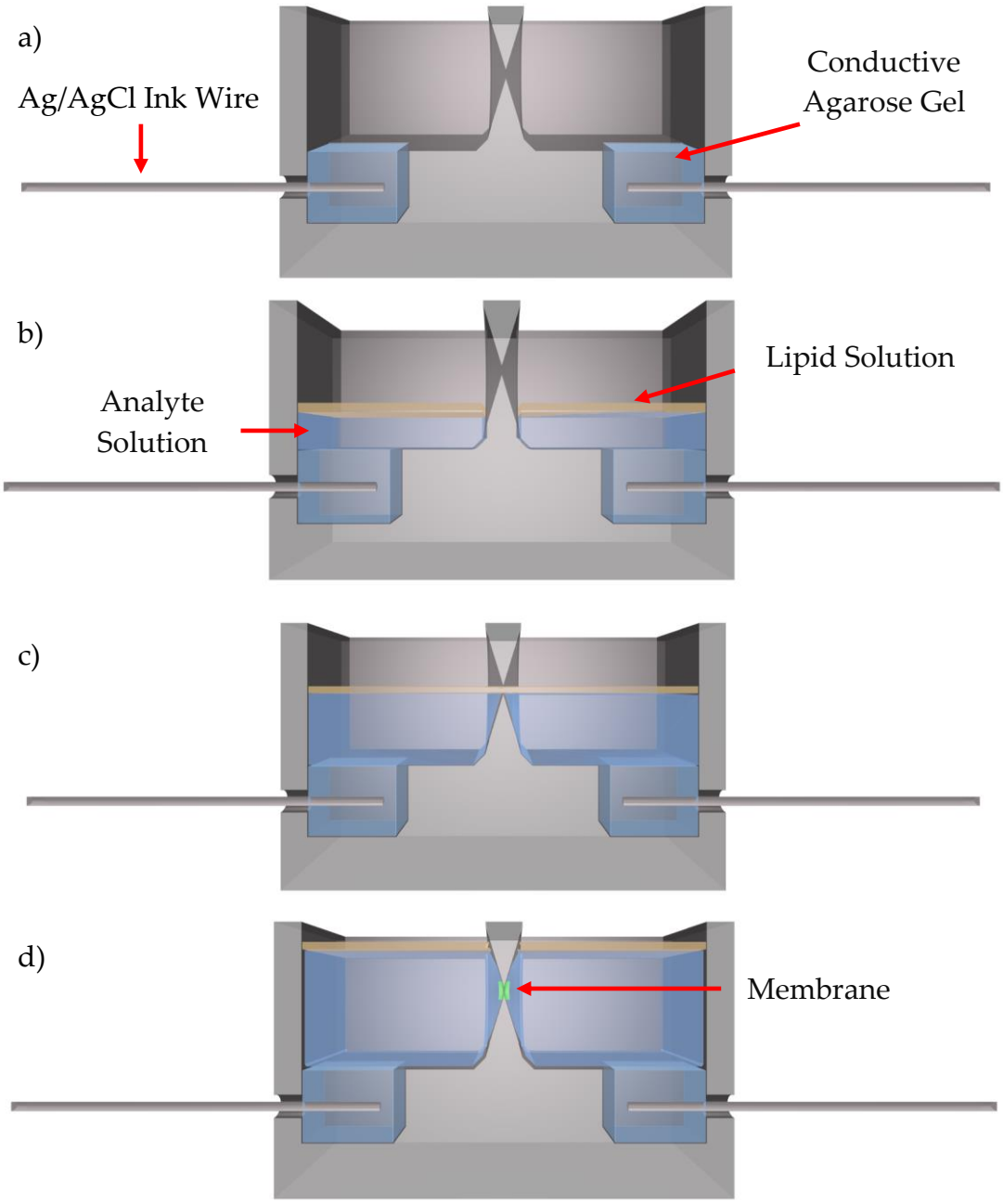

Figure 2. 1 – Diagrams of membrane formation using the Aperture device. (a) The device is fitted with the Ag/AgCl wires (silver rods) and agarose gel (light blue) is used to cover them. (b) Electrolyte solution (darker blue) is added to each side, and asolectin-in-decane (brown) is pipetted on top. (c) The electrolyte level is raised via additions using pipettes until the lipid solutions connect both sides through the aperture. (d) The level is further raised so that a membrane (green) forms across the aperture.

2.2.5 – D.I.B. Membrane Formation

The D.I.B. cells were prepared by fitting one of the reference electrodes into the base and fixed using glue on the outside of the device, carefully, so as to not apply any glue to the ink-covered area of the electrode (Figure 2. 2a). An agarose gel (see above, Section 2.1.4, ~65 μℓ) was added into the electrode compartment to submerge the electrode completely. The appropriate electrolyte solution (300 μℓ) for that electrode was then added to cover the agarose and so that the water level was easily visible. A layer of asolectin-in-decane (100 μℓ, 25 mg asolectin per 1 mℓ decane) was deposited on top of the electrolyte by pipetting against the wall of the cell and left for a short time for the lipids to self-assemble as a monolayer at the water-decane interface (Figure 2. 2b).

The second electrode was prepared by passing it through a glass capillary tube so that around 1 cm protruded from the bottom of the tube and then cut so as to leave enough wire at the top to allow it to be connected to the reference/counter cable. The wire was glued to the capillary at the top and, once the glue had dried, the Ag/AgCl ink was applied to completely cover the exposed wire and left to dry. A small droplet of agarose gel, the same as that used for the first electrode, was then pipetted onto the tip of the second electrode to act as an anchor for the droplet, which might otherwise fall off the electrode. This electrode was then inserted into the micro-manipulator (World Precision Instruments M3301-M3) and positioned above the device, before being connected to the potentiostat (Figure 2. 2c).

An electrolyte droplet (4 μℓ) was pipetted onto the agarose anchor and the suspended electrode was then lowered slowly through the lipid solution until the droplet contacted the other monolayer at the water-decane interface (Figure 2. 2d). The electrode was then raised slightly (~5 μm) so that the droplet would settle on the monolayer at the boundary between the lower aqueous electrolyte and the upper lipid-in-decane phase. This small raise was so that the pressure on the droplet – and membrane – from mechanical forces caused by the micromanipulator would hopefully be minimised, and to make sure that it was not possible for the agarose drop to interfere with the

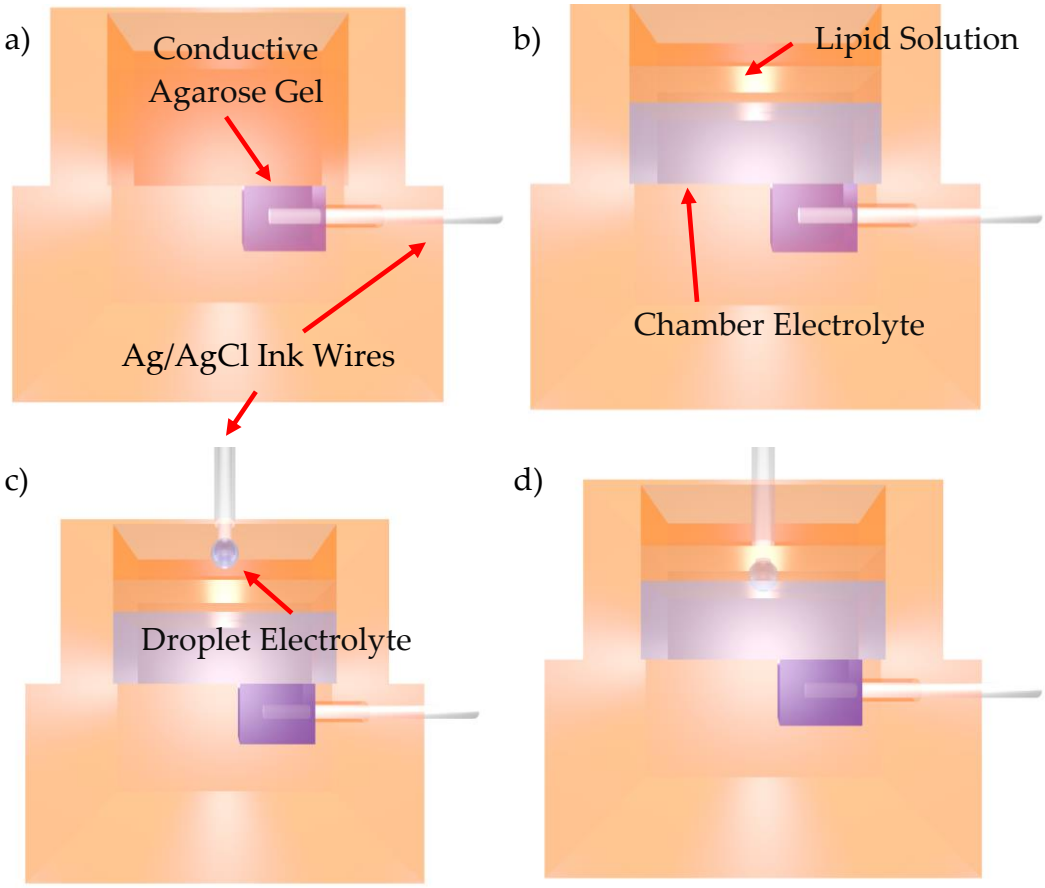

Figure 2. 2 – Membrane formation in the D.I.B. device. (a) The device is prepared with the ink wire electrode (silver rod) and agarose gel (dark blue). (b) The electrolyte (light blue) and lipid solution (orange) are added into the chamber. (c) The droplet-electrode is positioned above the device and lowered through the lipid solution. (d) The droplet solution is lowered through the lipid solution until it comes into contact with the chamber solution and a bilayer membrane forms.

membrane interface. The resistance and capacitance values were calculated from the CV data collected after this step and compared to literature values to confirm whether a membrane had formed.

2.3 – AuNP Preparation

Stock solutions of $HAuCl_4$ (~0.05 M) were prepared using the same method as described above (Section 2.1.1). The Agilent Cary 8454 UV-Vis spectrophotometer and Hellma absorption cuvettes - black sided (400 μℓ) were used for all UV-Vis measurements.

2.3.1 – Mercapto-Carborane Functionalised 2-3 nm AuNPs

2.3.1.1 – Preparation

Mercapto-carborane functionalised 2-3 nm AuNPs (carb-AuNPs) were prepared following a literature method[147,148]. A 1:1:3 molar ratio of Au^{3+}:mercapto-carborane:$NaBH_4$ was used in this synthesis, with the total volume of solvent (methanol and Milli-Q water) after all additions being 20 mℓ.

$HAuCl_4$ (60 μmol) was added to methanol (~15 mℓ) in a conical flask with a stirrer bar; resulting in a clear yellow solution. A solution of mercapto-carborane (60 μmols) in methanol (~1.5 mℓ) was prepared and then added to the flask mixture. The solution changed in colour from yellow to orange over a period of ~5-10 minutes. After this, a fresh solution of $NaBH_4$ (180 μmols, ~1.5 mℓ methanol) was prepared and, once the effervescence had subsided, rapidly added to the solution under vigorous stirring. The solution immediately turned black. This was left for 20 minutes to allow the process to complete.

The resulting dark brown solution was transferred to a round-bottomed flask and the solvent was removed using a rotary evaporator at 28 °C. The residue was washed three times with diethyl ether (3 x 3 mℓ) to remove any unreacted capping ligands. The carb-AuNPs are slightly soluble in diethyl ether, and so a high proportion of the product is lost in these washing steps. Once washed, the remaining AuNPs were re-dispersed in iso-propanol (10 mℓ) and filtered and transferred, using a syringe filter, into another flask to remove unwanted water-soluble reactants from the AuNPs. The iso-propanol was then removed via rotary evaporation at 31 °C. Finally, the AuNPs, a dark-brown residue, were re-dispersed in a small amount of ethanol (200 μℓ) and, once the majority of the AuNPs had been dispersed in the ethanol, a larger amount of Milli-Q water (1.8 mℓ). The carb-AuNP solution was then transferred to a glass vial to be used as a stock solution, which was kept at room temperature.

2.3.1.2 – UV-Vis Spectroscopy

Carb-AuNP stock solution (40 μℓ) was diluted using Milli-Q water (360 μℓ) and was run against a blank solution comprising Milli-Q water (396 μℓ) and ethanol (4 μℓ), accounting for the 10% ethanol in the stock solution (Figure 2. 3).

The shape of the curve, without a SPR peak seen, is characteristic of AuNPs that are smaller than 3 nm diameter, confirming that the AuNPs had been prepared successfully and had not formed larger sized AuNPs. The concentration of the stock solution was then calculated from the absorbance value at the wavelength 400 nm using the Beer-Lambert Law (Eq. 8, Section 1.6.5) using known ε values[142].

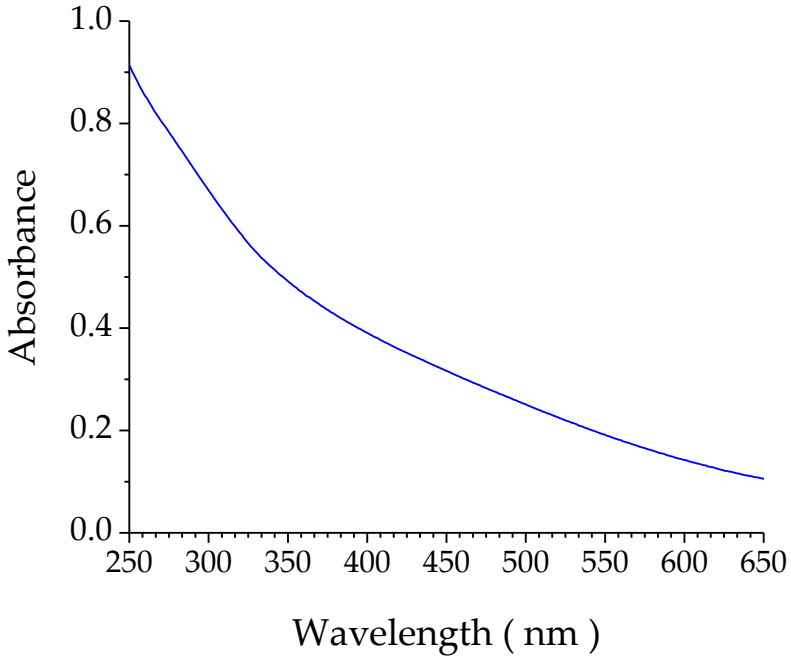

Figure 2. 3 – UV-Vis spectrum of the carb-AuNPs in Milli-Q water. The blank used was a 1% ethanol in water solution, to account for the ethanol in the carb-AuNP stock.

2.3.2 – 12-Crown-4-CH2-SH Functionalised 2-3 nm AuNPs

2.3.2.1 – Preparation

12-Crown-4-CH2-SH functionalised 2-3 nm AuNPs were prepared using a similar method to the carb-AuNPs[142]. A 1:1 molar ratio of $HAuCl_4$ (19 μmol) and the ligand, 12-crown-4-CH_2-SH (19 μmols, 3.74 μℓ) were added to methanol (3 ml) in a 5 ml glass round-bottomed flask with a stirrer bar. The solution, which was a pale-yellow colour, was left to stir for 5 minutes. During this time, an excess of $NaBH_4$ (89.1 μmol) was dissolved in methanol (0.5 mℓ) and, once the effervescence had subsided, rapidly added to the flask under vigorous stirring. The solution immediately turned black and was left for 20 minutes whilst stirring to allow the reaction to complete. The solvent was removed by rotary evaporation at 28 °C until a dry, black/brown residue coated the flask. This was washed with toluene (3 x 3 ml) and then diethyl ether (3 x 3 ml) and left to dry in air. Once dry, the product was dissolved in isopropanol (2-3 ml) and syringe-filtered into a new round-bottomed flask in order to remove unwanted excess $NaBH_4$ and other water-soluble impurities. The filtrate obtained was a clear dark brown solution. The isopropanol was then removed via rotary evaporation at 30 °C until completely dry, and a dark brown residue was left coating the flask. The final product was re-dispersed in Milli-Q water (2 ml) and transferred to a glass sample vial to use as a stock solution of the functionalised 12-crown-4 AuNPs. The stock solutions were kept at room temperature. Throughout the thesis, these particles will be referred to as crown-AuNPs.

The solubility of the crown-AuNPs in toluene and diethyl ether is poor compared to the carb-AuNPs, so significantly less of the product is lost in the washing stages of the preparation. It is, therefore, possible to make these

crown-AuNPs in smaller batches (3 mℓ) compared to the carb-AuNPs (20 mℓ) and produce a similar amount of usable AuNPs.

2.3.2.2 – UV-Vis Spectroscopy

To ensure that the crown-AuNPs made were the desired size and that they were of sufficient quality for experimentation, a UV-Vis spectrum (Figure 2. 4) of the crown-AuNPs was obtained. Crown-AuNP stock solution (20 μℓ) was diluted using Milli-Q water (380 μℓ) and was run against a blank solution comprising Milli-Q water (400 μℓ).

From the UV-Vis spectrum, it can be seen that there is no SPR absorption peak present, which indicates that small (<3 nm) crown-AuNPs and the shape of the absorbance curve is identical to the 2-3 nm crown-AuNPs that had been analysed using microscopy[142]. The concentration was then calculated as above in Section 2.3.1.2.

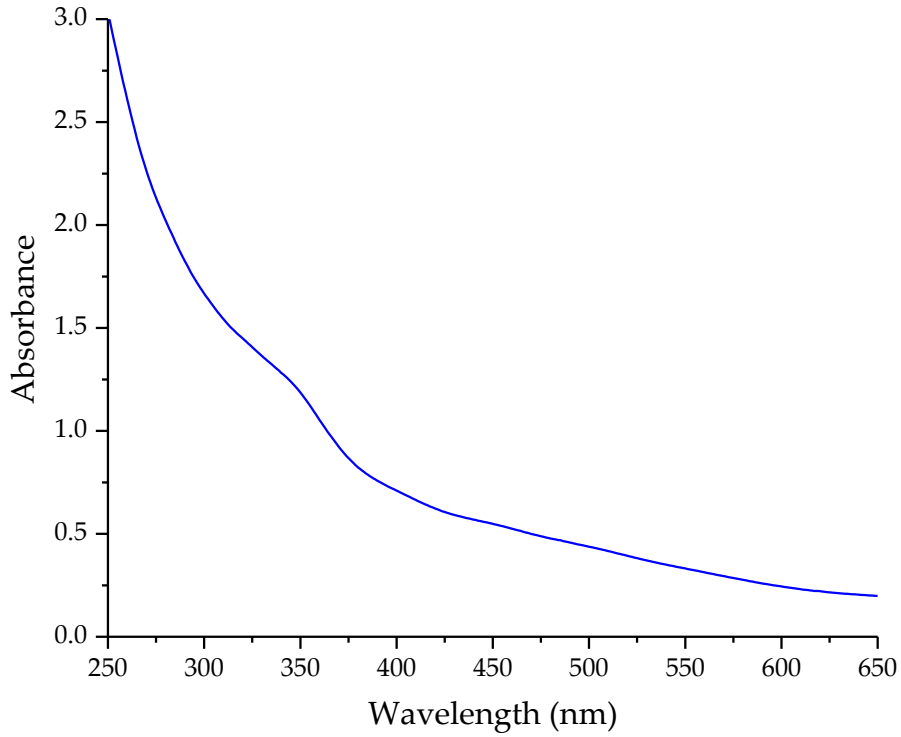

Figure 2. 4 – UV-Vis Spectrum of the crown-AuNPs stock in Milli-Q water. The absorbance value at 400 nm is used to calculate the concentration of the stock solution.

There is a small "rise" at around 350 nm wavelength, not seen in the carb-AuNP spectrum, but seen in almost all 12-crown-4-, 15-crown-5-, and 18-crown-6- AuNP UV-Vis spectra[142]. An explanation for this has not yet been assigned.

2.4 – Analytical Procedures

2.4.1 – Electrochemistry Experiments

Two potentiostats were used throughout the study. All experiments using the Aperture membrane formation method were run using a Metrohm μAutolab III. All experiments using the D.I.B membrane formation method were undertaken using a Metrohm PGSTAT302N. The software used to control the potentiostats was Metrohm Autolab Nova 1.10. All experiments were repeated at least three times.

The "standard" electrochemical experiment consists of one solution and three electrodes: a working electrode (W.E.), a polarisable electrode where the reaction of interest takes place; a reference electrode (R.E.), a non-polarisable electrode that maintains a constant potential difference compared to the solution, and a counter electrode (C.E.) which is used to prevent high current going through the R.E.. Passing high currents through a R.E. causes degradation of the electrode surface and the constant potential would be lost.

As previously discussed in Section 1.5.4, phospholipid membranes have high resistance and function as insulators. Solutions on either side of them can be thought of as effectively electrochemically separated. When applying potentials and currents across the membrane, therefore, an experimental set-up that deviates from the "standard" three-electrode model is required. To accurately control or monitor the potential across the membrane, a non-polarisable electrode is needed on either side of the membrane. In this way,

the potential of the solutions on either side of the membrane is known, as it is set by the non-polarisable electrode in each solution.

Due to the membrane being highly resistive, the amount of current that flows through the system is low, and so it is possible to remove the two polarisable electrodes, that would otherwise protect the non-polarisable electrodes from degradation due to high current flow, from the set-up and use only two non-polarisable electrodes. This greatly reduces experimental difficulties and the two electrode system has been used for the electrochemical study of membranes consistently[131,149–151]. These electrodes were termed Reference Electrode 1 (R.E.1) and Reference Electrode 2 (R.E.2). R.E.1 was connected to the potentiostat using the working electrode cable, and R.E.2 was connected to the potentiostat using both the reference electrode cable and counter electrode cable (Figure 2. 5).

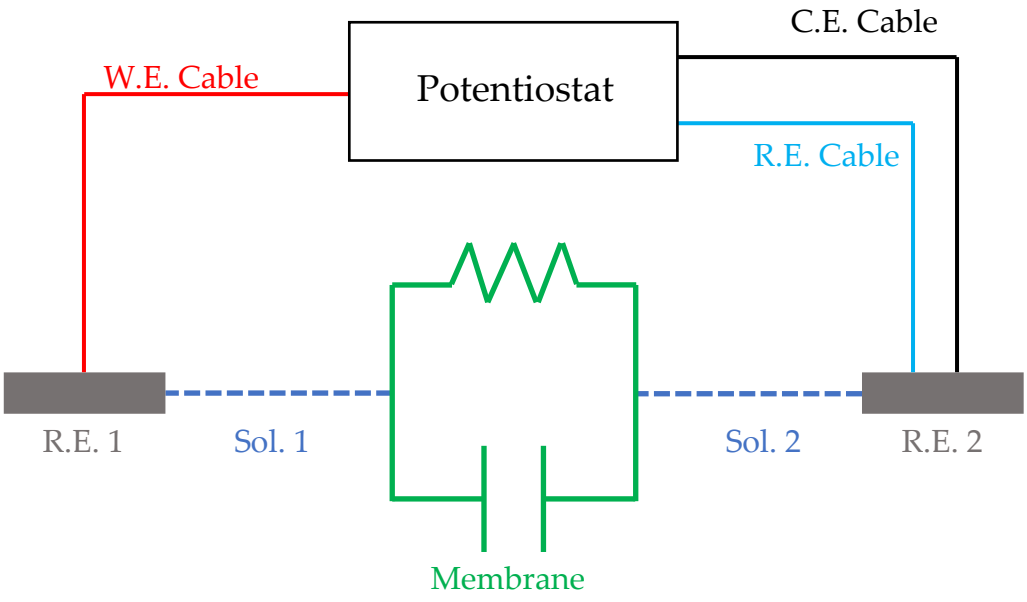

Figure 2. 5 – The electrical circuit of the experimental set-up. The working electrode cable is connected to R.E. 1. Both the reference electrode cable and the counter electrode cable are shorted together and connected to R.E. 2.

Where solution 1 (Sol. 1) and R.E. 1, are on one side of a membrane, and solution 2 (Sol. 2) and R.E. 2 are on the other side, applying a potential to R.E. 1 will also raise the potential of Sol. 1 by the same amount, as the potential difference between solution and non-polarisable electrode is constant. In this way, it is possible to measure or apply a potential across the membrane (Figure 2. 6). There will be low currents through the membrane which will cause degradation of the R.E.s, but this will take place slowly. It is possible to use them for successive experiments, but they become unusable after several uses and need to be replaced regularly. As the R.E.s needed to be continually replaced, using commercial non-polarisable electrodes would be uneconomical, and so less costly reference electrodes were prepared following the procedure described in Section 2.2.2.

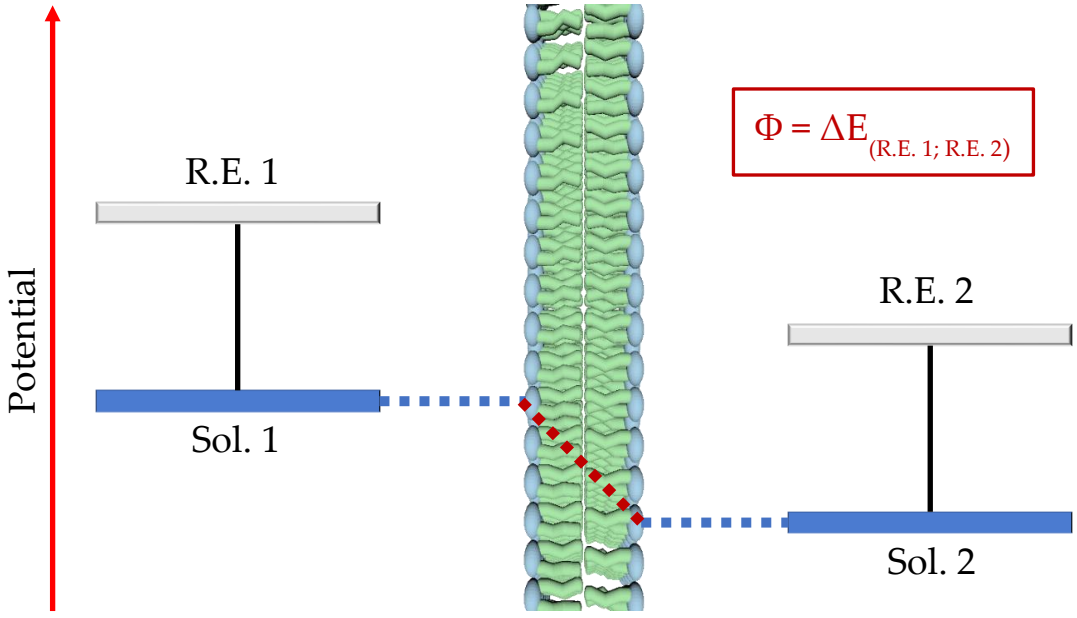

Figure 2. 6 – Potential diagram of the two-electrode system. The two R.E.s maintain a constant potential difference between their respective solutions (black line). By using two identical R.E.s, the potential drop across the membrane (Φ, in volts), i.e the potential difference between Sol. 1 and Sol. 2, will be identical to the potential difference (ΔE) between the two R.E.s

2.4.1.1 – Aperture Membranes: Base Membrane and Gramicidin Testing

Cyclic voltammetry experiments on membranes in Section 3.2 used a scan rate of 2 mVs^{-1} and a scan range from -40 mV to +40 mV when using the aperture membrane formation method described above in Section 2.2.4. The analyte used for these experiments was 0.1 M KCl.

The exceptions to this were experiments that were run on aperture membranes with gramicidin involved. These experiments had a reduced scan rate (1 mVs^{-1}) and a reduced range (-10 mV to +10 mV) as it was expected that the conductance through the membranes would be much higher due to the presence of a natural ionophore. By lowering the scan range, the current passing through the system would be reduced, helping to prevent unnecessary degradation of the Ag/AgCl electrode wires until they were replaced. If the electrodes showed a significant change (±5 mV) in the potential difference compared to the value during the first experiment in which they were used, a new cell and electrodes were prepared immediately. This was done to prevent possible anomalies and artefacts arising due to compromised Ag/AgCl electrodes.

The gramicidin-divalent cation blocking experiment was set up using 0.1 M KCl as the analyte solution, and a lipid solution that also contained gramicidin (200 nM). The membrane was formed, and a continuous CV was run with scan rate 1 mVs^{-1} between +10 mV and -10 mV. At 7750 seconds, $CaCl_2$ (0.1 M, 20 μℓ) was added to each side of the membrane.

2.4.1.2 – D.I.B. Membranes: Base Membrane and Gramicidin Testing

These methods refer to the membranes discussed in Section 3.3. The cyclic voltammetry parameters (scan rate and scan range) were identical for all experiments (base and gramicidin) using the D.I.B. membranes formed. The

cells were made daily rather than weekly, and so the risk of degradation of the electrodes due to excessive currents and continual use, and how that would affect the measurements, was thought to be low. The scan rate for all experiments was 2 mVs^{-1} and the scan range was between +50 mV to -50 mV. The membranes were all formed using the D.I.B membrane formation method described above in Section 2.2.5. Five symmetric membranes were studied:

pH1 symmetric membrane: **R.E.1:** 100 mM HCl; **R.E.2**: 100 mM HCl

pH2 symmetric membrane: **R.E.1:** 10 mM HCl; **R.E.2**: 10 mM HCl

pH3 symmetric membrane: **R.E.1:** 1 mM HCl; **R.E.2**: 1 mM HCl

pH4 symmetric membrane: **R.E.1:** 0.1 mM HCl; **R.E.2**: 0.1 mM HCl

pH5 symmetric membrane: **R.E.1:** 0.01 mM HCl; **R.E.2**: 0.01 mM HCl

For the zero-current potential measurements, a D.I.B membrane was formed using a solution of HCl at pH 2 (0.01 M HCl) with 200 nM gramicidin dissolved in the lipid in decane solution and the zero-current potential was measured. The electrolyte on the droplet was then replaced with a solution of pH 3, and the zero-current potential was recorded again. This was repeated, replacing the droplet solution with solutions of pH 4, 5, and 6.

2.4.1.3 – Aperture Membranes: carb-AuNPs Potential Step Experiments

These methods refer to the membranes discussed in Section 4.2 and were formed using the aperture method with following solutions on each side of the membrane:

Na^+ symmetric membrane: **R.E.1:** 100 mM NaCl; **R.E.2**: 100 mM NaCl.

K^+ symmetric membrane: **R.E.1:** 100 mM KCl; **R.E.2:** 100 mM KCl.

Na^+ vs K^+ membrane: **R.E.1:** 100 mM NaCl and 1 mM KCl; **R.E.2:** 1 mM NaCl and 100 mM KCl.

Na^+ vs Cs^+ membrane: **R.E.1:** 100 mM NaCl and 1 mM CsCl; **R.E.2:** 1 mM NaCl and 100 mM CsCl.
Li^+ vs Cs^+ membrane: **R.E.1:** 100 mM LiCl and 1 mM CsCl; **R.E.2:** 1 mM LiCl and 100 mM CsCl.
Na^+ vs Mg^{2+} membrane: **R.E.1:** 100 mM NaCl and 0.67 mM $MgCl_2$; **R.E.2:** 1 mM NaCl and 67 mM $MgCl_2$.

For the symmetric stepping measurements, the potential of R.E.1 was controlled, and stepped repeatedly between +80 mV and -80 mV, with each step occurring 90 seconds after the previous one. The current was recorded every 0.5 seconds.

Immediately after the symmetric stepping measurement was finished, the progressive stepping measurement was started. The potential of R.E.1 was stepped to +80 mV and then -80 mV for the first two steps to confirm the current values were similar to the last values of the symmetric stepping measurement. After this, the potential was stepped to 0 mV, and progressively higher potentials were applied, in increments of 10 mV, until ±80 mV was reached again.

Once both the symmetric stepping and progressive stepping experiments had been completed on the base membrane, the measurements were repeated, this time with the carb-AuNPs present. 200 nM of the carb-AuNPs were added to each side of the membrane after at least two of the potential steps had been completed at the beginning of the symmetric stepping measurement. This was done to confirm that the membrane had not changed significantly during the period of time between measurements. The addition of the carb-AuNPs during the measurement meant that it was possible to see what the initial effect of adding the AuNPs to each side of the membrane was. The convection caused by adding the AuNPs to the solutions briefly distorted the current

measured at the same time. This distortion was later used as a signal to identify the exact moment of AuNP addition on the current vs time recordings.

The addition of AuNPs to both solutions was introduced towards the bottom of the reservoirs and the pipette was angled so that the tip was directly under the membrane. The process was carried out slowly and with care as the movement of the pipette in the solutions would inevitably cause small eddies to form which could disrupt and break the membrane.

2.4.1.4 – D.I.B. Membranes: carb-AuNPs Zero-Current Potential Experiments

These methods refer to the membranes discussed in Section 4.3. The membranes were formed using the following solutions on either side of the membrane:

100 mM NaCl membrane: **R.E.1:** 100 mM NaCl; **R.E.2**: 100 mM NaCl.
1 mM NaCl membrane: **R.E.1:** 1 mM NaCl; **R.E.2**: 1 mM NaCl.
100 mM KCl membrane: **R.E.1:** 100 mM KCl; **R.E.2**: 100 mM KCl.
100 mM RbCl membrane: **R.E.1:** 100 mM RbCl; **R.E.2**: 100 mM RbCl.
100 mM $MgCl_2$ membrane: **R.E.1:** 100 mM $MgCl_2$; **R.E.2**: 100 mM $MgCl_2$.

Each symmetric membrane was set up using the D.I.B. technique with 0.1 nM carb-AuNPs on both sides of the membrane. The zero-current potential was then set to be continuously measured during the experiment. Different dilutions (0.1%, 1%, 10%, and 100% stock concentration) of the carb-AuNPs (3 μℓ) were then added to the chamber solution in stages so that the concentration in the chamber solution would increase but the droplet solution would remain constant.

The change in the potential after each addition was calculated and then a Nernst plot was obtained by plotting the change in membrane potential

against the natural logarithm of the ratio between the carb-AuNP concentrations on either side of the membrane. The charge on the carb-AuNPs was then calculated from the gradient of a straight-line fit to the data using the software Origin.

2.4.1.5 – D.I.B. Membranes: Crown-AuNPs Cyclic Voltammetry

These methods refer to the membranes discussed in Section 5.2. Two sets of symmetric membranes were formed, one set with 1 μM crown-AuNPs on both sides of the membrane (**X** = 1), and another set using 5 μM crown-AuNPs (**X** = 5). Each set of membranes formed were as follows:

pH1 membrane: **R.E.1:** 100 mM HCl and **X** μM crown-AuNPs; **R.E.2**: 100 mM HCl and **X** μM crown-AuNPs.
pH2 membrane: **R.E.1:** 10 mM HCl and **X** μM crown-AuNPs; **R.E.2**: 10 mM HCl and **X** μM crown-AuNPs.
pH3 membrane: **R.E.1:** 1 mM HCl and **X** μM crown-AuNPs; **R.E.2**: 1 mM HCl and **X** μM crown-AuNPs.
pH4 membrane: **R.E.1:** 0.1 mM HCl and **X** μM crown-AuNPs; **R.E.2**: 0.1 mM HCl and **X** μM crown-AuNPs.
pH5 membrane: **R.E.1:** 0.01 mM HCl and **X** μM crown-AuNPs; **R.E.2**: 0.01 mM HCl and **X** μM crown-AuNPs.

Each set also had a unique membrane prepared. For the 1 μM crown-AuNP set a pH1.5 membrane and for the 5 μM crown-AuNP solutions, a membrane at ~ pH1.5 was tested:

pH 1.25 membrane: **R.E.1:** 55 mM HCl and 1 μM crown-AuNPs; **R.E.2**: 55 mM HCl and 1 μM crown-AuNPs.

pH1.5 membrane: **R.E.1:** 31.6 mM HCl and 5 μM crown-AuNPs; **R.E.2**: 31.6 mM HCl and 5 μM crown-AuNPs.

After completing the experiments with 5 μM crown-AuNPs both sides of the membrane for pH1 and pH5, the R.E.2 solution was removed and replaced with a solution at the same pH but without crown-AuNPs and the membranes were analysed again using cyclic voltammetry. These are discussed in Section 5.2.2.

For the electron transfer experiments that are discussed in Section 5.9, a similar method was used, where a membrane was formed, and the droplet solution was replaced. Two membranes were studied:

Ru^{2+} membrane: **R.E.1:** 10 mM HCl, 1 μM crown-AuNPs and 1 mM $[Ru(NH_3)_6]Cl_2$; **R.E.2**: 10 mM HCl and 1 μM crown-AuNPs.

Ru^{3+} membrane: **R.E.1:** 10 mM HCl, 1 μM crown-AuNPs and $[Ru(NH_3)_6]Cl_3$; **R.E.2**: 10 mM HCl and 1 μM crown-AuNPs.

CVs were taken of these membranes and then the R.E.2, solution was replaced with a solution containing the other ion of the redox couple at the same concentration, and the CVs were taken again and compared.

2.4.1.6 – D.I.B. Membranes: Crown-AuNPs Potential Measurements

These methods refer to the membranes discussed in Section 5.3. The membranes were formed via the D.I.B. method, and the zero-current potential of the system was measured. Two sets of experiments were undertaken, one varying the AuNP concentration on either side of the membrane, and the other set varying the H^+ concentration. To create the different membranes, the chamber solution was kept constant at the highest concentration used, and the droplet solution was continually replaced with lower and lower concentrations once measurements had been taken. The starting analyte used for the study of varying the AuNP concentrations was a pH2 solution with 1 μM crown-AuNPs for both the droplet solution and the chamber solution. The

zero-current potential was then measured. The starting analyte used for the study of varying the pH was a pH1 solution with 1 μM crown-AuNPs for both the droplet solution and the device solution. The zero-current potential was then measured.

For the potential measurement described in Section 5.7.1, a symmetrical pH1 membrane was prepared with 1 μM AuNPs on each side of the membrane as well and the zero-current potential was measured. The droplet solution was then replaced with a pH0 solution of HCl and 1 μM crown-AuNPs, and the zero-current potential was measured again.

2.4.2 – Zeta Potential Measurements of crown-AuNPs

3 μM crown-AuNP solutions (1 mℓ) at multiple H^+ concentrations (0.1 mM, 0.25 mM, 0.05 mM, 1 mM, 2 mM, 3 mM, 4 mM, 5 mM, and 10 mM) were prepared in Eppendorfs using the crown-AuNP stock solution, the relevant HCl stock solutions and Milli-Q water. The pH of the solutions were checked using a pH meter. Immediately before a solution was to be pipetted into the ζ-potential cell, the solution was shaken manually for ~30 seconds to make sure the protons were distributed throughout the sample evenly, and then left for ~30 seconds to allow the solutions to equilibrate. The solutions were then injected into a ζ-potential cell and placed into the Zetasizer to begin the measurements.

All ζ-potential measurements were run using a Malvern Zetasizer Nano ZS Zen3600. Each sample was measured three times, with each measurement an average ζ-potential value of at least 10 runs. These experiments are discussed in Section 5.4.

2.4.3 – Optical and UV-Vis Study of Crown-AuNPs

2.4.3.1 – Optical Solutions

These experiments are discussed in Section 5.6.1. The stock crown-AuNP solution (50 μℓ) was diluted with Milli-Q H_2O and the HCl stock solutions to form 500 μℓ solutions at pH 1, 2, 3 and 4. To these, n-decane (500 μℓ) was then added.

Another solution of crown-AuNPs in pH1 was prepared in a similar way, however replacing the n-decane with chloroform.

2.4.3.2 – UV-Vis Study

The results from these experiments are discussed in Section 5.6.2. The Agilent Cary 8454 UV-Vis spectrophotometer and Hellma absorption cuvettes - black sided (400 μℓ) were used for all samples.

Eight 1 mℓ solutions of crown-AuNPs (5% volume of stock crown-AuNP solution in the 1 mℓ solutions) in solutions of varying pH (two solutions each of pH 1, 2, 3 and 4) were prepared in separate lo-bind Eppendorfs, confirming with the pH meter that the proton concentrations were correct. n-Decane (500 μℓ) was then added to one solution at each of the pH values. The solutions which had not been mixed with decane were named the "standard solutions", and the samples that had been mixed were called the "latent solutions".

The latent solutions were shaken manually for 60 seconds and, after allowing 10 seconds for phase separation, the aqueous solution (400 μℓ) was transferred using a pipette to another Eppendorf. All eight aqueous solutions were then analysed. The blank solution used for all solutions was Milli-Q water.

Chapter 3 – Electrochemical Study of Phospholipid Bilayer Membranes

In this section, two distinct methods of phospholipid bilayer membrane formation that allow for the study of the membranes electrochemically will be introduced and discussed. Each method will be tested for validity, with physical properties of the produced membrane calculated and compared to the known literature. The natural ionophore gramicidin will be used to confirm the presence and integrity of the membranes, using a different method for each of the two ways of bilayer formation.

3.1 – Ag/AgCl Ink Electrode Test

To confirm that the use of the ink-wire electrodes would be viable, they were tested by comparing their potential drift with commercial Ag/AgCl electrodes. The electrodes were suspended in a 0.1 M KCl solution, and the zero-current potential was measured. The potential was monitored over a 30-minute period (Figure 3. 1). The potential drift was then calculated in terms of μVh^{-1}. The commercial electrodes had a drift of 81.3 ± 0.75 μVh^{-1} whereas the potential drift using the ink-wire electrodes was 334 ± 2.50 μVh^{-1}. The potential difference between the ink-wire electrodes was smaller than the difference between the two commercial electrodes. The commercial electrodes are compartmentalised in their own salt solutions, which are then connected to the electrolyte solutions via a porous frit. The extra connections between the electrode-solutions and the electrolyte solution are believed to be the cause of the larger potential difference measured. The ink-wire electrodes do not have this extra connection, as they are immediately in contact with the

electrolyte solution and so the measured potential difference should be from the electrodes themselves.

The commercial electrodes, unsurprisingly, had a lower rate of drift compared to the ink-wire electrodes and the potential was less erratic during the timeframe, however, the performance of the ink-wire electrodes was deemed within acceptable limits, and were used in all electrochemical experiments on the membranes.

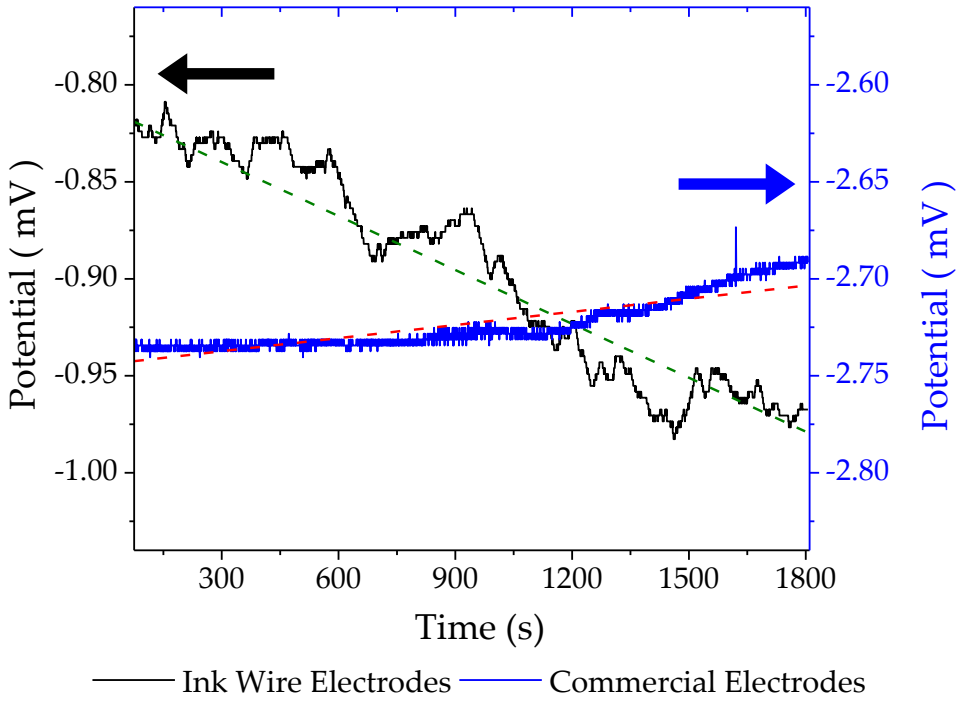

Figure 3. 1 – Comparison of the potential drift of the Ink Ag/AgCl electrodes (black) compared to the commercial reference electrodes (blue). The two y-axes have the same range to allow better comparison. The fitted straight lines used to calculate the drift are shown as green (ink-wire) and red (commercial) dotted lines.

3.2 – Electrochemical Analysis of the Aperture Membranes

3.2.1 – Cell Design

There are many ways in which to prepare a phospholipid bilayer membrane for electrochemical study as described in Section 1.5, of which several were attempted. One of the methods that produced robust membranes and repeatable results was based on Montal and Mueller's design[122,123], the Aperture method. Monolayers of lipids are deposited onto two reservoirs of electrolyte, which are separated by a wall with a small vertical aperture

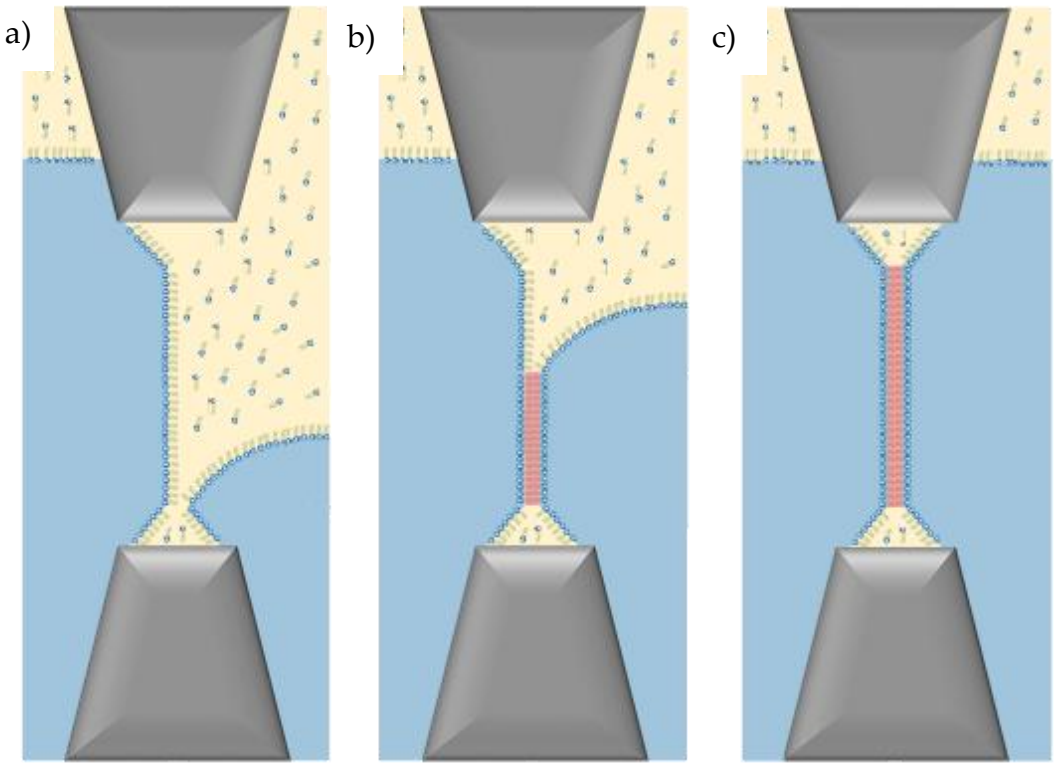

Figure 3. 2 – Membrane formation in the aperture system. Electrolyte solutions (blue) on either side of the aperture each have a monolayer of lipids (blue heads and green tails) at the interface with n-decane (yellow). (a) One side of the membrane is raised above the aperture opening (b) The water level on the right side is slowly raised, folding the monolayers onto each other, forming a membrane (shown in red). (c) When both solutions on either side cover the aperture, the membrane formation is completed, usually with a solvent annulus.

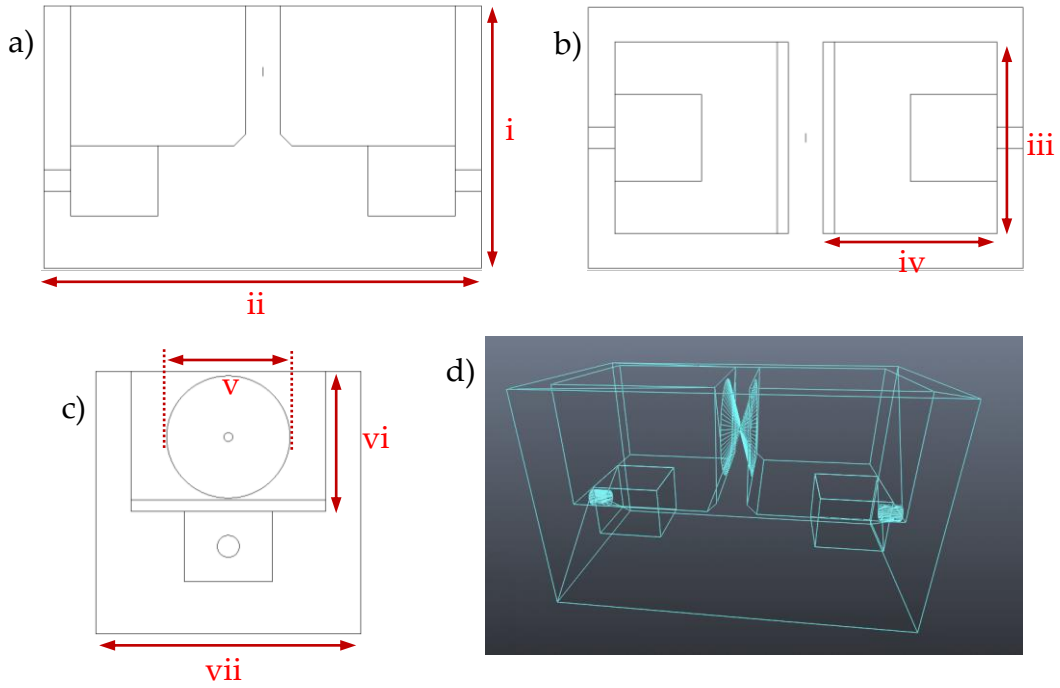

Figure 3. 3 – Design Schematic of the 3D-printed electrochemical cell used in the Aperture method of membrane preparation. (a) 2D Front view. (b) 2D Top View. (c) 2D Side View. (d) Wireframe 3D Model. The dimensions of the cell are as follows: (i) 15 mm (ii) 25 mm (iii) 11 mm (iv) 10 mm (v) 7 mm (vi) 8 mm (vii) 15 mm. The aperture is 300 μm in diameter.

connecting the two chambers. The two monolayers are then brought into contact through the aperture creating the bilayer membrane (Figure 3. 2).

The design of the electrochemical cell (Figure 3. 3) used to form aperture membranes comprises two reservoirs that are connected via an aperture. The aperture is a circular hole of 300 μm diameter that tapers out in a conical fashion to allow the smoothest transition between the two reservoirs and the aperture. Electrode compartments were added at the bottom of the reservoirs to allow the Ag/AgCl ink-wire electrodes to be fixed into the device, simplifying the experimental set-up, removing the need for electrode holders.

3.2.2 – Base Membrane Behaviour

The membranes were formed as described in Section 2.2.4, and the experiments described in Section 2.4.1.1. The membranes were monitored

using CVs during formation. The resistance through the aperture was considerably higher when the solutions were separated by the membrane compared to when they were connected (Figure 3. 4). The electrolyte solutions used were 0.1 M KCl.

The capacitance and resistance of the membranes formed using this method were calculated at 0.65±0.108 μFcm^{-2} and 5.4±0.784 $M\Omega cm^2$ respectively. These agreed with the literature although given how resistive some membranes formed can be, the resistances of these membranes were towards the lower values. The area of the membranes formed was difficult to accurately calculate as the resin used was opaque, and so the size was estimated to be the size of the whole aperture: $7.07x10^{-4}$ cm^2. The membrane formation, however, inevitably forms a solvent torus around the aperture leading to a smaller membrane area than the entire aperture area[152].

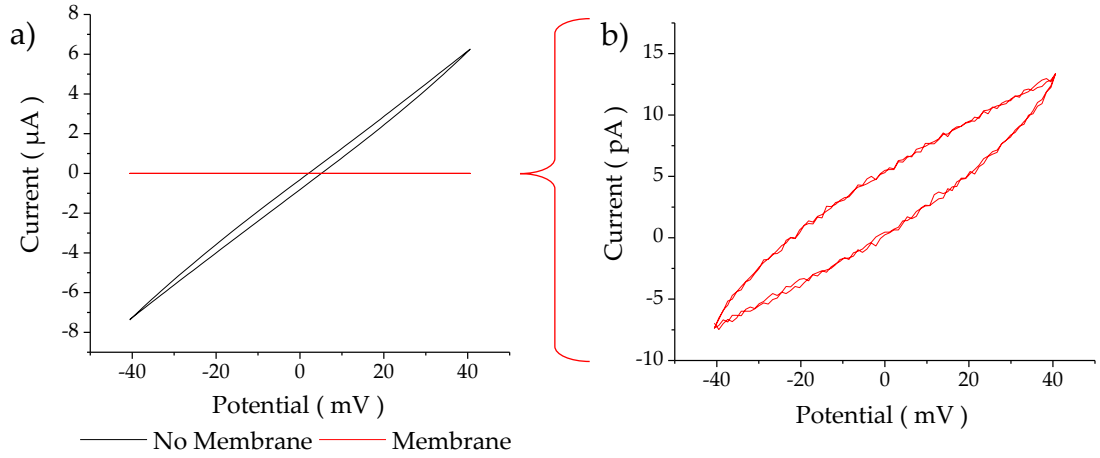

Figure 3. 4 – (a) CVs showing the high resistance through the system when a membrane separated two 0.1M KCl electrolyte solutions (red) compared to when they were connected (black). (b) A magnified view of the CVs of the membrane. All scans rates were 2 mVs^{-1}.

When the membranes had been formed, potential step experiments were also run to observe their behaviour under constantly applied currents (Figure 3. 5). The resistance and capacitance could also be calculated as separate components from their corresponding regions of the data. The resistance was 66.7 $M\Omega cm^2$, more aligned with the expected value according to the literature. The capacitive component of the membrane is negligible shortly after a potential step and does not influence the resistance calculation, but it may have influenced the previous resistance calculation from the CV data as the potential is a transient variable. The capacitance was calculated to be 0.60 ± 0.047 μFcm^{-2}, similar to the CV analysis.

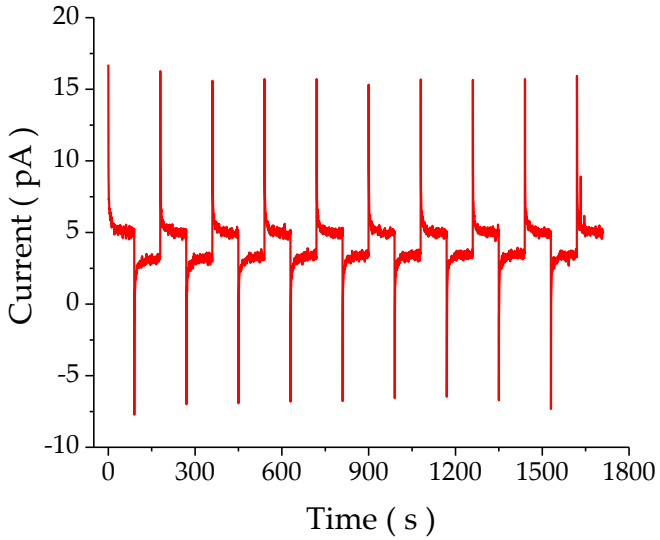

Figure 3. 5 – Typical potential step measurement of the Aperture membranes. Potential steps were alternated between ±80 mV every 90 seconds.

3.2.3 – Natural Ionophore Test: Gramicidin

As discussed in the introduction, there are many different natural ionophores that allow charge to transfer through a bilayer membrane. One of these, gramicidin D, was used to examine whether the membranes formed were appropriate to be used to study interactions with ionophores.

3.2.3.1 – Cyclic Voltammetry

The potential range between which the CVs were measured was reduced from ±40 mV to ±10 mV for the measurements involving gramicidin. As the measurements would be done over a long period of time, this was to reduce the risk of rapid electrode degradation during the measurement in the case of high currents through the circuit. The scan rate was reduced to 1 mVs^{-1}.

With the addition of gramicidin to the aqueous phase, the current began to increase until the membrane ruptured at ~1500 s (Figure 3. 6), the steady increase in conductance of the membrane being caused by the formation of

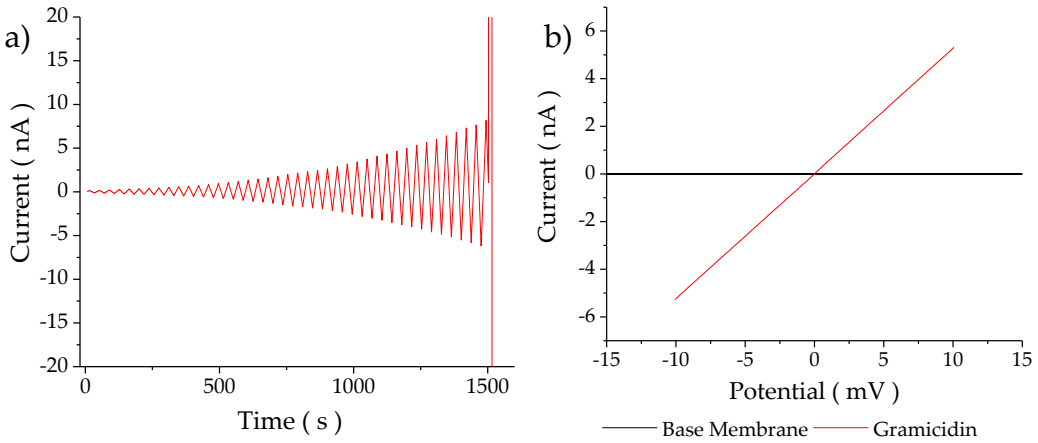

Figure 3. 6 – (a) A continuous CV (I vs t) showing the gradual increase in current as gramicidin channels open, scan range -10 mV to +10 mV and scan rate 1 mVs^{-1}. The membrane breaks at ~1500 s, as seen by the large increase in current. (b) A comparison of the 0.1 M KCl base membrane (black) with the final CV (I vs E) of the gramicidin-loaded membrane (red) before the membrane break occurred.

gramicidin channels. The final CV before the break was compared against the base membrane. The increase in conductance from 233 pS to 526 nS implies that ~43,800 channels were open at the time of membrane rupture, as a gramicidin single-channel conductance is ~12 pS in 0.1 M KCl[14]. Although the membrane broke before the current stabilised, it demonstrated that membrane disruption is a rapid process and can be identified immediately.

3.2.3.2 – Blocking Gramicidin with a Divalent Ion

As discussed in Chapter 1, divalent cations bind too strongly to the binding sites at the entrances of the channels created in the membrane by gramicidin D, blocking them. This prevents other ions and water molecules from diffusing through the pore. As a further test, Ca^{2+} was added to a gramicidin membrane to block it. The membranes were formed using 0.1 M KCl electrolyte solutions, with gramicidin already present in the lipid solution, to remove the need for extra additions that could risk membrane rupture.

The addition of 0.1 M $CaCl_2$ (20 μℓ) on both sides of the membrane directly below the aperture led to an immediate decrease in the current passing through the system (Figure 3. 7), demonstrating the blocking effect of the divalent cation Ca^{2+}. The conductance decrease across the membrane was 4.37 μS, 85% of the original signal. ~364,000 gramicidin channels would have had to have been blocked for this decrease. The area that the gramicidin channels would occupy in the membrane was calculated to confirm that this was a reasonable amount. Each cylindrical gramicidin channel has an outer diameter of 16 Å and so 364,000 gramicidin channels would only constitute ~1.14×10^{-3} % of the entire membrane area[153]. This is entirely reasonable.

As the investigations using gramicidin all returned expected results, the aperture method of membrane formation was established as an electrochemical platform for the AuNP-membrane interactions.

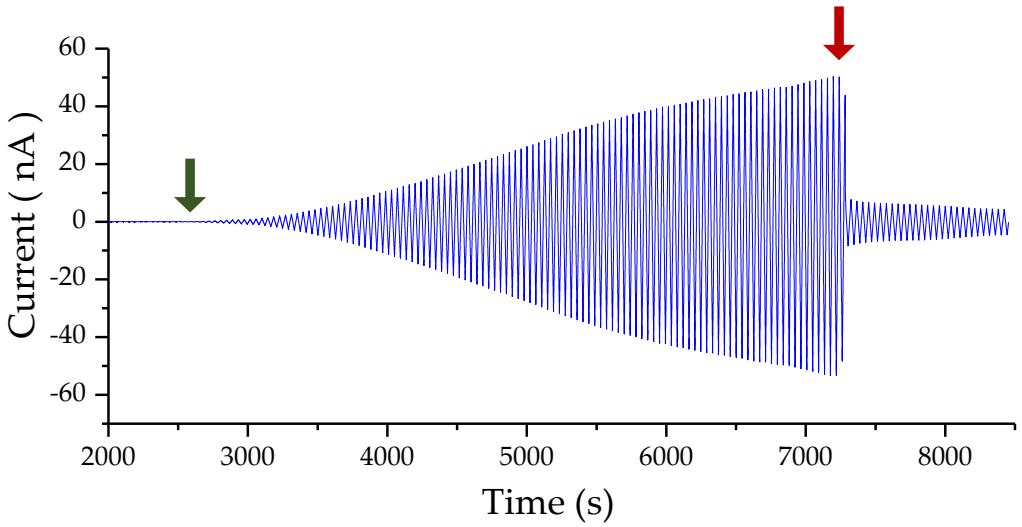

Figure 3. 7 – Continuous CV (I vs t) of a gramicidin-membrane. The membrane forms (green arrow) and the current through the membrane increases as gramicidin starts to dimerise and create channels. An addition of $CaCl_2$ on each side of the membrane occurred at ~7750 s (red arrow) and an immediate decrease in current is seen. The electrolyte solutions prior to the $CaCl_2$ addition were 0.1 M KCl. The scan rate was 1 mVs^{-1} with a potential range of -10 mV to +10 mV.

3.3 – Electrochemical Analysis of the D.I.B. Membranes

3.3.1 – Cell Design

An alternative membrane formation method that produced verifiable membranes was a modification of a D.I.B. system. In a standard D.I.B. membrane, two droplets are suspended on electrodes in an organic phase[128,131,132]. Lipids are dissolved in either the organic bath or in the aqueous droplets and, acting as a surfactant, form a monolayer around the droplets. They are then manoeuvred, using micro-manipulators, so that they come into contact with each other and the bilayer membrane is formed. Whilst

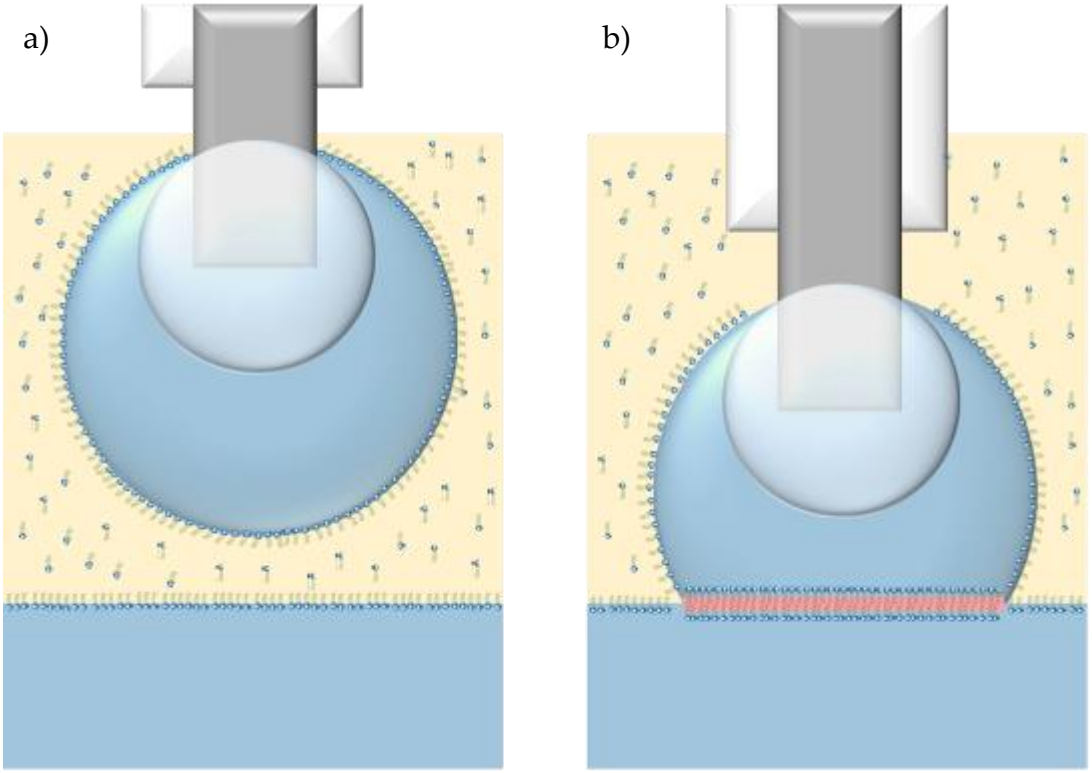

Figure 3. 8 – Membrane formation using a simplified D.I.B. system. Aqueous solutions are in blue, and the lipid solution in yellow. An aqueous droplet is suspended above another aqueous solution using an Ag/AgCl wire (grey) encased in a glass capillary tube (white), with agarose gel acting as an anchor (pale blue circle). (b) The droplet is then lowered through the lipid solutions until a bilayer membrane (red) is formed by contacting the two lipid monolayers formed at each organic-aqueous interface.

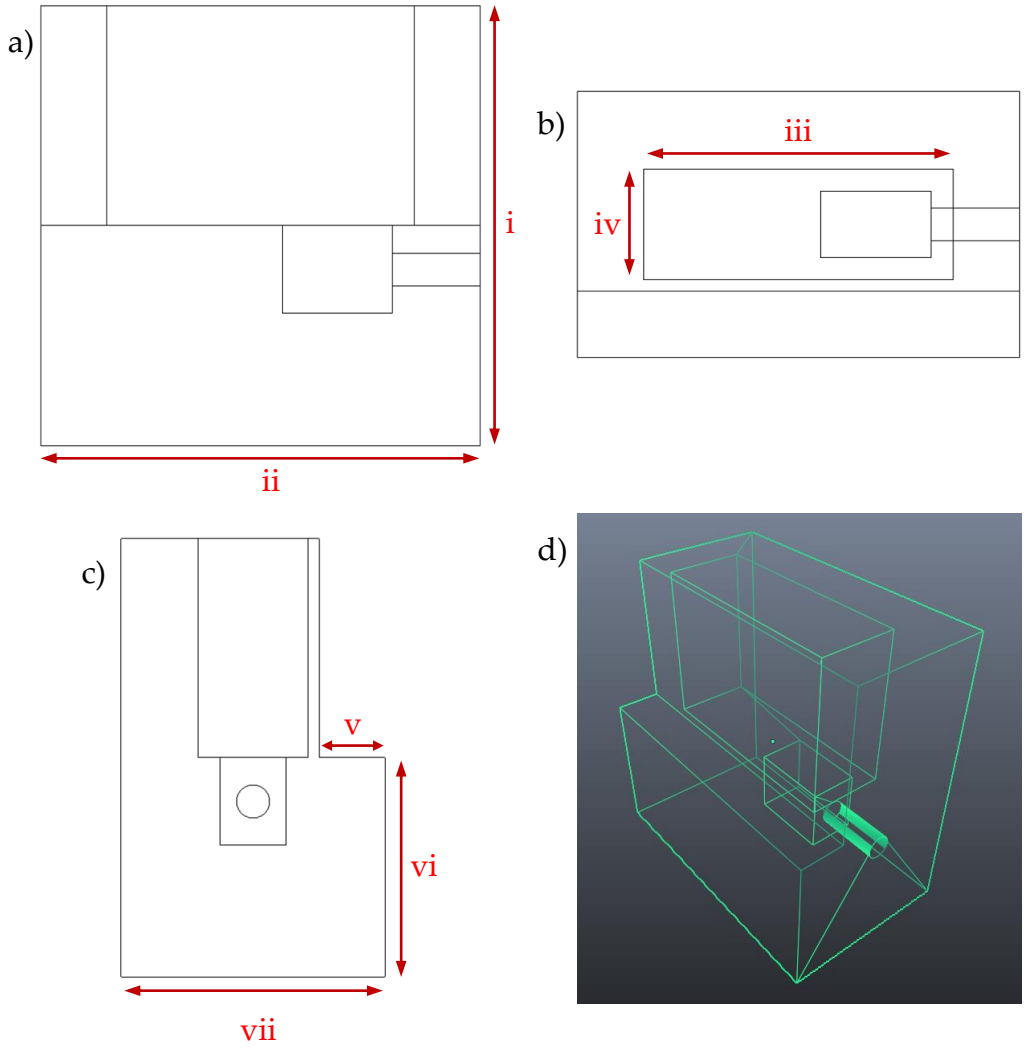

Figure 3. 9 – Design Schematics of the 3D-printed electrochemical cell used in the D.I.B. membrane preparation method. (a) 2D Front view. (b) 2D Top View. (c) 2D Side View (d) Wireframe 3D Model. The dimensions of the D.I.B. cell are as follows: (i) 20 mm (ii) 20 mm (iii) 14 mm (iv) 4 mm (v) 3 mm (vi) 10 mm (vii) 12 mm.

micromanipulators are required to achieve positional control of the droplet, it is much simpler to create the membranes when this equipment is available compared to the aperture membrane formation method. To minimise space and complexity, the system was modified so that only a single micromanipulator was necessary, and bears resemblance to work by Tsofina *et al*[154]. The electrolyte droplet suspended on an electrode was lowered through an asolectin-in-decane solution until it was in contact with a second electrolyte solution (Figure 3. 8).

Rather than an aperture separating two electrolyte reservoirs, one electrolyte solution is contained in the 3D-printed cell, with a lipid solution on top of it (Figure 3. 9). The other electrolyte solution is suspended on a reference electrode above. The design of the cell had an enlarged base so that the entire liquid chamber was raised off the ground to make it easier to see when the droplet had come into contact with the other electrolyte through the decane phase.

Cells conforming to the above were produced using 3D printing techniques explained in Section 2.2.1 and the membrane preparation can be found in Section 2.2.5.

3.3.2 – Base Membrane Behaviour

The D.I.B. membranes were tested using HCl as the electrolyte. CVs were conducted using solutions at pH 1 through 5 and the conductance compared (Figure 3. 10). The expectation was that CVs should not change appreciably when changing the electrolyte concentrations. The conductance of the solutions should be masked by the highly resistive membrane, which should impede the current through the electrical circuit and be the dominant feature in the measurements.

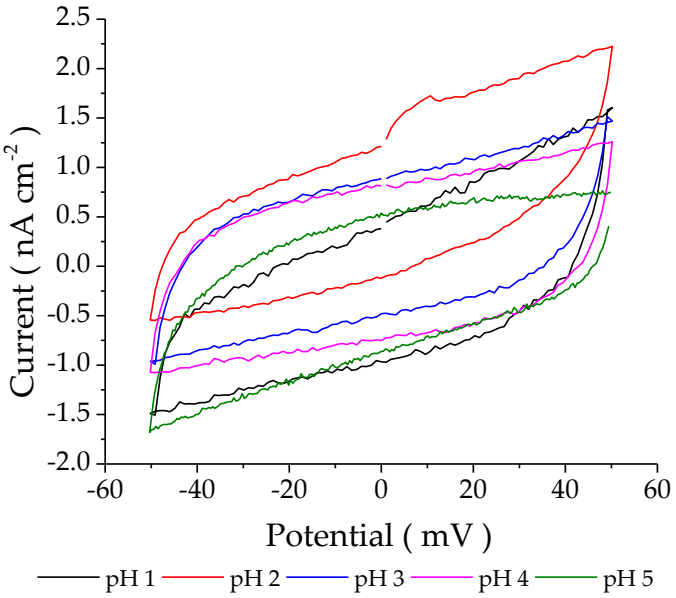

Figure 3. 10 – Base membrane CVs at pH 1, 2, 3, 4 and 5.

The CVs obtained at the various H^+ concentrations showed minimal variance in the conductance values for the different pH membranes (Table 3. 1). The capacitances of the membranes were, on average, 9.18±2.23 nF, which corresponds to a specific capacitance of 0.520±0.126 μFcm^{-2} which is again commensurate with literature membrane values[2,124,137]. The larger deviation in the values of the capacitance of the membranes formed by this method compared to the aperture style is presumed to be a consequence of the lack of membrane area control. As there is no defined space in which the membranes are formed, the area of the membranes can only be estimated. It is calculated from the area of the greater circle of the 4 μℓ droplet. This was $3.05x10^{-2}$ cm^2 and was used for all droplet calculations. The conductance values do not show any significant correlation with the proton concentration of the electrolyte

Table 3. 1 – Conductance and capacitance values for phospholipid membranes at pH 1 to 5.

	pH1	pH2	pH3	pH4	pH5
Conductance (nS cm^{-2})	19.73	20.94	14.22	11.58	15.16
Capacitance (nF)	10.32	9.53	8.96	8.58	11.52

solutions. From this, it was concluded that the membranes were functioning as predicted.

3.3.3 – Natural Ionophore Test: Gramicidin

3.3.3.1 – Cyclic Voltammetry

Gramicidin was, again, used to verify that the membranes could be used for the charge transport experiments. CVs on membranes at pH 1, 2, 3 and 4 were run, and the conductance calculated. The conductance across the D.I.B. membranes increased with the addition of gramicidin for all pHs (Figure 3. 11). With increasing concentration of H^+, the conductance through the membrane increased proportionally to the proton concentration, following the Debye-Hückel-Onsager equation[155]:

$$\Lambda_m = \Lambda_m^0 - (A + B\Lambda_m^0)\sqrt{c} \qquad \text{(Eq. 9)}$$

Where Λ_m is the molar conductivity (S mol^{-1}), Λ_m^0 the limiting molar conductivity (S mol^{-1}), A (S $mol^{½}$ $dm^{-1½}$) and B ($mol^{-½}$ $dm^{1½}$) are constants, and

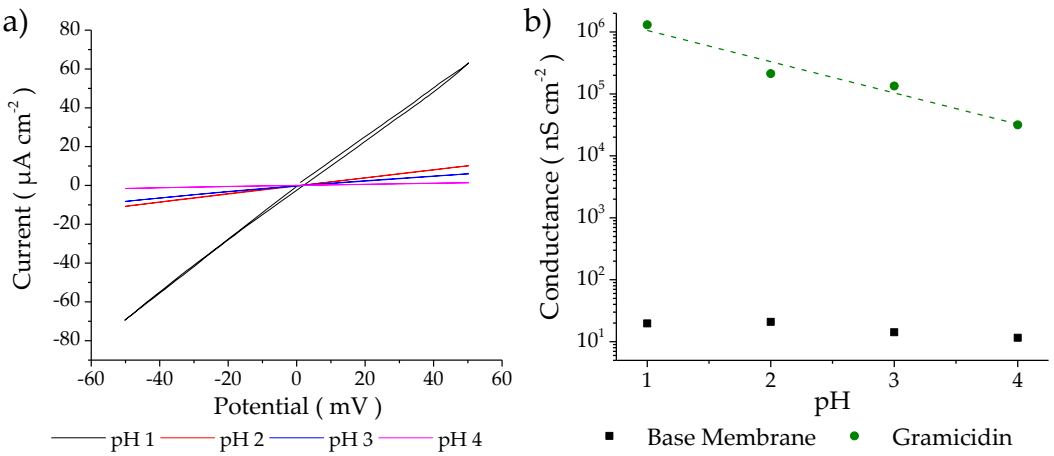

Figure 3. 11 – (a) CVs of gramicidin membranes at pH 1, 2, 3 and 4 using HCl as the acid. (b) A logarithmic plot of the conductance calculated from the gradient of the CVs, comparing base (black) and gramicidin-loaded membranes (green) at pHs 1,2, 3 and 4. The straight line fit for the gramicidin data shows linear proportionality between the conductance and [H^+](green dotted line).

c the electrolyte concentration (mol dm^{-3}). Typically, the direct proportionality between conductance and concentration is usually only valid for low concentrations of strong electrolytes, where $\Lambda_m^0 >> ((A + B\Lambda_m^0)\sqrt{c})$. It has been shown, though, that conductance through gramicidin channels is directly proportional to ion concentration, up to 1 M ion solutions[14].

3.3.3.2 – Zero-Current Potential Study

A second verification method using gramicidin was also performed on D.I.B. membranes. The selective ability for gramicidin to transport only cations and not anions was tested. When the membrane is only permeable to one ion, the zero-current potential should follow the Nernst-Donnan equation (Eq. 6, Section 1.6.3).

The potential of the membrane was measured for several asymmetric membranes by varying the H^+ concentration of the droplet solution, the R.E. 2 side of the membrane (Figure 3. 12) as described in Section 2.4.1.2.

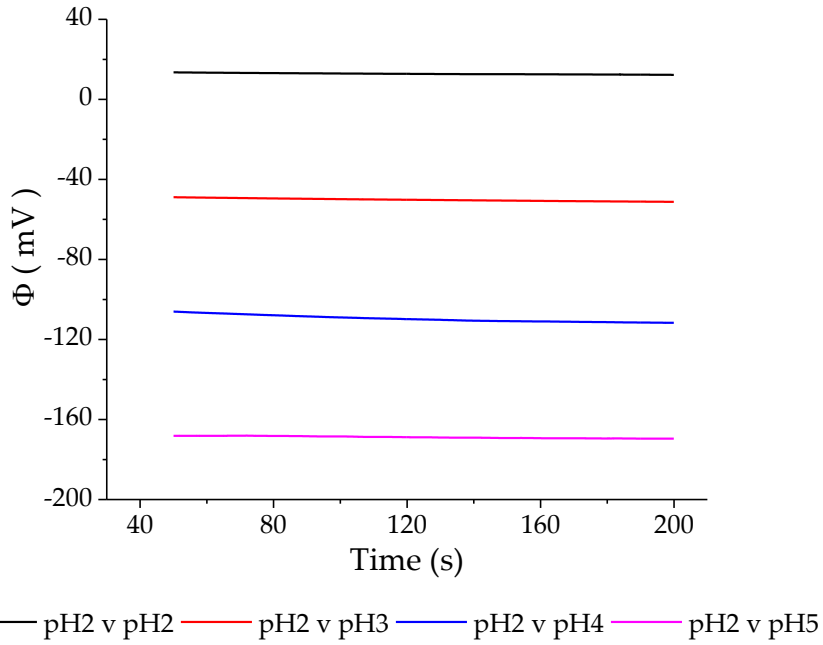

Figure 3. 12 – Zero-current potential measurements for various asymmetric pH-membranes in the presence of gramicidin. As the H^+ concentration decreases on the R.E. 2 side of the membrane, the measured potential of the R.E. 1 side becomes more negative.

The average potential for each membrane was then plotted against $ln\frac{[H]_{R.E.2}}{[H]_{R.E.1}}$ (Figure 3. 13). This type of graph has been coined a "Nernst Plot" throughout the thesis. The gradient of the line of best fit can be used to calculate the experimental charge on the partitioning ion and, for the H^+, was found to be +0.976. This was in accordance with the expected value of +1 for H^+ and meant that the membranes were performing as theory would dictate and could be used for further investigations.

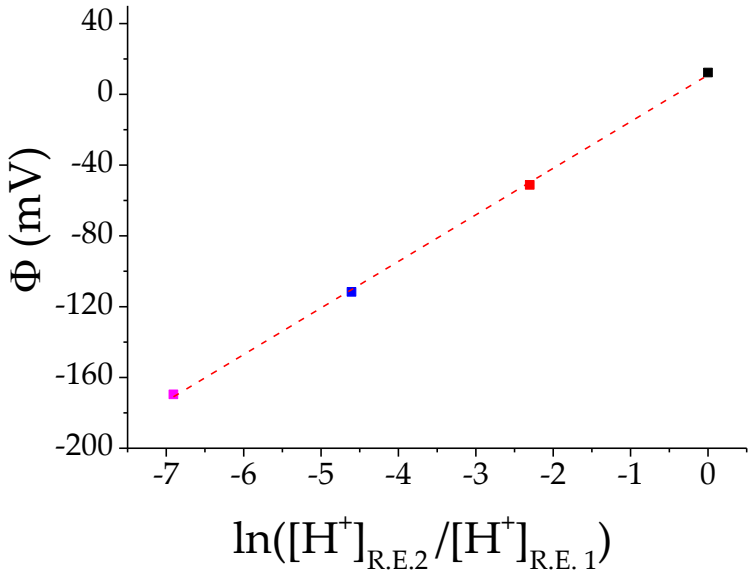

Figure 3. 13 – Nernst plot of the average membrane potential vs the H^+ concentration ratio. As a test, the charge can be calculated from the gradient of the straight line of best fit (red dashed line) and was found to be +0.976, close to the expected value of +1 for H^+.

3.4 – Comparisons between Aperture and D.I.B Membranes

Both methods of membrane formation produced phospholipid bilayers that were able to be electrochemically analysed. The resistance and capacitance of both methods were in accordance with literature values (Table 3. 2)[2,156,157]. The two properties were similar across both devices which was expected as the same lipids and organic solvent were used, although they were lower for D.I.B membranes in both instances.

The capacitance was varied more compared to the resistance of the membranes between the two formation methods. The D.I.B membranes had a lower capacitance compared to aperture membrane, and this is thought to be because of an increased amount of solvent incorporated within the membrane. Solvent-free membranes have a higher capacitance compared to membranes with trapped solvent molecules within them[139]. These solvent molecules disrupt the membrane and increase the width, reducing the capacitance. The formation of the aperture membranes is a slower and more controlled process, and the whole membrane is not formed at once, which should lead to less solvent molecules getting trapped. The formation is also from the bottom of the membrane up, and so the less dense solvent should be able to escape upwards during membrane formation. The D.I.B membranes, however, are formed relatively quickly, and they are formed horizontally. Solvent in the centre of the membrane may not be pushed out upon

Table 3. 2 – Resistance and capacitance of the membranes formed by aperture and D.I.B membranes, with the ranges from literature for reference.

	Aperture Membranes	D.I.B Membranes	Literature Values
Resistance (MΩ cm^2)	67	61	10 – 1000
Capacitance (μF cm^{-2})	0.60	0.52	0.3 - 1

membrane formation, leading to more solvent molecules incorporated in the D.I.B membranes. This would lead to the lower capacitance of the D.I.B membranes.

The standard deviation is also higher for the D.I.B membranes, although this is believed to be due to uncontrolled membrane area size. All of the membranes formed following the aperture method were constrained by the aperture itself. There is no set area for the membrane to form using D.I.B cells, and the membrane area could be affected by multiple factors, such as the shape of the agarose gel anchor.

Unlike the membranes prepared using the Aperture method, the zero-current potential for D.I.B membranes was not constant across all devices when transporters were not present. This can be seen from the CVs in Section 3.3.3.1: pH2 was measured on one device, pH1 and 5 were using a different device, and pH3 and 4 were run on another. The difference in zero-current potentials across devices means that potential measurements can only be compared for experiments that were run on the same device, using the same electrode pair.

Although not definitive, the proposed rationale currently is that the non-identical environment of the suspended electrode across devices causes this issue. It was almost impossible to prepare identical agarose gel anchors on the suspended electrode; the coverage and volume was different for each electrode prepared. This is not the case for the chamber electrode, or the two electrodes used in the preparation of the aperture membranes.

3.5 – Chapter 3 Conclusions

The formation and testing of phospholipid membranes prior to AuNP experiments was imperative, as well as testing the ink-wire Ag/AgCl reference electrodes. The electrodes performed to a satisfactory standard, although not as stable as commercial variants.

Two methods of membrane formation, the Aperture and D.I.B. methods, were verified using gramicidin, a natural ionophore. Each method produced membranes with capacitance and conductance values in accordance with other literature. The aperture method produced membranes that were robust with consistent capacitance and resistance. However, in practise, their preparation proved delicate and time-consuming, and it was not possible to perform the number of experiments necessary within the allotted time.

The D.I.B. method was designed to allow more rapid changing of solutions and for easier asymmetric membrane comparisons. The drawback of using the D.I.B.s was that zero-current potentials varied across devices, and potential comparisons could only be done on measurements run on the same device. The D.I.B. method was used to produce membranes with both carb-AuNPs and crown-AuNPs.

With two electrochemical platforms now finalised, the study of AuNP interactions with the membrane could now begin.

Chapter 4 – Ion-Selective Transport via Carborane-Functionalised AuNPs

Having established an electrochemical platform to investigate phospholipid bilayer membrane interactions, incorporating functionalised AuNPs was now possible. This chapter will focus on 2-3 nm AuNPs that have been functionalised with a mercapto-carborane ligand (carb-AuNPs) as described in Section 2.3.1. These carb-AuNPs had shown promise in regard to ion storage and switchable hydrophobicity in past research[148].

Results from an electrochemical study of the carb-AuNPs using a variety of different cations will be presented. The conductance through the membrane upon the addition of the carb-AuNPs, calculated from potential step analysis will be established and the relative selectivity of the AuNPs for each of the ions, calculated based on the permeability of the membrane to each ion, will also be discussed. A section of the work in this chapter has contributed to an article published in ACS Nano (M. P. Grzelczak, S. P. Danks, R. C. Klipp, D. Belic, A. Zaulet, C. Kunstmann-Olsen, D. F. Bradley, T. Tsukuda, C. Viñas, F. Teixidor, J. J. Abramson and M. Brust, *ACS Nano*, 2017, **11**, 12492–12499)[158]

The ability of the carb-AuNPs to self-partition across the membrane, polarising the membrane will be investigated and the charge on the carb-AuNPs in different electrolytes was estimated based on these measurements.

4.1 – Mercapto-carborane-AuNPs

Carborane has an icosahedral structure with the molecular formula $C_2B_{10}H_{12}$ (Figure 4. 1). Carborane exhibits the usual structural isomers ortho-, meta- and para-, referencing where the carbon atoms are in the structure, relative to each other. The ortho-carborane – where the carbon atoms are adjacent to each

other in the structure – was the only variant used in this study, and any reference to carborane from here on will be referencing the ortho-carborane molecule.

For use as a ligand for AuNP synthesis, a thiol group can be added as a functional group to one of the carbon atoms[146]. As ligands, the mercaptocarborane molecules are thought to be densely packed together, more so than usual alkane-thiol ligands, due to hydrogen bonding between rigid structures, and thermo-gravimetric analysis has been used to estimate that for 2 nm core sized AuNPs, there are 0.6 carborane ligands for every gold atom (surface and core). The icosahedral structure of the mercapto-carborane molecule means that, even with a close-packing array of the ligands on the gold surface, there are inevitably gaps in the ligand shell, and these gaps allow ions which are small enough to flow into the core-shell "voids" – the space created between the Au core and the carborane ligands. Further reduction of the AuNP is possible, which causes the core to become negatively charged, at which point cations are attracted to the negatively charged core and enter the

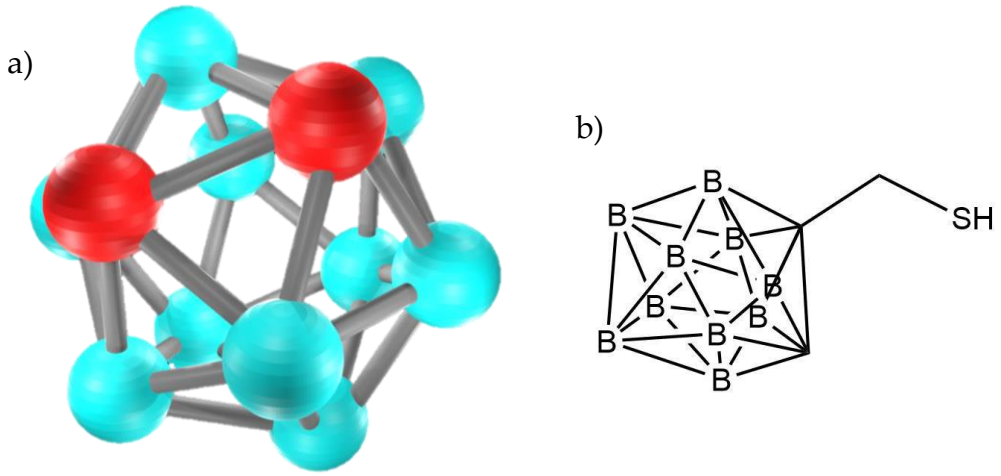

Figure 4. 1 – (a) Ball and stick structure of ortho-carborane, with the hydrogen atoms ignored for clarity. The carbon atoms are the red spheres, and the boron atoms are the blue spheres. (b) Structure of mercapto-carborane, with the hydrogen on the atoms forming the icosahedra omitted for clarity.

voids. This has been shown by Li nuclear magnetic resonance spectroscopy. It has been shown that the carb-AuNPs have the ability to reversibly switch between hydrophobic and hydrophilic behaviour, depending on the number of ions in the core-shell voids[148] (Figure 4. 2). When the particles have many cations loaded in the shell, the carb-AuNPs are hydrophilic and are dispersible in water. Conversely, when the carb-AuNPs are loaded with many cations, they become hydrophobic. When hydrophobic, the carb-AuNPs also have the ability to go into biological cells and position themselves in the phospholipid bilayer of the cells. Due to these characteristics, it was thought that they had the potential to act as ionophores.

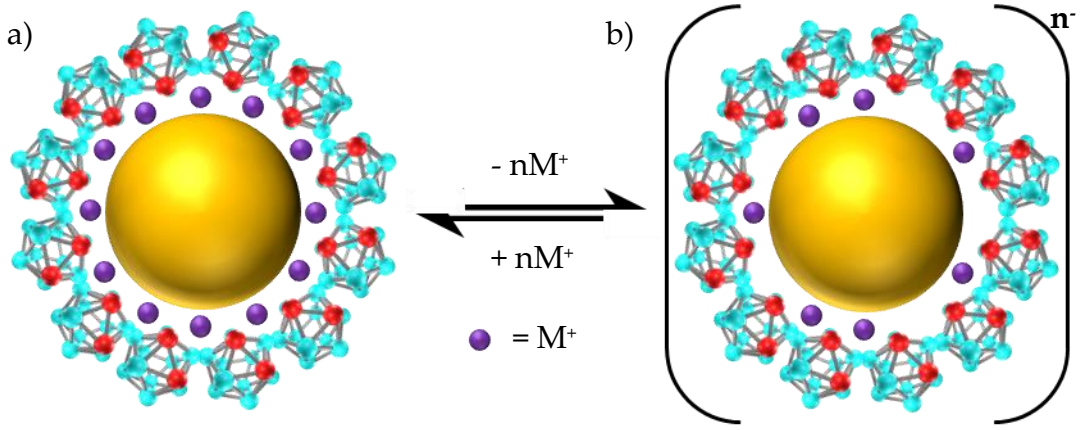

Figure 4. 2 – The carb-AuNPs exhibit reversible hydrophobicity. (a) The hydrophobic uncharged complex to (b) the hydrophilic poly-anion. The thiol-linkages between the mercapto-carborane and the AuNP have been removed for clarity.

4.2 – Carb-AuNPs as Ionophores

It had been identified using vesicle-based fluorometry experiments, that the carb-AuNPs have the ability to generate a membrane potential when the AuNPs are only on one side of the membrane[158]. They also generate potentials when an electrochemical gradient is present for either Na^+ or K^+. They do not, however, seem to interact with Mg^{2+}. The study was also able to identify that the carb-AuNPs were able to depolarise a membrane that had been initially polarised by the inclusion of a natural ionophore in the vesicle membranes, such as gramicidin or valinomycin.

The investigation presented here was run to study the carb-AuNPs under potentiometric control, with the added benefit of being able to incorporate them on both sides of the membrane, which is not possible for vesicle experiments. The main study of the carb-AuNPs undertaken was a set of potential step experiments, changing the cations present on either side of the membrane to see whether the currents through the membrane were affected by the different cations. The procedure followed is in accordance with Section 2.4.1.3; the base membranes were subject to symmetric and progressive stepping measurements first to establish a baseline, and this was followed by the addition of the carb-AuNPs and a second set of symmetric and progressive stepping measurements.

The contribution to the current of the anion used in the preparation of the membranes studied, Cl^-, was assumed to be negligible for two reasons. Firstly, Cl^- has the largest ionic size of all the ions used in this study (see Table 1. 1), including Cs^+ and considering minimal current was seen attributed to Cs^+ it was thought to be unlikely that Cl^- ions would be able to enter the voids. Secondly, it is negatively charged, and unlike the cations, it should be repelled by the negatively charged carb-AuNPs.

Throughout this section, except for the first measurement, the current (y-axis) has been cropped for clarity of the residual currents in all the applicable figures presented; the capacitive current observed at the beginning of each potential step was not of interest for this particular part of the study and is not entirely shown in most instances.

4.2.1 – Symmetric Membranes using Na^+ and K^+

As referred to above, it has been identified that the addition of the carb-AuNPs could facilitate a potential across a membrane when Na^+ and K^+ were present on one side of the membrane, and also depolarise a membrane that had been already polarised by valinomycin, a natural ionophore. This led us to believe that by using these ions on either side of the membrane, ion transport across the membrane would be observed as an increase in the current through the system.

For the first experiment, a simple, symmetric membrane was formed using 100 mM NaCl on both sides of the membrane and, once the baseline had been established, carb-AuNPs were added on both sides of the membrane. The addition of the carb-AuNPs caused an increase in the current flowing through the membrane, with an increase in current of 7.98 $nAcm^{-2}$ when R.E.1 was polarised to +80 mV and 7.23 $nAcm^{-2}$ when polarised the opposite way (-80 mV) compared to the standard membrane (Figure 4. 3). The progressive stepping experiment was then used to observe how the current changed with potential; for example, did the current follow Ohm's law and behave like a traditional ionophore like valinomycin and gramicidin? Or was there a potential below +80 mV where the carb-AuNPs become activated and an increase in current was only seen once this potential had been reached like a voltage-gated channel? From the results shown in the graph (Figure 4. 4), the

current did not have an activation potential, and the current was increased for all potential steps (except for the 0 mV applied potential).

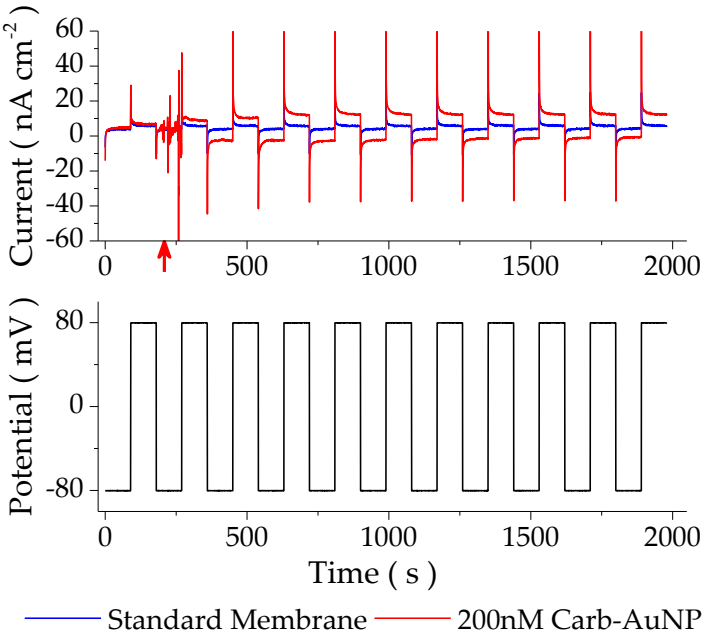

Figure 4. 3 – Top: Symmetric stepping experiment of a Na^+ vs Na^+ membrane comparing the current before (blue) and after (red) an addition of carb-AuNPs. The AuNP addition occurred at around 230 s, indicated by the red arrow. Bottom: The potential-trace from the same experiment.

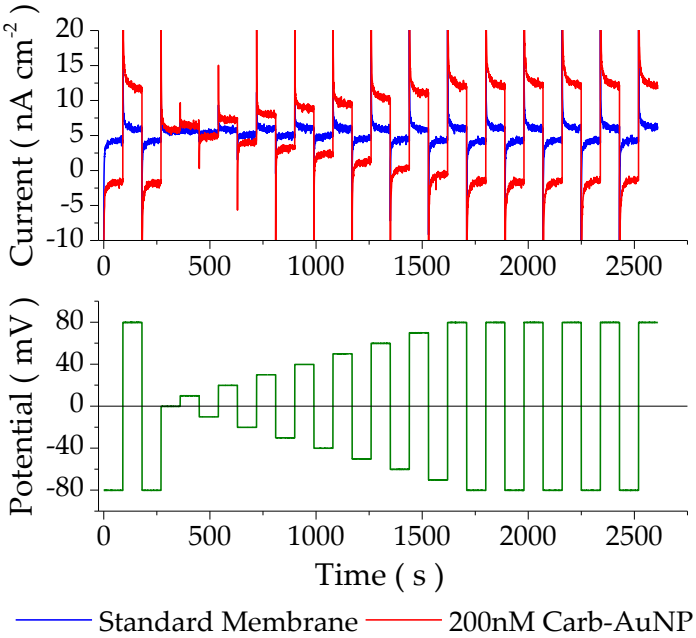

Figure 4. 4 – Top: Progressive stepping experiment on the Na^+ vs Na^+ membrane, comparing the current through the system before (blue) and after (red) the addition of carb-AuNPs. Y-axis cropped to show resistive currents more clearly. Bottom: The potential trace of the same experiment (green).

Analysis of a K^+ vs K^+ membrane was carried out next, to see whether the change in the cation species had an effect on the induced current through the system. The experiment was repeated but using 100 mM KCl on both sides of the membrane. The current generated when the carb-AuNPs were added was considerably lower than that of the Na^+ vs Na^+ membrane for the symmetric and progressive stepping experiments (Figure 4. 5 and Figure 4. 6, respectively) with the increase in conductance through the membrane caused by the addition of the carb-AuNPs being only 1.64 $nAcm^{-2}$ and 1.78 $nAcm^{-2}$ at +80 mV and -80 mV respectively, approximately one-fifth of the increase in current through the Na^+ vs Na^+ membrane.

It is hypothesised that the lower current measured through the membrane is likely to be due to a difference in the number of ions that are able to be transported at one time. A lower current through the circuit could mean that fewer ions are travelling through the membrane. If the space inside the core-

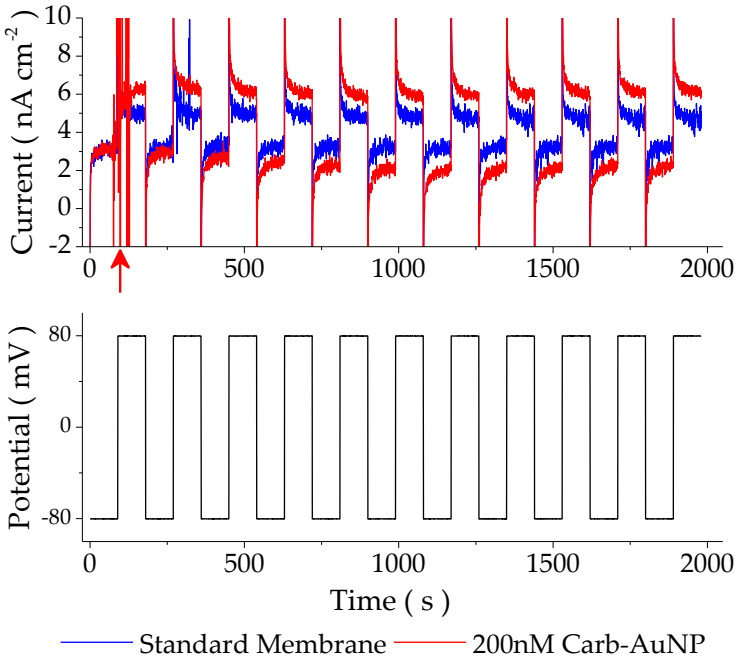

Figure 4. 5 – Top: Symmetric stepping experiment of a K^+ vs K^+ membrane comparing the current before (blue) and after (red) an addition of carb-AuNPs. The AuNP addition occurred at around 100 s, indicated by the red arrow. Y-axis cropped to show resistive currents more clearly. Bottom: The potential-trace of the same experiment.

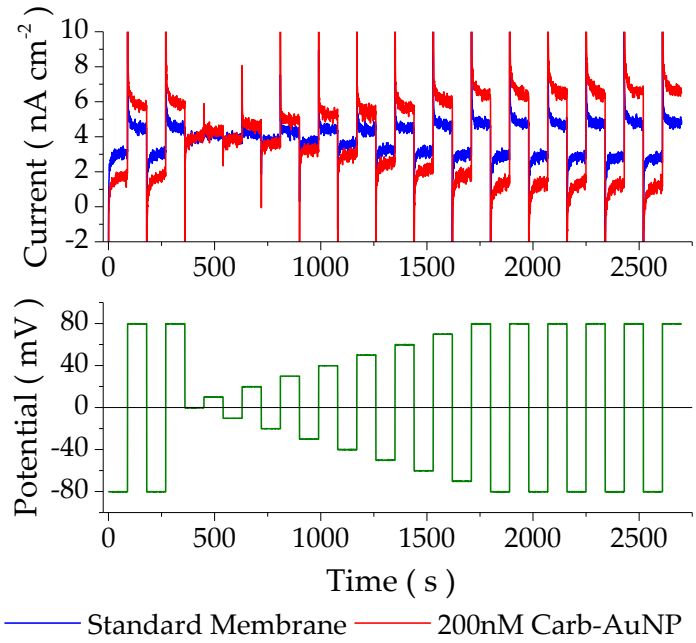

Figure 4. 6 – Top: Progressive stepping experiment on the K^+ vs K^+ membrane, comparing the current through the system before (blue) and after (red) the addition of carb-AuNPs. Y-axis cropped to show resistive currents more clearly. Bottom: The potential trace of the experiment (green).

void shells is what dictates the number of ions that can be carried, then it should be dependent on the size of the ions involved, which is dependent on whether the ions are hydrated or not. Given that a lower current is seen for K^+ compared to Na^+, it suggests that the ions in the voids do not have a hydration shell as K^+ has a larger ionic radius compared to Na^+ without a hydration shell but it is smaller than Na^+ with a hydration shell (Table 1. 1). This suggest that the ionic radius without the hydration shell is a significant factor in the magnitude of the current passing through the circuit.

From the progressive stepping measurements, it is possible to create an I vs E graph, which can then be used to calculate the increase in conductance through the membrane due to the carb-AuNPs. The baseline currents are subtracted from the currents measured after the addition of the carb-AuNPs. The average current at each potential is then plotted versus said potential to create the I vs E graphs.

The I vs E graphs of both the Na^+ membrane and the K^+ membrane show near-linear behaviour confirming adherence to Ohm's law (Figure 4. 7). This suggests that the carb-AuNPs are not "activated" like a ligand- or voltage-gated ionophore. As the currents follow Ohms law, the increase in conductance through the membrane due to the addition of the carb-AuNPs can be calculated from the gradient of the line of best fit. The values for the Na^+ and K^+ membranes were 74.6 nS cm^{-2} and 19.8 nS cm^{-2}, respectively.

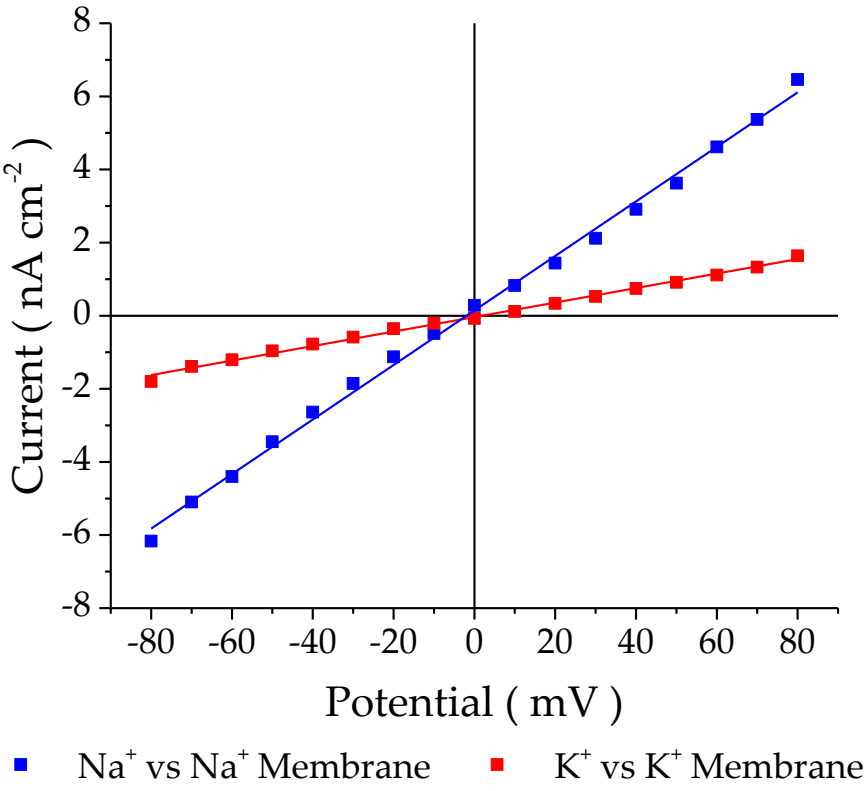

Figure 4. 7 – I vs E graphs of the symmetric Na^+ membrane (blue) and the symmetric K^+ membrane (red). Using Na^+ leads to a higher current through the membrane compared to K^+. Straight lines have been fitted to the data to show ohmic behaviour for both of the Na^+ (blue line) and K^+ (red line) symmetric membranes.

4.2.2 – Electrochemical Gradient Study

4.2.2.1 – Na^+ vs K^+

Having seen how the carb-AuNPs interacted with the Na^+ and K^+ symmetrical membranes, a Na^+ vs K^+ membrane was studied to observe how an electrochemical chemical gradient affected the current generated by the addition of the AuNPs (Figure 4. 8). Upon the addition of AuNPs to the solutions on both sides of the membrane, a steady rise in the current passing through the system was seen (Figure 4. 9), taking more time to stabilise than the previous symmetric membranes and eventually stabilising around 900 s after the addition. This was due to a change in the position where the AuNPs were added. Rather than add the carb-AuNPs directly under the membranes, as done in the above measurements, the particles were added on the other side of the reservoir chamber, further away from the membrane. This was to observe whether the initial spike in the current seen during the addition process could be reduced, slowing the degradation of the reference electrodes. This did not affect the current spike upon addition but meant that the carb-AuNPs had to diffuse towards the membrane from further away, and so this change was reverted for experiments following this one. The increase in current compared to the standard membrane during the last potential steps was found to be 9.60 $nAcm^{-2}$ (3.s.f) when the R.E. 1 was polarised to +80 mV and 13.9 $nAcm^{-2}$ (3.s.f) when it was -80 mV (Figure 4. 10).

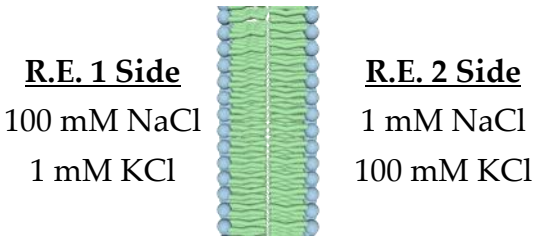

Figure 4. 8 – Experimental set-up of a Na^+ vs K^+ membrane, showing the concentrations of each chloride-salt on both sides of the membrane.

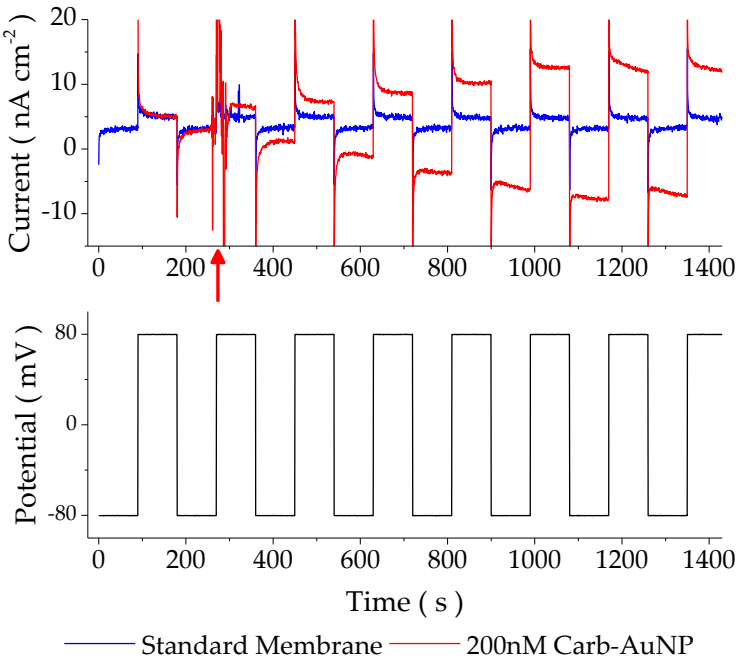

Figure 4. 9 – Top: Symmetric stepping experiment of a Na^+ vs K^+ membrane comparing the current before (blue) and after (red) an addition of carb-AuNPs. The AuNP addition occurred at around 270 s, indicated by the red arrow. Y-axis cropped to show resistive currents more clearly. Bottom: The potential-trace from the same experiment.

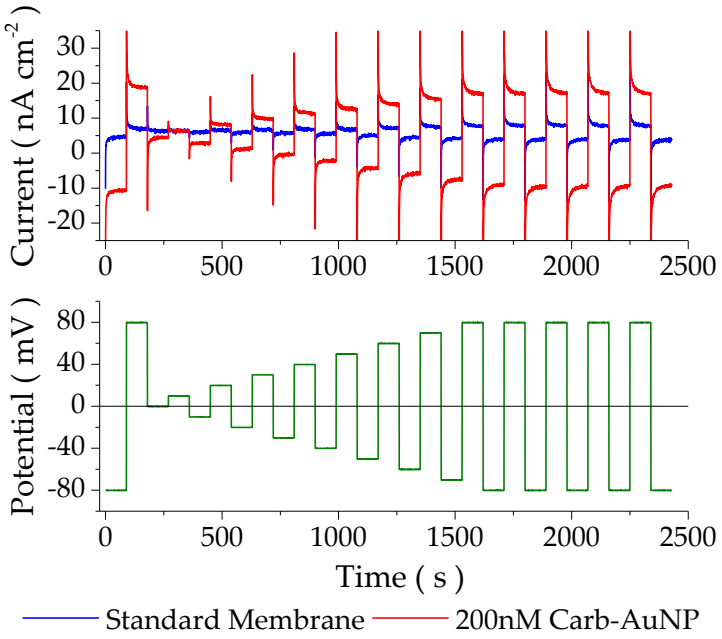

Figure 4. 10 – Top: Progressive stepping experiment on the Na^+ vs K^+ membrane, comparing the current through the system before (blue) and after (red) the addition of carb-AuNPs. Y-axis cropped to show resistive currents more clearly. Bottom: The potential trace of the same experiment (green).

The difference between the increases in current arising from different polarisations of R.E. 1 can give an indication of which ion is preferentially transported. The larger increase in current occurring when the applied potential of R.E.1 is negatively polarised, which would encourage K^+ to be transported across the membrane down its concentration gradient, would indicate that the AuNPs are more selective to K^+ compared to Na^+. Considering the Na^+ vs Na^+ membrane gave a much higher conductance through the membrane than the K^+ vs K^+ membrane, the selectivity for K^+ is surprising, and some rationales for this behaviour are proposed in Section 4.2.2.5.

The I vs E graph (Figure 4. 11), is a straight-line graph as in the previous experiments, confirming adherence to Ohm's law, and thus the conductance through the membrane can be calculated from the gradient of the line. For the Na^+ vs K^+ membrane, the increase in conductance after addition of the carb-AuNPs compared to the base membrane was found to be 150 nScm-2. This was over one and a half times higher than that of the increase in conductance from both the Na^+ vs Na^+ membrane and the K^+ vs K^+ membrane combined (94.4 nScm-2), indicating that the chemical gradient across the membrane is enhancing the transport of charge across the membrane. The increase in conductance due to the chemical gradient in the Na^+ vs K^+ membrane, with the same amount of carb-AuNPs in the membrane, could suggest that there are points in the transport mechanism that allow for the diffusion of the ions freely through the membrane and, as it is entropically favourable due to the concentration gradients, lead to the higher conductance. This would mean that the AuNPs are creating a pathway for the ions to move through the membrane much like the standard ionophores such as gramicidin and valinomycin, where the charged carb-AuNPs are not the only contributors to the current through the membrane.

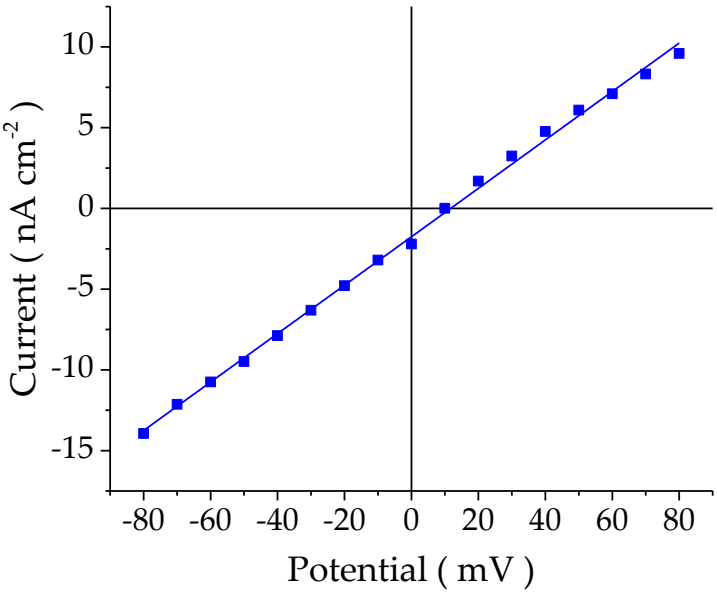

Figure 4. 11 – I vs E graph of the Na^+ vs K^+ membrane, showing the current generated by the carb-AuNPs, with a straight line fitted to the data. The membrane zero-current potential has been shifted to +11.7 mV (3.s.f.), indicating the carb-AuNPs are more selective to K^+ than Na^+.

4.2.2.2 – Na^+ vs Cs^+

The two ions, K^+ and Na^+, are relatively similar in size with K^+ being slightly larger. To see whether the size of the ion was an important factor as hypothesised, K^+ was replaced with Cs^+, a larger ion. By comparing Na^+ and Cs^+, it could be expected that the transport of the ions would be much more asymmetric across the membrane.

Accordingly, membranes were formed using NaCl and CsCl solutions (Figure 4. 12). In this case, when the potential was set at -80 mV – the polarity that would encourage the transport of Cs^+ down its concentration gradient, there was little increase in current through the membrane (Figure 4. 13). However, the increase in current at +80 mV, associated with the transport of the Na^+ down its concentration gradient, is at a similar level measured for the same current in the Na^+ vs K^+ membrane at around 10 $nAcm^{-2}$. Such a low increase in current when the membrane was polarised to enhance Cs^+ transport through the system suggests that the Cs^+ was barely transported.

The progressive stepping data shows a large shift towards higher currents at the smaller applied potentials. It requires a relatively large potential to cause positive charge to flow from the Cs^+ side of the membrane to the Na^+ side (Figure 4. 14). This suggests that Cs^+ transport is highly unfavourable compared to Na^+ transport. It is maybe surprising that transport attributed to Na^+ ions transferring towards the Cs^+ side still occurs when the potential

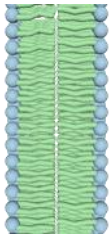

Figure 4. 12 – Experimental set-up of a Na^+ vs Cs^+ membrane, showing the concentrations of each chloride-salt on both sides of the membrane.

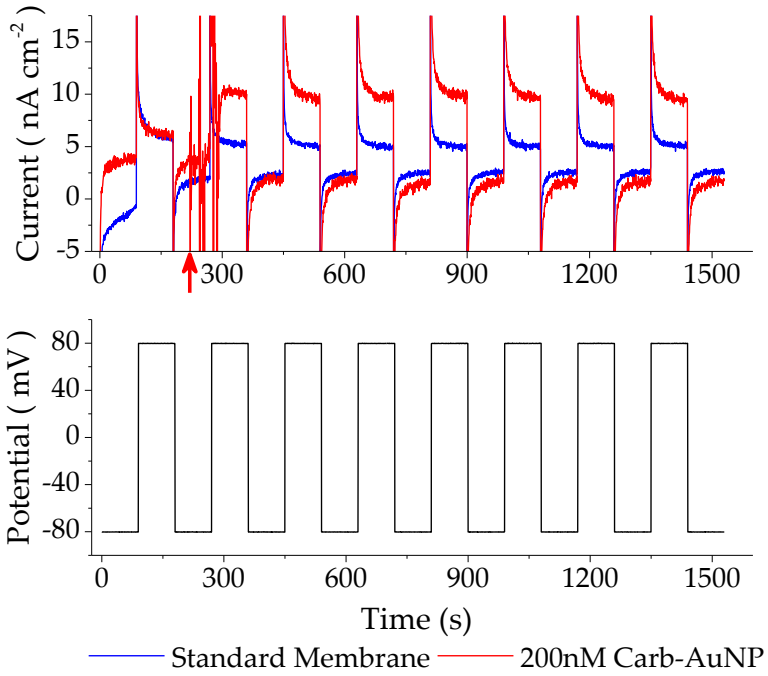

Figure 4. 13 – Top: Symmetric stepping experiment of a Na^+ vs Cs^+ membrane, comparing the current before (blue) and after (red) the addition of carb-AuNPs. The AuNP addition occurred at around 210 s, indicated by the red arrow. Y-axis cropped to show resistive currents more clearly. Bottom: The potential-trace of the same experiment.

applied would hinder said transfer. The currents at -10 and -20 mV are still more positive than those for the baseline membrane. When a potential of 0 mV is applied to the system, more current flows through the system compared to the base membrane as well. This suggests that the zero-current potential of the membrane has been shifted to a more negative potential, which then implies that the membrane is more permeable to Na^+ compared to Cs^+.

The conductance of the membrane from the I vs E graph was calculated to be 45.7 $nScm^{-2}$, which is considerably lower than even the Na^+ vs Na^+ membrane (Figure 4. 15). Surprisingly, the Na^+ electrochemical gradient did not have an effect large enough to enable increased transport. The large Cs^+ ions may be slowing down the process of ion transfer into and out of the core-shell voids, reducing the current flow.

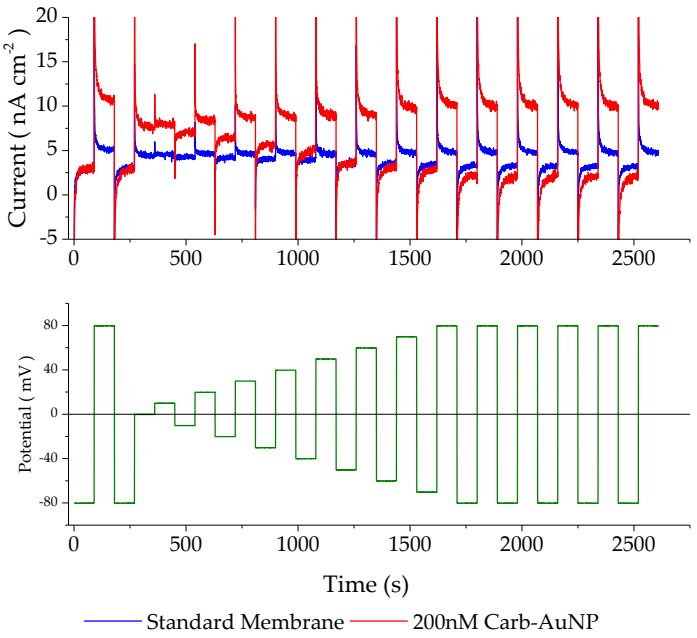

Figure 4. 14 – Top: Progressive stepping experiment on the Na^+ vs Cs^+ membrane, comparing the current through the system before (blue) and after (red) the addition of carb-AuNPs. Y-axis cropped to show resistive currents more clearly. Bottom: The potential trace of the same experiment (green).

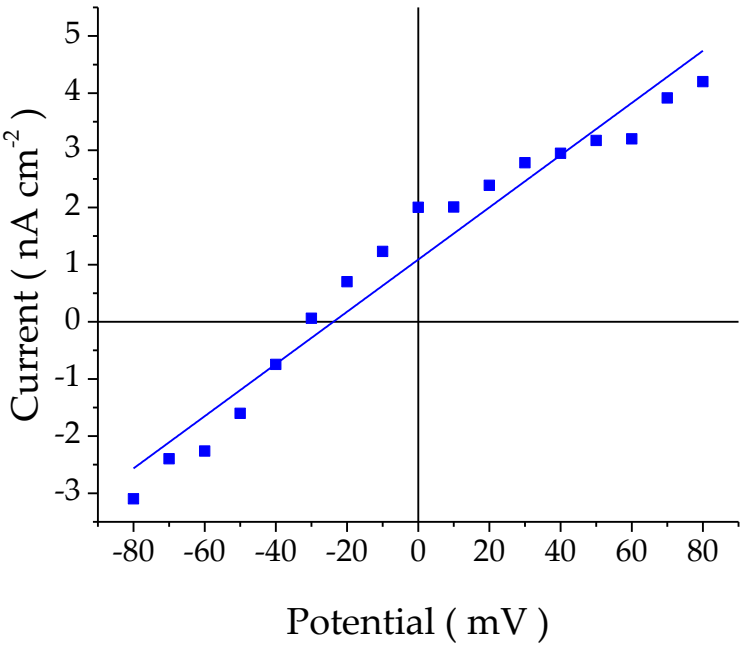

Figure 4. 15 – I vs E graph of the Na^+ vs Cs^+ membrane, showing the current generated by the carb-AuNPs, with a straight line fit of the data. The membrane zero-current potential has been shifted to -23.8 mV (3.s.f.), indicating the carb-AuNPs are more selective to Na^+ than Cs^+.

4.2.2.3 – Li^+ vs Cs^+

Based on the previous experiments, where Na^+ is shown to be transported much more than Cs^+, the size of the ions was deemed an important factor in the current generated by the addition of the carb-AuNPs. Due to the proposed transport mechanism of the carb-AuNPs, which is limited by the core-shell voids of the particles, it was reasoned that using the smallest ion would give larger conductance through the membrane as a larger number of them could be held within the voids. A membrane was formed using Li^+, the smallest alkali metal ion, and Cs^+, the largest available alkali metal ion, as the two cationic species and the stepping and progressive stepping experiments were studied (Figure 4. 16).

The addition of the carb-AuNPs to the solution caused the current corresponding to Li^+ being transported favourably to increase dramatically, increasing to >20 $nScm^{-2}$ just after the carb-AuNP addition, whilst the Cs^+ transport current increased only slightly (Figure 4. 17). The increase corresponding to the Cs^+ current is higher for this membrane than for Na^+ vs Cs^+. It could be that a proportion of the Cs^+ current generated is actually due to the small concentrations of Li^+ (or Na^+ in the experiments in Section 4.2.2.2), implying that transport due to Cs^+ was maybe even less than previously thought.

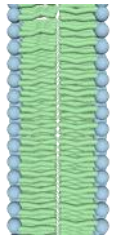

Figure 4. 16 – Experimental set-up of a Li^+ vs Cs^+ membrane, showing the concentrations of each chloride-salt on both sides of the membrane.

It can be seen that immediately after the addition, relatively little current is produced when R.E.1 is polarised negatively, which would encourage Cs^+ transport down the concentration gradient. After a period of time, however, the additional current does start to increase. This may be due to the other ion, Li^+ in this case, slowly equilibrating between the two solutions and after a period of time had passed, the concentration of Li^+ was large enough on the Cs^+ side of the membrane to contribute a significant amount of current (Figure 4. 18).

The progressive stepping experiment showed that the entire stepping profile had been shifted to more positive current measurements, much like the Na^+ vs Cs^+ membrane before, but the shift in the membrane zero-current potential

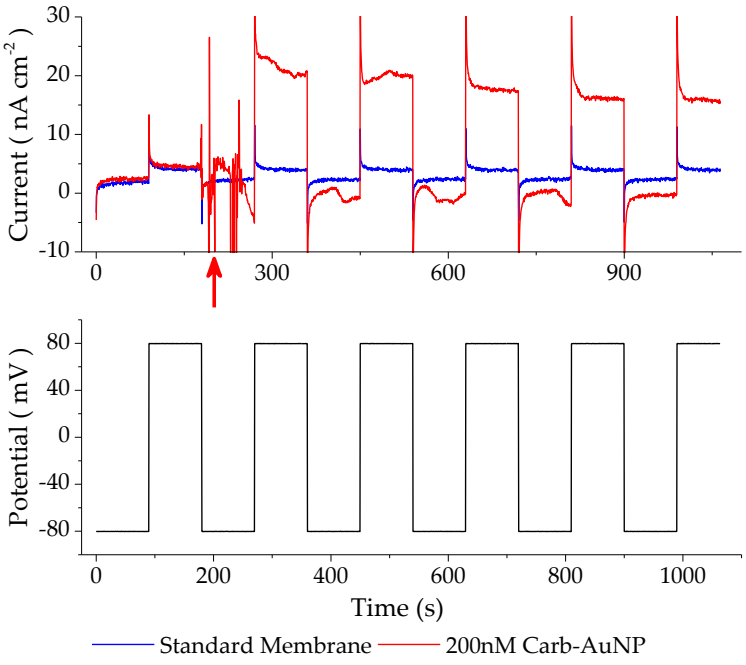

Figure 4. 17 – Top: Symmetric stepping experiment of a Li^+ vs Cs^+ membrane, comparing the current through the system before (blue) and after (red) the addition of carb-AuNPs. The AuNP addition occurred at around 200 s, indicated by the red arrow. Y-axis cropped to show resistive currents more clearly. Bottom: The potential trace of the same experiment.

was the highest that had been seen so far, with the Li^+ vs Cs^+ membrane differential being -35.19 mV (Figure 4. 19).

Directly comparing these results with those for Na^+ vs Cs^+, it can be seen that the current through the membrane caused by the addition of the carb-AuNPs is much larger for the Li^+ vs Cs^+ membrane than for the Na^+ vs Cs^+ membrane, and this was the case as the conductance calculated from the I vs E graph was 78.8 $nScm^{-2}$. This is in keeping with the provisional theory that the current is dependent on the size of the ions, in that more ions of smaller size are able to enter the core-shell voids, leading to greater transport of charge.

Although the Li^+ vs Cs^+ membrane has a higher conductance compared to the Na^+ vs Cs^+, the conductance is still not as high as the Na^+ vs K^+ experiment. This suggests that the high conductance seen in the Na^+ vs K^+ experiment is down to the fact that both species are able to transfer well and do not inhibit each other.

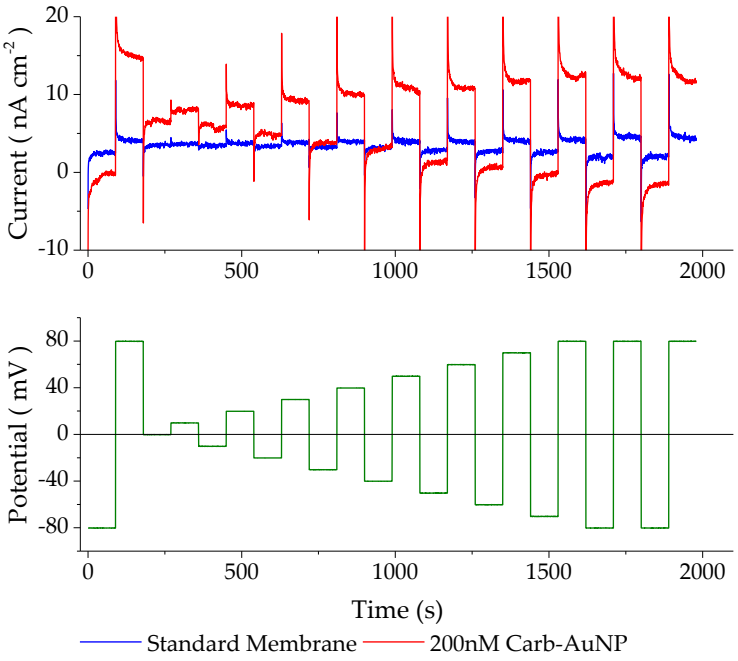

Figure 4. 18 – Top: Progressive stepping experiment of the Li^+ vs Cs^+ membrane, comparing the current through the system before (blue) and after (red) the addition of carb-AuNPs. Y-axis cropped to show resistive currents more clearly. Bottom: The potential trace of the same experiment (green).

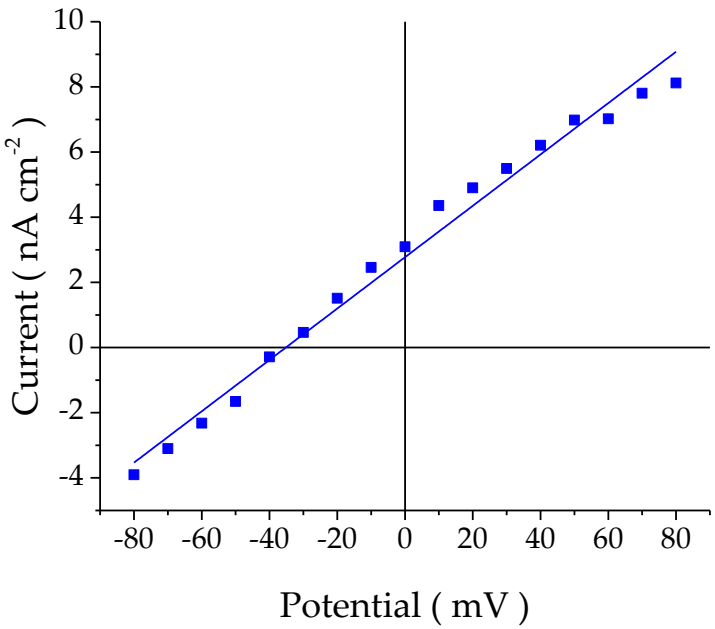

Figure 4. 19 – I vs E graph of the current generated by the carb-AuNPs for the Li^+ vs Cs^+ membrane, with a straight line fitted to the data. The zero-current membrane potential has been shifted to -35.2 mV (3.s.f.), indicating the carb-AuNPs are more selective towards Li^+ than Cs^+

4.2.2.4 – Na^+ vs Mg^{2+}

The final potential step experiments that were undertaken used NaCl and $MgCl_2$ solutions to form the membrane (Figure 4. 20). From vesicle experiments run in parallel with this research, it had been identified that Mg^{2+} may be a poor complexation ion for the carb-AuNPs, where using $MgCl_2$ on one side of the membrane and NaCl or KCl on the other side would cause the membrane to become polarised in such a way that would indicate preferential Na^+ or K^+ transport, respectively. Studying this ion electrochemically could help to support this theory.

Mg^{2+} transport across the membrane from the R.E.2 side of the membrane, where it is a high concentration, to the R.E.1 side would be more prominent when the R.E.1 side of the membrane was negatively charged, due to electrostatic attraction. The addition of the carb-AuNPs caused a large increase in current when the R.E.1 was set at +80 mV, but at -80 mV the current increased only slightly (Figure 4. 21). The low current when negatively charged suggests that the Mg^{2+} is poorly transported across the membrane, corroborating the vesicle study results.

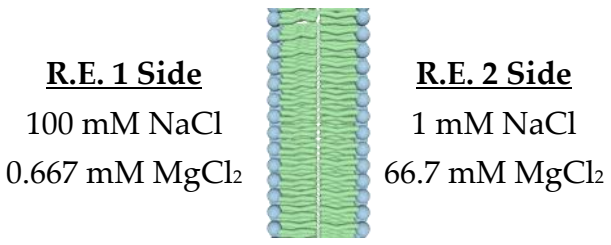

Figure 4. 20 – Experimental set-up of a Na^+ vs Mg^{2+} membrane, showing the concentrations of each chloride-salt on both sides of the membrane.

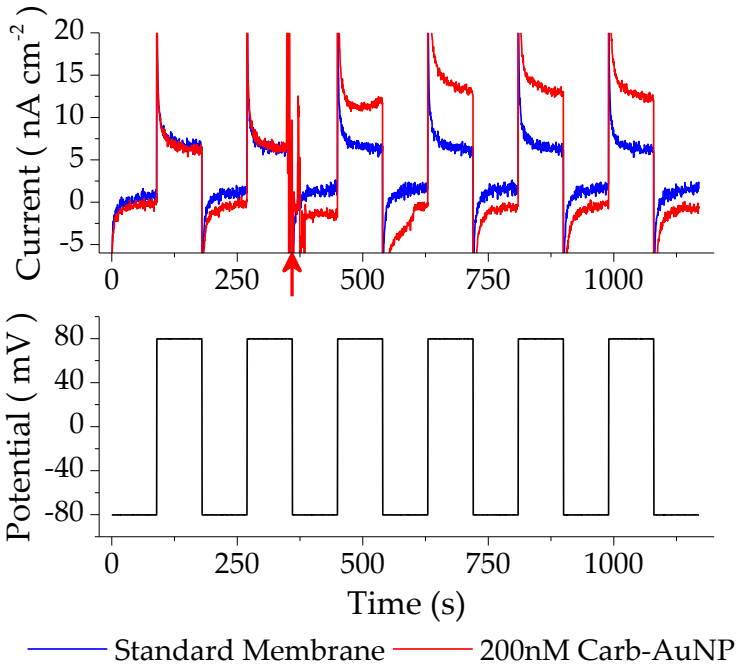

Figure 4. 21 – Top: Symmetric stepping experiment of a Na^+ vs Mg^{2+} membrane comparing the current before (blue) and after (red) an addition of carb-AuNPs. The AuNP addition occurred at around 360 s, indicated by the red arrow. Y-axis cropped to show resistive currents more clearly. Bottom: The potential-trace of the same experiment.

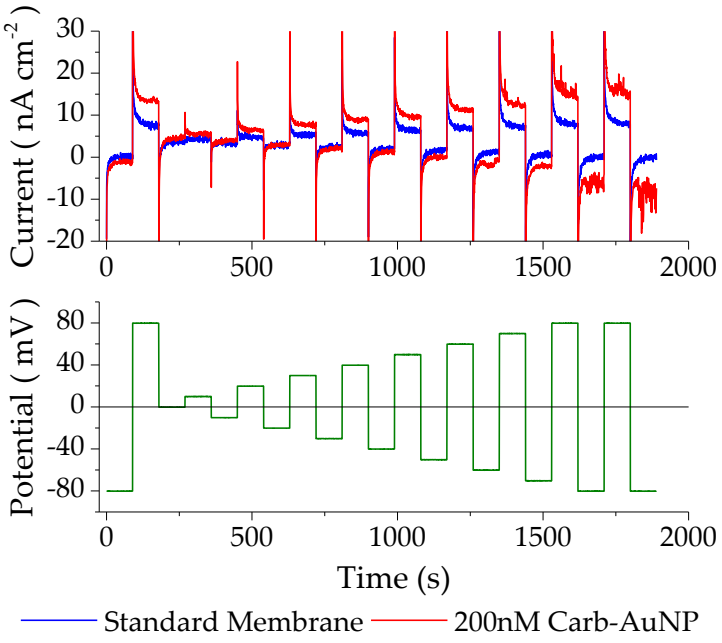

Figure 4. 22 – Top: Progressive stepping experiment on the Na^+ vs Mg^{2+} membrane, comparing the current through the system before (blue) and after (red) the addition of carb-AuNPs. Y-axis cropped to show resistive currents more clearly. Bottom: The potential trace of the same experiment (green).

Towards the end of the progressive stepping experiment, the current recording started to become erratic, and the membrane did rupture soon afterwards (Figure 4. 22). The current increase through the membrane before the break was measured to be 6.47 $nAcm^{-2}$ at +80 mV, corresponding to Na^+ transport and 1.55 $nAcm^{-2}$ at -80 mV corresponding to Mg^{2+} transport. This is a higher increase in current compared to the Na^+ vs Cs^+ membrane, but much lower than the other gradient membranes.

The erratic behaviour also gave rise to the non-linear behaviour at the extremes of the I vs E graph (Figure 4. 23). The conductance through the membrane was calculated at 66.1 $nScm^{-2}$, higher than that of the Na^+ vs Cs^+ membrane, suggesting that Mg^{2+} does not inhibit the transport of Na^+ as much as Cs^+.

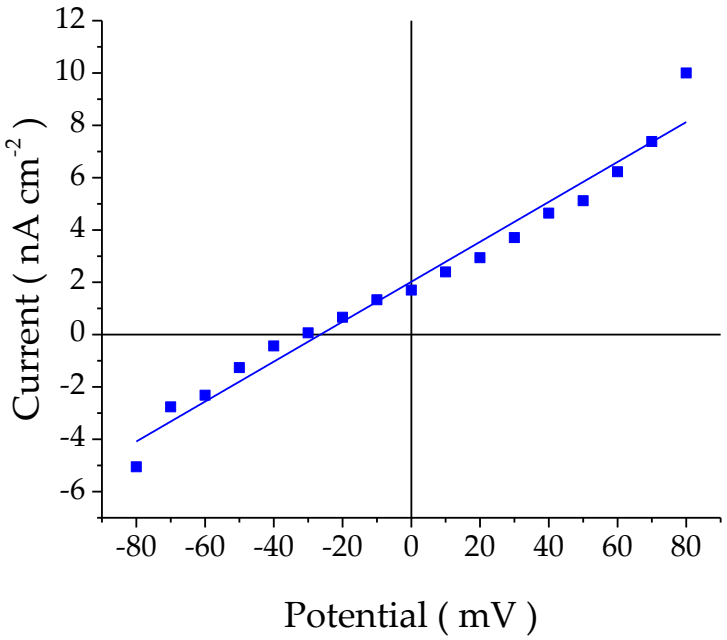

Figure 4. 23 – I vs E graph of the current generated by the carb-AuNPs for the Na^+ vs Mg^{2+} membrane, with a straight line fitted to the data. The zero-current membrane potential has been shifted to -26.5 mV (3.s.f.), indicating the carb-AuNPs are more selective towards Na^+ than Mg^{2+}.

4.2.2.5 – Summary of Conductance Data

The increases in conductance upon the addition of the carb-AuNPs for all of the membranes are summarised in Table 4. 1. The highest conductance across the membrane was the Na^+ vs K^+ membrane, which may be expected due to the use of two ions that were known to be able to complex with the carb-AuNPs, and the presence of their electrochemical gradients across the membrane. The lowest conductance of a membrane with an electrochemical gradient was Na^+ vs Cs^+ and considering that the Na^+ vs Na^+ membrane produced a larger increase in conductance, it is believed that Cs^+ , and Mg^{2+} must have been an inhibiting factor towards current transfer.

When looking at conductance only, the cations can be placed in series. By comparing the symmetric membranes, Na^+ gives greater current than K^+, by comparing the "vs Cs^+" membranes Li^+ produces more current than Na^+, and then by comparing the "Na^+ vs" data, it is calculated that $K^+ > Mg^{2+} > Cs^+$. This leads to the overall conductance series of:

$$Li^+ > Na^+ > K^+ > Mg^{2+} > Cs^+$$

This follows the series of increasing ionic size (see Table 1. 1), with Mg^{2+} the exception. This may be due to the much larger hydration shell that Mg^{2+} carries, and so the energy required to remove the shell is much larger than for all of the other cations. It is presently believed that there are two processes in this charge transport mechanism. The first step is that the cations must diffuse into and out of the core-shell voids of the carb-AuNPs. This equilibrium

Table 4. 1 – The increase in conductance through a membrane due to the addition of carb-AuNPs for all of the membranes studied (3.s.f).

	K^+ vs K^+	Na^+ vs Na^+	Na^+ vs K^+	Na^+ vs Mg^{2+}	Na^+ vs Cs^+	Li^+ vs Cs^+
Conductance (nS cm^{-2})	19.8	74.6	150	66.1	45.7	78.8

should be determined by both the enthalpy of hydration of the ions and ionic size of the ion. The ionic size of the ion determines whether the ions can enter the voids through the spaces between the carborane ligand spheres, where smaller ions should be able to enter more easily, and also the number of ions that can be held in them, where smaller ions would allow more to enter. The enthalpy of hydration only determines whether the ions can enter or not. For the monovalent cations, the enthalpy of hydration does not seem to be as important as ionic size, due to Li^+ producing the largest conductance. However, it seems that for Mg^{2+} the stability of the hydrated ion is too high and cannot remove the H_2O molecules to allow the ion to diffuse into the voids.

The second step is the carb-AuNP-ion complexes must travel across the membrane to transport the ions to the other side. This should be dependent on the charge on the complex which will be dependent on the number of ions that are located in the voids. This in-turn will be dependent on the size of the ion, with the voids being able to house more smaller ions than larger ones. This is believed to be the reason why the symmetric Na^+ vs Na^+ membrane gave a higher conductance through the membrane when compared to the symmetric K^+ vs K^+ membrane.

As alluded to in Chapter 1, it is possible to calculate the relative membrane-permeability of the ions from the zero-current potential. For monovalent ions, a modified version of the Nernst-Donnan equation for membranes that accounts for more than one permeating ion is used: the Goldman-Hodgkin-Katz equation[159,160]. The zero-current potential of a membrane with two permeating cations follows:

$$\Phi = \frac{RT}{z_{n/m}F} \ln\left(\frac{\rho_n[n^+]_{R.E.2} + \rho_m[m^+]_{R.E.2}}{\rho_n[n^+]_{R.E.1} + \rho_m[m^+]_{R.E.1}}\right) \quad \text{(Eq. 10)}$$

Where Φ is the zero-current membrane potential (V), R the universal gas constant (8.3145 J mol^{-1} K^{-1}), T the temperature (K), F the Faraday constant (96485 C mol^{-1}), $\rho_{n/m}$ the membrane permeability of ion *n* or *m* (mol s^{-1}), $[n,m]_{R.E.2}$ the concentration of ions *n* or *m* on the R.E.2 side of the membrane (mol dm^{-3}), and $[n,m]_{R.E,1}$ the concentration of ion *n* or *m* on the R.E.1 side of the membrane (mol dm^{-3}). $z_{n/m}$ is the charge on the permeating ion, n or m. This can be rearranged to find the relative membrane-permeability ratio between two monovalent ions:

$$\frac{\rho_m}{\rho_n} = \frac{\left([n^+]_{R.E.2} - [n^+]_{R.E.1}\, e^{\frac{\Phi F}{RT}}\right)}{\left([m^+]_{R.E.1}\, e^{\frac{\Phi F}{RT}} - [m^+]_{R.E.2}\right)} \quad \text{(Eq. 11)}$$

To calculate the relative permeabilities of both monovalent and divalent ions, the Goldman-Hodgkin-Katz equation cannot be used unmodified. It must be adapted to account for the +2 charge on the divalent ion. The most straightforward way to do this is using the Goldman current equation for ion flux, which for an ion, x, is:

$$J_x = \frac{\rho_x {z_x}^2 \frac{\Phi F^2}{RT}([x]_{R.E.1}\mathrm{A} - [x]_{R.E.2})}{A-1} \quad \text{(Eq. 12)}$$

Where $A = e^{\frac{z_X \Phi F}{RT}}$. At the zero-current potential, the net current across the membrane is zero, which can be represented as $0 = J_{Na} + J_{Mg}$ using Na^+ and Mg^{2+} as the two ions, since it is assumed that only these two cations are able to contribute to the current. The currents attributed to each ion must be equal and opposite: $J_{Na} = -J_{Mg}$. It is then possible to calculate the relative ionic permeabilities of the ions through the membrane Equating $J_{Na} = -J_{Mg}$, and cancelling down gives:

$$\rho_{Na}([Na]_{R.E.1}A - [Na]_{R.E.2}) = \frac{4\rho_{Mg}([Mg]_{R.E.2} - [Mg]_{R.E.1}A)}{\left(e^{\frac{\Phi F}{RT}} + 1\right)} \quad \text{(Eq. 13)}$$

This can then be re-arranged to calculate the relative permeability ratio for Na^+ transport through the membrane against Mg^{2+}, $\frac{\rho_{Na}}{\rho_{Mg}}$:

$$\frac{\rho_{Na}}{\rho_{Mg}} = \frac{4([Mg]_{R.E.2} - [Mg]_{R.E.1}A)}{\left(e^{\frac{\Phi F}{RT}} + 1\right)([Na]_{R.E.1}A - [Na]_{R.E.2})} \quad \text{(Eq. 14)}$$

From the progressive stepping data, I vs E graphs have been produced, from which the zero-current potentials can be calculated for each separate membrane environment. The zero-current potentials can be then used in the previous equations to calculate the relative permeabilities of the ions. The relative permeability ratio through the membrane will be caused by the selectivity of the carb-AuNPs.

The symmetric membranes had a zero-current potential of ~0 mV, which was expected. However, a potential was observed for the membranes that were

Table 4. 2 – The calculated zero-current potentials from the line of best fit of the I vs E graphs of each membrane (3.s.f.).

	Na^+ vs K^+	Na^+ vs Cs^+	Li^+ vs Cs^+	Na^+ vs Mg^{2+}
Zero-Current Potential (mV)	+11.7	-23.8	-35.2	-26.5

formed with an electrochemical gradient present (Table 4. 2). These values were then used to calculate the relative permeability ratios using Eq.11 for the monovalent cation pairs, and Eq. 14 for Na^+ vs Mg^{2+}.

The ratio between the permeabilities for the Na^+ vs K^+ membrane, $\frac{\rho_{Na}}{\rho_K}$, was 0.627 (3.s.f), which correlates to the carb-AuNPs transporting 1.59 K^+ ions for every 1 Na^+ ion. It is perhaps strange that the carb-AuNPs are more selective towards K^+ compared to Na^+ when a higher conductance was observed for the symmetric Na^+ membrane compared to the symmetric membrane formed using K^+. One possible explanation for this behaviour is that there are two/three major steps involved in the transport of ions across the membrane using ionophores: the take-up and release of the ions into and out of the core-shell voids, and the transport through the membrane. If the uptake/release of K^+ is a kinetically slower process than it is for Na^+, then less current will be observed.

There could also be an argument that the different ionic environments either side of the membrane alter the carb-AuNPs, with a different number of ions in the core-shell voids. The carb-AuNPs may have different charges either side of the membrane leading to a pseudo-electrochemical gradient of the AuNPs across the membrane as well. If this were the case, permeability ratios of the two carb-AuNP populations would also need to be accounted for, as well as the charge of the carb-AuNPs, and calculating permeability ratios for highly charged ions (> 3+, or < -3) is quite challenging.

The relative permeability ratio between Na^+ and Cs^+ was 2.58:1, indicating that for every Cs^+ ion transported, 2.58 Na^+ ions are transported in the other direction. The increased size of the Cs^+ may mean that uptake is a slow process and that fewer of the ions can reside inside the voids.

The permeability ratio for Li^+: Cs^+ was calculated to be 4.08:1, meaning 4 Li^+ ions are transferred for every 1 Cs^+ ion. Using the two ratios with Cs^+ as the standard, the Li^+:Na^+ selectivity ratio was estimated to be 1.58:1, similar to the K^+:Na^+ ratio.

The relative permeability ratio of Na^+:Mg^{2+} was 5.66:1. This is the highest selectivity for Na^+ against any ion so far, demonstrating that Mg^{2+} is indeed poorly transported, corroborating with what had been seen above, and in the previous research[148,158].

The Mg^{2+}: Na^+ ratio calculated was lower than that of the Cs^+:Na^+, identifying that Mg^{2+} was the lowest transported ion. However, it is observed again that the selectivity is not necessarily related to current through the membrane as the Na^+ vs Mg^{2+} membrane was more conductive than Na^+ vs Cs^+.

The relative permeabilities were converted to selectivities, using Na^+ as the standard (Table 4. 3), from which a different order in ion "effectiveness" arises for the selectivity series compared to the conductance series:

$$K^+ > Li^+ > Na^+ > Cs^+ > Mg^{2+}$$

The position of K^+ in this series is difficult to understand. It is possible that selectivity is dependent on a combination of both ionic size and hydrated size as above when discussing conductance, and that K^+, although not the leading candidate in either of them, may be the most favourable when both are taken into consideration.

Table 4. 3 – Relative selectivity of the cations, using Na^+ as the reference standard (2.d.p.).

	Li^+	Na^+	K^+	Cs^+	Mg^{2+}
Relative Selectivity	1.58	1.00	1.59	0.39	0.18

4.2.3 – Control Experiment using 2-3 nm PEG AuNPs

To confirm that the increase in conductance through the membrane was due to the addition of the carb-AuNPs, and their ability to store ions in the core-shell voids, a control experiment using the same sized AuNPs (2-3 nm) but using a different, polyethyleneglycol- (PEG)- based, ligand: HS-$(CH_2)_{11}$-$(CH_2CH_2O)_4$-OH, was carried out. The PEG-AuNPs were provided by Dr Marcin Grzelczak, who prepared them via the literature method[148].

The membrane used was the Na^+ vs K^+ membrane that produced the most current when using the carb-AuNPs. Upon the addition of PEG-AuNPs, little to no increase in current could be seen (Figure 4. 24). Throughout the entire progressive stepping experiment, there was similarly negligible change in the current passing through the system (Figure 4. 25).

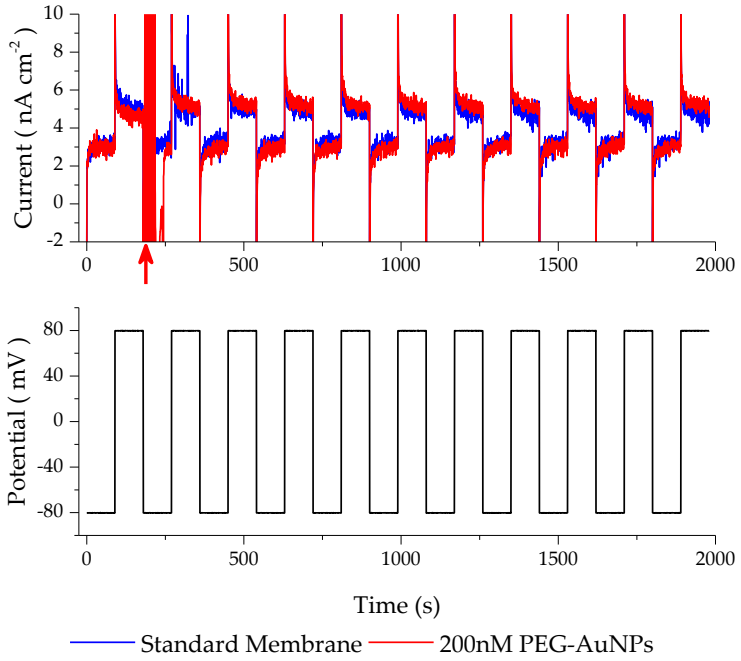

Figure 4. 24 – Top: Symmetric stepping experiment of a Na^+ vs K^+ membrane comparing the current before (blue) and after (red) an addition of PEG-AuNPs. The AuNP addition occurred at around 200 s, indicated by the red arrow. Y-axis cropped to show resistive currents more clearly. Bottom: The potential-trace from the same experiment.

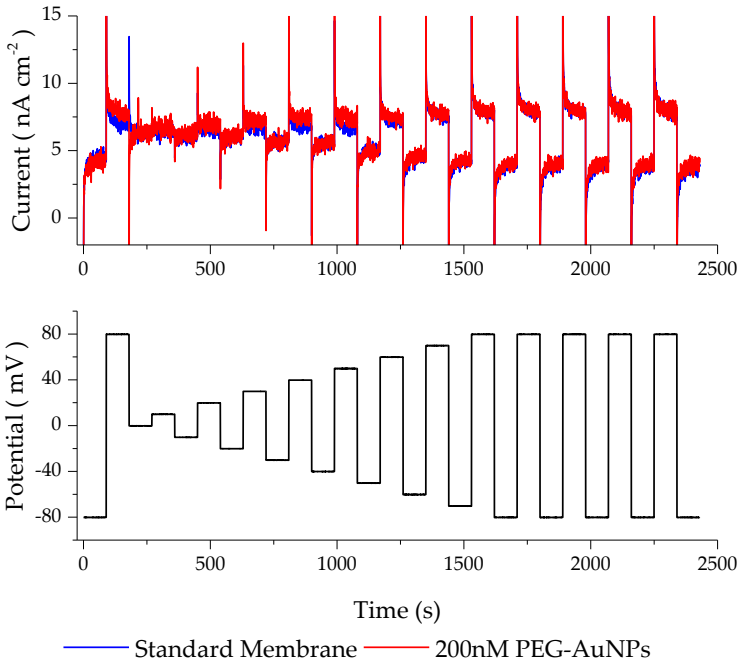

Figure 4. 25 – Top: Progressive stepping experiment on the Na^+ vs K^+ membrane, comparing the current through the system before (blue) and after (red) the addition of PEG-AuNPs. Y-axis cropped to show resistive currents more clearly. Bottom: The potential trace of the same experiment.

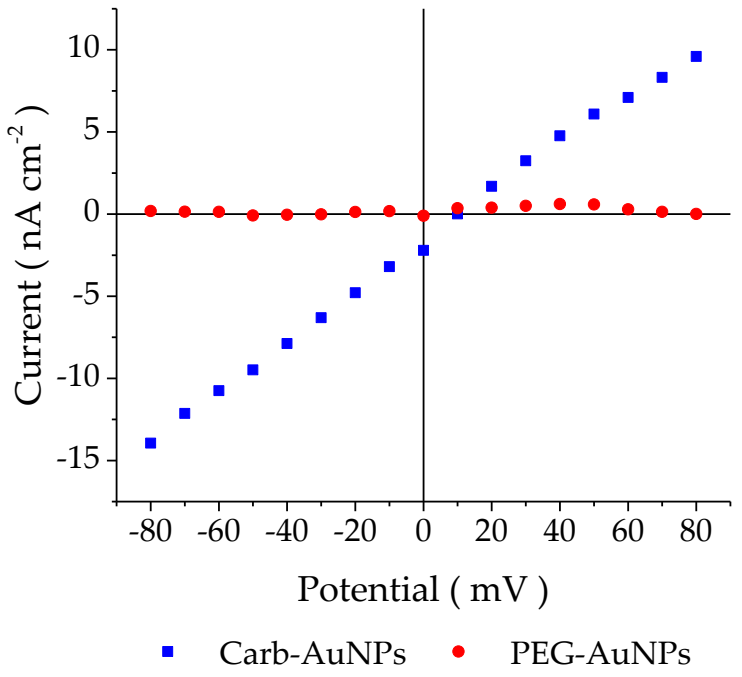

Figure 4. 26 – I vs E plot of the average increase in current due to the addition of carb-AuNPs (blue) and the same amount of PEG-AuNPs (red) through the membrane from the progressive stepping experiment of the Na^+ vs K^+ membrane.

The I vs E graph of the change in current through the membrane upon the addition of the PEG-AuNPs showed no ohmic behaviour, confirming that they do not affect the conductance of the membrane (Figure 4. 26). The addition of the same amount of PEG-AuNPs as the carb-AuNPs did not induce any increase in conductance through the membranes. The increase in currents seen in the previous results can justifiably be attributed to the carb-AuNP's ability to store and release ions from their core-shell voids. It is difficult to identify, however, whether it is ion transport through the membrane facilitated by the AuNPs, or whether the AuNP-ion complexes themselves pass through the membrane and generate the increase in current.

4.3 – Carb-AuNPs as Partitioning Poly-Ions

In view of the fact that the addition of the carb-AuNPs to the vesicle membranes produced a small membrane potential even with symmetrical solutions, the partitioning of the carb-AuNPs was studied by measuring how the zero-current potential changed when the concentration of the carb-AuNPs on only one side of the membrane was increased. The membranes used in these experiments were formed using the D.I.B. method according to Section 2.4.1.4.

4.3.1 – Nernst-Donnan Potential Study

4.3.1.1 – NaCl Solutions

Following on from the previous potential step experiments, Na^+ was the first cation to be studied to see whether the change in carb-AuNP concentration on one side of the membrane would cause a potential change across the membrane. For 100 mM NaCl, the potentials measured gave rise to a linear trend for the Nernst plot demonstrating that the carb-AuNPs do partition across the membrane (Figure 4. 27). The charge on the carb-AuNPs was calculated as -3.46 from the gradient of a fitted line. Considering the membrane is a hydrophobic barrier to smaller, monovalent ions, it is perhaps surprising that the carb-AuNP can partition through the membrane when such a charge is associated with it. The charge is likely to be distributed across the Au core with charge density likely to be low; the hydrophobic carborane

ligands must be able to mask this charge from the hydrophobic part of the membrane, to allow the carb-AuNPs to pass through the membrane.

With a high concentration of Na^+ in the solution, the number of ions that are present in the core-shell voids is expected to be much higher than in a lower concentration of Na^+. To test this, the same experiment was attempted, but this time 1 mM NaCl was used, rather than the 100 mM NaCl solution. The data measured also gave a linear trend, although the spread of the data about the line of best fit was greater than that for the 100 mM solution data. The charge on the carb-AuNPs was calculated to be -6.16 for the lower concentration solution, suggesting that the average carb-AuNP carried around two or three more Na^+ ions in the higher concentration of 100 mM NaCl than the lower one. This would suggest that, for the gradient solutions used in previous experiments, when a potential was applied, the carb-AuNPs would partition towards the positively charged side of the membrane. The

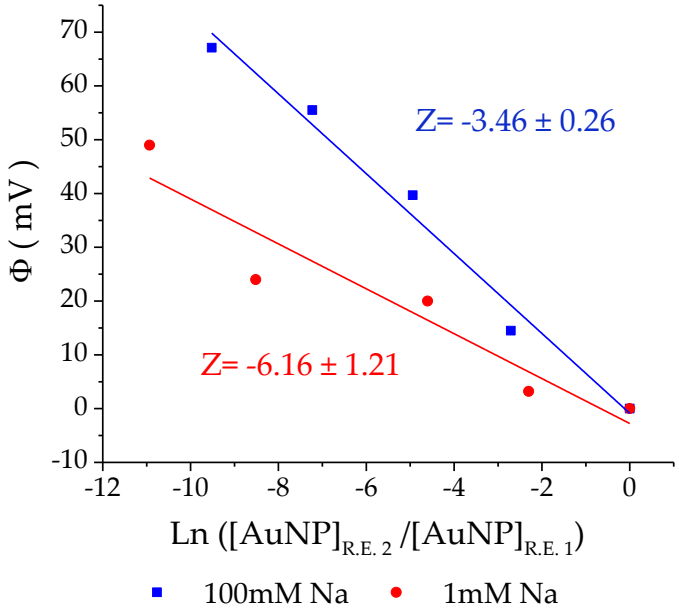

Figure 4. 27 – Nernst plot for two different concentrations of NaCl, 100 mM NaCl (blue) and 1 mM NaCl (red), changing the ratio of AuNPs on either side of the membrane. The charge on the AuNPs for each solution was calculated from the gradient of the linear fit of each set of data, and these were found to be -3.46 in 100 mM NaCl and -6.16 in 1 mM NaCl

carb-AuNPs would then be able to release the ions that were in the core-shell voids into the solution down their concentration gradient, and the ions on that side of the membrane could then enter the spaces left. Once the membrane was polarised the other way, the same situation would occur, which is why the effect of an enhanced current when an electrochemical gradient was present can be seen. The entropically favoured mechanism would encourage the ions to diffuse out, increasing the amount of charge transported in the same timeframe compared to symmetric membranes – where there is no extra encouragement for the ions to diffuse out of the voids except for the electrochemical stimulus.

4.3.1.2 – KCl Solutions

Similar experiments were also attempted with potassium, but the 100 mM solution of KCl did not seem to follow the Nernst-Donnan equation, with the potential not increasing linearly with the logarithm of the carb-AuNP ratio; but instead appearing more like an exponential or polynomial increase (Figure 4. 28). In order to make a comparison with the Na^+ solutions, the charge was never-the-less calculated assuming a linear relationship. The value calculated from the gradient of the line of best fit for the carb-AuNPs in the KCl solution was -3.14. This is less negative than the NaCl solution of the same concentration, indicating that more K^+ has been taken up in the core-shell voids. This is unexpected, as the core-shell voids would require less K^+ to fill them being larger than Na^+. However, from the potential step measurements, the selectivity of K^+ is higher than Na^+, and if it is assumed that the voids are not full at 100 mM, this would be consistent with the current

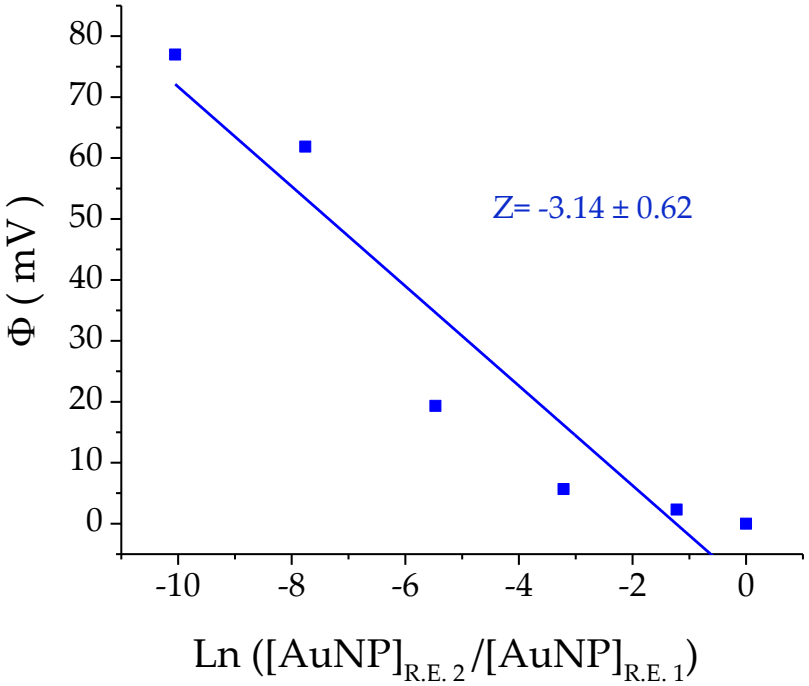

Figure 4. 28 – Nernst plot for the carb-AuNPs in a 100 mM KCl solution. The charge on the complex was calculated from the gradient of a straight line fitted to the data, and was found to be -3.14

theory. Since the relationship between the zero-current potential and the logarithm of the carb-AuNP ratio does not appear linear, the calculation of the charge using the gradient cannot be relied upon.

4.3.1.3 – RbCl Solutions

100 mM RbCl was the next solution selected for experimentation – the first time this cation was studied. With Rb^+ being the next-largest alkali metal ion after K^+, it was used to confirm whether the non-linear behaviour was consistent. Like the 100 mM KCl solution, the zero-current potential was not linearly dependent on the logarithm of the carb-AuNP ratio (Figure 4. 29). However, a similar effect was observed. The final additions of a large amount of carb-AuNPs produced a much larger potential shift compared to the earlier additions, suggesting an exponential or polynomial relationship. For the purpose of comparison with Na^+ and K^+, the charge on the carb-AuNPs was again calculated assuming linear behaviour. The charge was more negative

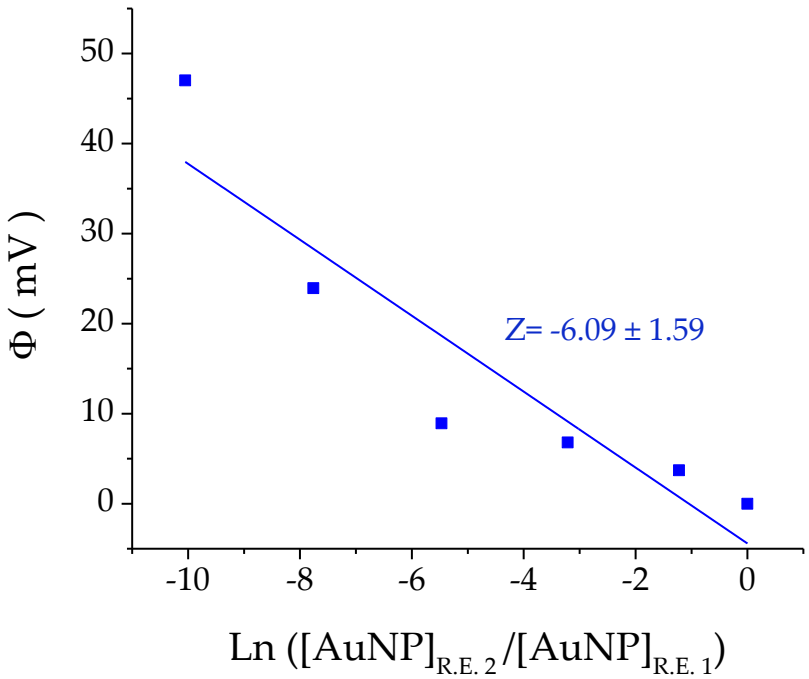

Figure 4. 29 – Nernst plot for the carb-AuNPs in a 100 mM RbCl solution with the fitted straight line that was used to calculate the charge on the carb-AuNP complex, which was found to be -6.09.

for Rb^+, -6.09, suggesting that the number of Rb^+ ions in the core-shell voids was lower than for the Na^+ and K^+ experiments, consistent with the hypothesis that the size of the ions is significant.

4.3.1.4 – $MgCl_2$ Solutions

The last salt studied to investigate how using a solution of it affected the behaviour of the carb-AuNPs was 100 mM $MgCl_2$. From the potential step experiments, it is known that the conductance attributed to the AuNPs complexing with Mg^{2+} is poor. So far, it is unknown whether the poor conductance is due to Mg^{2+} not being able to enter the voids and thus not getting transported, or whether the Mg^{2+} ions are unable to exit once inside due to a greater attraction to the negative Au core. The charge on the carb-AuNPs would give an indication of whether Mg^{2+} are able to reside in the core-shell voids. If they are, the charge calculated will be more positive. However, if they do not occupy the voids of the carb-AuNP, the charge would be more negative.

The Nernst plot again does not show linear behaviour (Figure 4. 30), however, the charge calculated for Mg^{2+} gives the most negative so far, indicating that Mg^{2+} is not entering the voids. This may be due to the hydration shell of Mg^{2+} being too strongly bound to the ion, and thus the large hydrated Mg^{2+} is not able to diffuse between the carborane ligands into the voids. With this being the case, it is not surprising that Mg^{2+} was found towards the lower conductance end of the series presented previously.

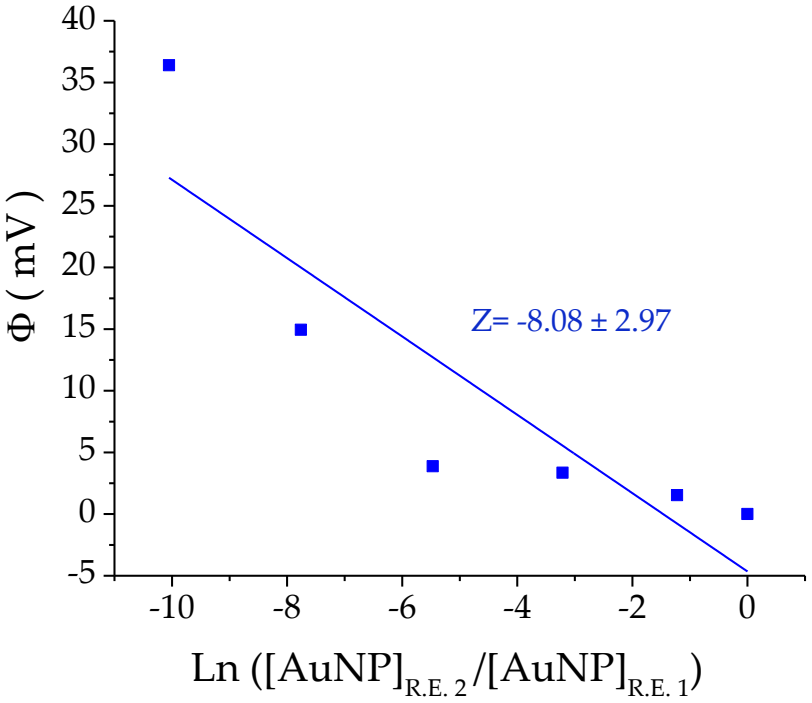

Figure 4. 30 – Nernst plot for the carb-AuNPs in a 100 mM $MgCl_2$ solution, with the fitted straight line that was used to calculate the charge on the carb-AuNP complex, which was found to be -8.08.

4.3.2 – Linear Behaviour Comparisons

If only the first four points of the Nernst plots are considered, all of the ions show relatively linear behaviour (Figure 4. 31), and the charges of the carb-AuNPs in the ionic solutions calculated from the gradients of the lines of best fit give a distinct series of Mg^{2+} (most negative) < Rb^{+} < K^{+} < Na^{+} (least negative) (Table 4. 4).

This could be explained by considering the total capacity of the core-shell voids, assuming that Mg^{2+} is not able to interact with the carb-AuNPs.. When the carb-AuNPs are low in concentration, there may be an excess of cations, and so the voids will become saturated. A larger number of smaller cations would be able to enter the core-shell voids and would lead to a more positive charge on the complex. The maximum number of ions in the core-shell voids would decrease with increasing ionic radius. It is noteworthy that the charge on the carb-AuNPs is not dictated by the selectivity of the ion, calculated from the potential step experiments, but the size of the cation. This observation may

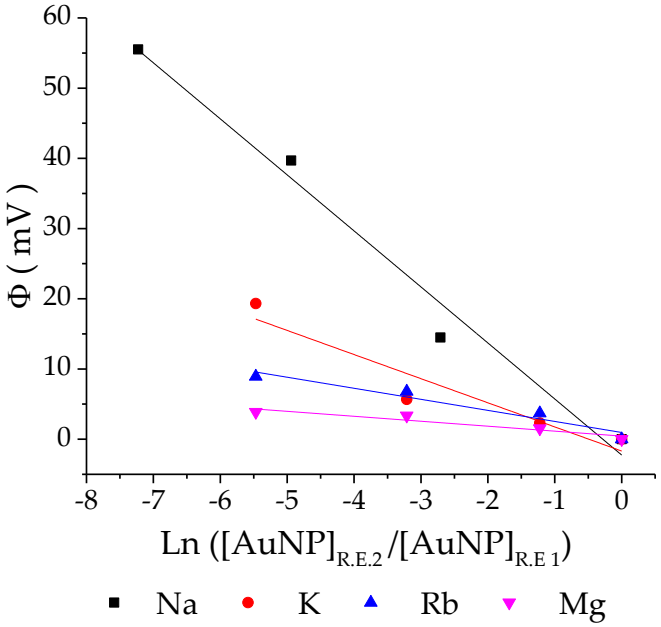

Figure 4. 31 – Nernst plot using only the first four points for each ion, each with a fitted line. The solutions were all 100 mM to make sure the complexing ions were all the same concentration.

Table 4. 4 – Calculated charges of the carb-AuNPs using the lines of best fit from the above Nernst plots that use only the first 4 points (3.s.f.).

	Na^+	K^+	Rb^+	Mg^{2+}
Carb-AuNP Charge	-3.22	-7.47	-16.4	-36.4

also explain why the current is relatively low for the symmetric K^+ vs K^+ membrane compared to Na^+ vs Na^+.

The difficulty with these experiments is that following the addition of the AuNPs, there is no way to stir the solution as this action may cause the membrane to break. This means that it is difficult to ensure that the solution is homogeneous. The concentration of the carb-AuNPs at the membrane may vary from the expected concentration, which would mean that the theoretical ratio of AuNP concentration could vary significantly from the experimental ratio, and the theoretical ratios consequently may not correspond to the measured potential. The low volume additions for the lower concentrations make this particularly likely. Without the opportunity for sufficient mixing of the solution, a significant proportion of the AuNPs may not reach the membrane. It is also challenging to angle the pipette so that the AuNPs are delivered to the membrane without compromising its structural integrity. Finding a solution to this problem could bring about carb-AuNP concentrations which would be more consistent with those expected at the membrane, and a more linear behaviour might be revealed.

4.4 – Shuttle Mechanism

The mechanism of ion transport for these carb-AuNPs is thought to be different from that of standard ionophores such as gramicidin and valinomycin. This is primarily due to the carb-AuNPs not being able to facilitate a membrane potential in accordance with Nernst-Donnan theory on their own (Figure 4. 32).

When in aqueous solutions, the carb-AuNPs are negatively charged polyanions and position themselves on the positive side of the membrane. They are able to complex the cations on that side of the membrane and become more neutral. They then position themselves further into the hydrophobic part of the membrane as they become less electrostatically repulsed by the other, negatively charged, side of the membrane and are thought to be able to flip across it. Once on this side of the membrane, the ions are released from the core-shell voids, causing the AuNPs to lose their positive charges, becoming more negatively charged again. The carb-AuNPs then flip back to the positive side of the membrane due to the electrostatic attraction, ready to collect more cations. The process repeats itself, shuttling the cations from the positive side of the membrane to the negative.

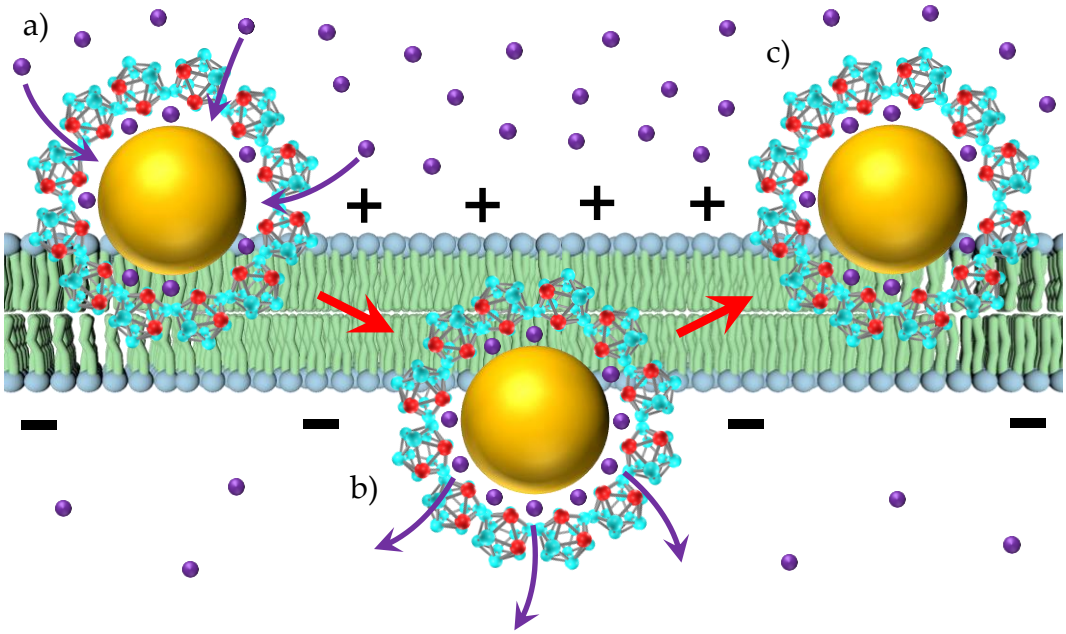

Figure 4. 32 – Proposed mechanism of ion transport using carb-AuNPs. (a) the carb-AuNPs (gold circles surrounded by red and blue carborane molecules) take up cations (purple circles) into the core-shell voids and become more positively charged. (b) They flip across the membrane to the negatively polarised side and release the cations, making the AuNPs more negatively charged. (c) The carb-AuNPs flip back across the membrane to the positively polarised side, at which point they can begin to take up cations again.

This shuttle mechanism cannot work in the opposite direction. This is because the flipping action of the carb-AuNPs would not be able to function. If the AuNPs release the cations on the positive side of the membrane, hyper-polarising the membrane, the carb-AuNPs would become more negatively charged and would not be able to flip back over to the negative side of the membrane to restock on cations due to electrostatic repulsion effects.

The carb-AuNPs accumulate ions in the core-shell voids, similar to the complexation of ions by valinomycin, but it is believed that they are not able to translocate across the membrane without a stimulus. However, when a potential across the membrane is already present, created by electrochemical means or by another ionophore present in the solution, the carb-AuNPs act as a rectifier, reducing that potential.

4.5 – Chapter 4 Conclusions

The carb-AuNPs have been shown to increase the currents that flow through a membrane in the presence of multiple ions, and the selectivity of the AuNPs has been calculated based on the zero-current potential of the membrane when chemical gradients between different ions were present.

Currents through the membrane were much higher when a chemical gradient was present across the membrane, compared to symmetrical membranes. This is thought to be due to an entropic double effect where the loading and release of the cations into/out of the carb-AuNPs down their concentration gradients on either side of the membrane occurs faster - increasing the current through the system. The faster releasing and loading mean that the flipping of the carb-AuNPs across the membrane can also happen faster as well, hence the double effect.

The partitioning carb-AuNPs with core-shell voids acting as traps for monovalent ions would suggest that a smaller ion, with the hydration shell removed, would lead to the most current and this is generally the result seen from these experiments. It is thought that the hydration shell of Mg^{2+} is too strongly bound to be removed, resulting in it not being able to diffuse into the voids. The charges calculated for the carb-AuNPs are also consistent with smaller ions being able to complex more – reducing the inherent negative charge on the carb-AuNPs. The selectivity is generally consistent with this hypothesis but with one exception, K^+. This is believed to be because both hydrated and ionic size of the ion is important for selectivity, and K^+ seems to fall in the best overall position when both dependents are combined.

Chapter 5 – Proton Transfer via 12-Crown-4 Functionalised AuNPs

In previous work carried out in the group, it had been identified that AuNPs functionalised with a 12-crown-4-CH_2-SH ligand were able to complex protons[142]. A series of experiments were undertaken to identify whether it would be possible to transport these protons across a membrane using the functionalised 12-crown-4 AuNPs and to try and identify the mechanism of transport if this was indeed the case.

In this chapter, a small introduction on 12-crown-4 will be given with reasons for it being the ligand of choice for the proton transport study. Results from electrochemical studies on the 12-crown-4 AuNPs using CVs and potential measurements will be presented and the possible mechanisms of proton transport are discussed. Finally, 12-crown-4 AuNPs will be compared to the natural ionophore gramicidin and an attempt at electron transfer will be discussed.

5.1 – 12-Crown-4-CH_2-SH Functionalised AuNPs (2-3 nm)

The focus of this chapter is primarily on proton transport and is not intended to be specifically aimed at 12-crown-4. It is known that both 15-crown-5 and 18-crown-6 are able to complex protons[161]. However, they were not used as although they may be able to complex protons, they are much more selective for other ions (notably Na^+ and K^+ respectively) compared to protons. To make sure that the currents or potentials that arose from the experiments were due to the proton transportation and not the other ions (which may get into the

solution from the ionic agarose gels that surround the reference electrodes), 12-crown-4 was the ligand chosen for the study.

As discussed in Section 1.3.1.2, crown ethers are a set of organic heterocyclic molecules with a characteristic motif of repeating -CH_2-CH_2-O- ether linkages that form a ring. 12-crown-4 is a crown ether with 4 of these linkages in the ring system and is one of the smaller crown ethers, next to 9-crown-3 and 1,4-dioxane, also known as 6-crown-2. The molecule that was used in the AuNP synthesis is 12-crown-4-CH_2-SH, a thiolated variant which enabled it to bind to, and act as a ligand for, the AuNP (Figure 5. 1).

Each of the oxygen atoms in the ring system has lone pairs that are directed into the centre of the molecule, creating a negatively charged cavity in the centre. This allows complexation with cations that can fit into it. The size of the cavity for 12-crown-4 is 120-150 pm in diameter and is known for being selective for the Li^+ ion[162,163]. From the previous work done in the Brust group, 12-crown-4 functionalised AuNPs have shown the ability to complex protons and transfer from H_2O to chloroform at acidic H^+ concentrations (pH3)[142]. It was then thought that by controlling the pH of the solutions on either side of the membrane, it would be possible to cause these crown-AuNPs to enter the hydrophobic region of the membrane and act as a channel, where protons could pass through the membrane, utilising the 12-crown-4 ligands. As 12-

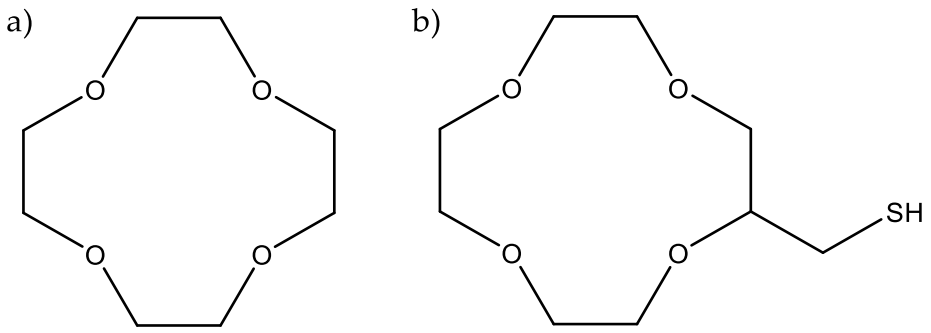

Figure 5. 1 – (a) Structure of 12-crown-4. (b) Structure of 12-crown-4-CH_2-SH, the ligand used to prepare the 12-crown-4 AuNPs.

crown-4 is a smaller ligand compared to 15-crown-5 and 18-crown-6, it was also thought that it would be more beneficial for electron transfer, where larger ligands may hinder the process.

5.2 – Cyclic Voltammetry Study

Once the crown-AuNPs had been made and characterised (Section 2.4.1.5), they could be studied. The first series of experiments used cyclic voltammetry to see whether the functionalised crown-AuNPs would facilitate charge transfer across the membrane. These experiments consisted of analysing the change in conductance across a D.I.B. membrane with the addition of the crown-AuNPs to the HCl solutions before the membrane formation. This was performed on multiple membrane environments, varying the concentration of the protons between pH1 and pH5. Two sets of data were produced with two different amounts of crown-AuNPs added to each of the separate proton concentrations.

5.2.1 – Crown-AuNPs on both sides of the Membrane

The first series of experiments used the same solutions on either side of the membrane to remove any other factors and possible unknowns from the process when trying to establish whether the crown-AuNPs caused a change in the conductance of the phospholipid membrane.

5.2.1.1 – 1 μM Crown-AuNP Experiments

Having confirmed that all the membranes were stable throughout the range of different pHs, the next experiments included the addition of the crown-AuNPs to the solution. 1 μM solutions of the crown-AuNPs, the same concentration as the test experiments with gramicidin in Section 3.3.3, were used. pH2 (10 mM HCl) was the first solution to be studied, as it was hypothesised that the high concentration of HCl would remove bulk transport

issues and that there would be enough protons for the crown-AuNPs to complex. Comparing the solutions with and without crown-AuNPs, an increase in current passing through the system can be seen when the crown-AuNPs were present (Figure 5. 2). The conductance increased from 20.94 $nScm^{-2}$ for the standard pH2 membrane to 136.40 $nScm^{-2}$ with the addition of the crown-AuNPs. This increase in conductance appeared to indicate that the crown-AuNPs were acting as a proton transporter and that the flow of protons through the membrane was the cause of the current. The next experiments were intended to investigate how a change in the proton concentration would affect the trans-membrane current, and so pH1 and pH3 solutions were prepared and studied with the crown-AuNPs present. The prediction was

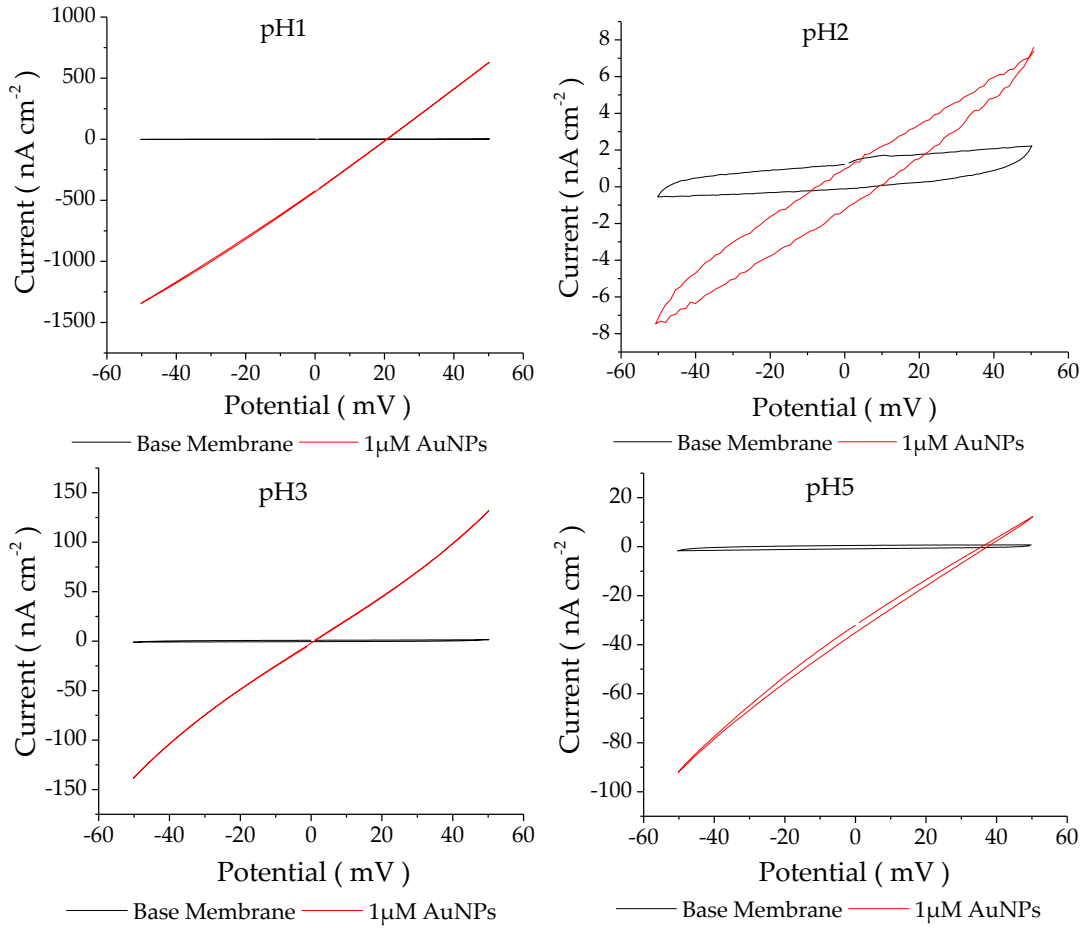

Figure 5. 2 – CVs comparing the standard membranes (black) to membranes with 1 μM crown-AuNPs in the solutions on both sides of the membrane (red) at various pHs (see the graph titles). Scan rate = 2 mVs^{-1}.

that pH1 membrane would see a higher current flow through it and that the pH3 membrane would see a lower current, reflecting the change in proton concentrations compared to pH2.

The experiment using pH1 solution did follow the prediction as the increase in current was larger than that of the pH2 membrane, leading to a large increase in conductance from 19.73 $nScm^{-2}$ without crown-AuNPs to 19.36 μScm^{-2} with the crown-AuNPs, one thousand times more conductive. The conductance increase was larger than expected, however, as the solution was around one hundred times more conductive than the pH2-crown-AuNP solution, and consequently indicated that the current did not seem to be linearly related to proton concentration.

When pH3 was studied, it was anticipated that the current would be less than that of pH2 but, contrary to expectations, this was not the case. The conductance for the pH3 membrane was much higher than that of the pH2 membrane, increasing from 14.22 $nScm^{-2}$ to 2.52 μScm^{-2}, nearly 20 times the conductance of the pH2 membrane with crown-AuNPs. This did not make sense at the time as it was thought that proton transfer was the overriding contributor to the current through the membrane.

The membranes studied to this point had all been relatively acidic, and so to see whether the crown-AuNPs could induce a current through the membrane in less acidic solutions, an experiment using pH5 was also attempted. This was a relatively low concentration for an electrolyte, and so the current through the system was expected to be much lower than previous measurements. There was, surprisingly, a higher conductance through the membrane compared to the pH2 experiment; the value of the conductance through the system calculated at 1.00 μScm^{-2} being similar in magnitude to the pH3 membrane.

Table 5. 1 – Conductance values for the 1 μM crown-AuNP solutions on both sides of the membrane in the different pHs (3.s.f.).

	pH1	pH2	pH3	pH5
Conductance (S cm^{-2})	$1.94x10^{-5}$	$1.36x10^{-7}$	$2.52x10^{-6}$	$1.00x10^{-6}$

The protons appear to be affecting the conductance, but the relationship shows no simple proportionality (Table 5. 1). Consequently, there must be another reason why the conductance fluctuates so. As the crown-AuNP concentrations in the solutions were kept constant across the different pH HCl solutions, their contributions to the current may have an effect more important than first hypothesised, suggesting that the assumption that the crown-AuNPs would act as an ionophore similar to gramicidin or valinomycin was unfounded. It is also unknown as to why this should lead to a minimum conductance at pH2.

Side Note: Unfortunately, the pH4 experiments using the 1 μM crown-AuNP solutions did not produce repeatable conductance results, with only a few measurements showing increases in current, and so are not reported.

5.2.1.2 – 5 μM Crown-AuNP Experiments

Experiments with a higher concentration of crown-AuNPs in the solutions were run to see how the current changed with the concentration of crown-AuNPs, as it has already been seen how pH affects conductance. The crown-AuNP concentration in the solutions was increased from 1 μM to 5 μM. It was hoped that by increasing the number of AuNPs in the solutions, more of them would be able to transport ions across the membrane, increasing the current flowing through the system.

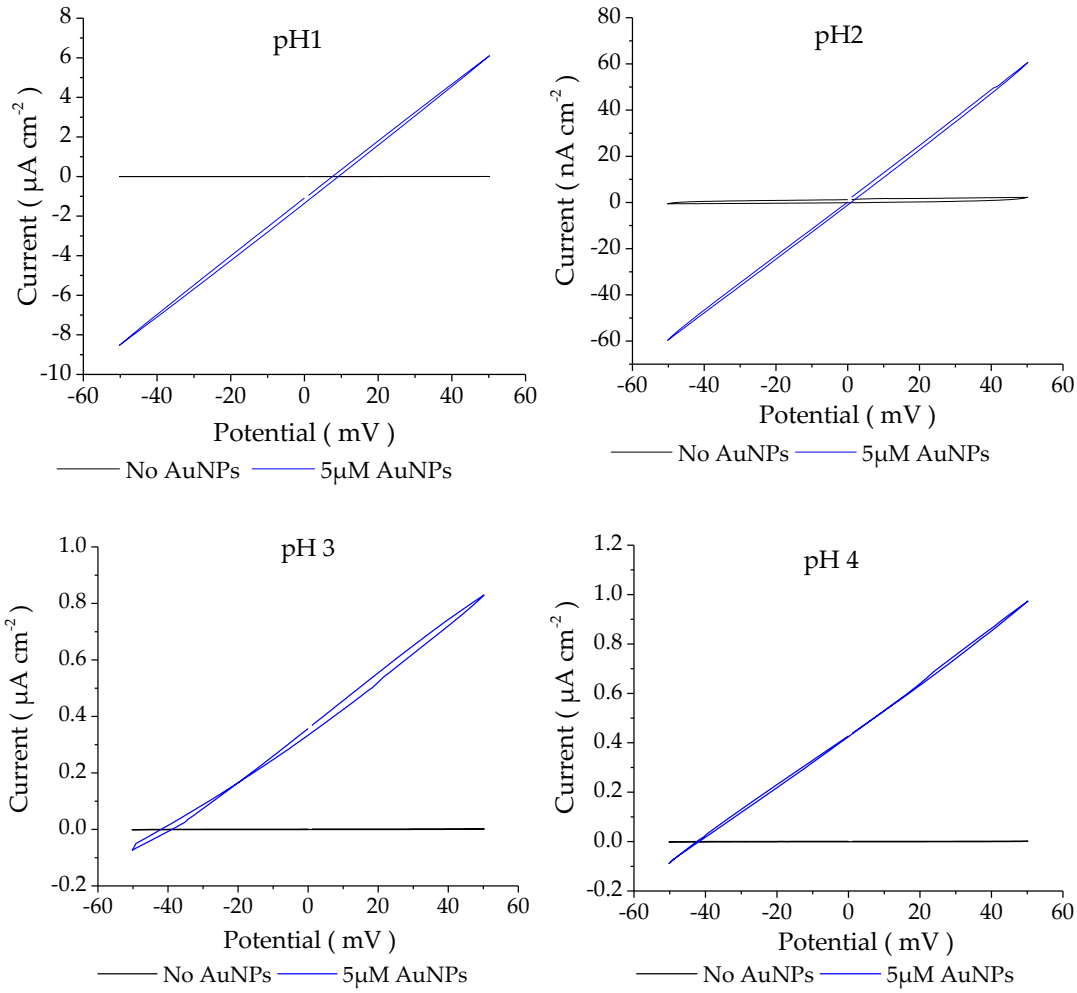

Figure 5. 3 – CVs comparing the standard membranes (black) to membranes with 5 μM crown-AuNPs in the solutions on both sides of the membrane (blue) at various pHs (see graph titles). Scan rate = 2 mVs^{-1}.

Table 5. 2 – Conductance values for the 5 μM crown-AuNP solutions on both sides of the membrane in the different pHs (3.s.f.).

	pH1	pH2	pH3	pH4
Conductance (S cm-2)	1.46×10^{-4}	1.19×10^{-6}	9.05×10^{-6}	1.11×10^{-5}

An increase in current was again seen for all crown-AuNP membranes compared to the standard membranes (Figure 5. 3). For pH1 the increase in current through the system was again high, with the highest calculated conductance observed at 146 μScm^{-2} (Table 5. 2). There was also an increase over the 1 μM crown-AuNP solutions, confirming that the AuNPs are involved in the charge transport and that the currents are dependent on them.

Side Note: As for the pH4 experiments using the 1 μM crown-AuNP solutions, none of the pH5 experiments using the 5 μM crown-AuNP solutions gave reliable/repeatable conductance results, and as they could not be compared to the other results, they were omitted.

5.2.1.3 – Between pH1 and pH2

There are striking similarities between the results of the two sets of experiments. In both, there is a minimum conductance at pH2, with a sharp rise in conductance moving to pH1 and a smaller rise at pH levels above 2. In order to investigate the change from pH2 to pH1, separate experiments using both crown-AuNP concentrations were carried out. For the 1 μM crown-AuNP solutions, 55 mM HCl - the mean H^+ concentration between pH1 and pH2 membranes - was studied. This is close to pH1.25 (Figure 5. 4). The conductance is calculated at 1.51 μScm^{-2}, just less than for the pH3 membrane. It is interesting that when the conductance of the solutions at pH 1, 1.25, and 2 are converted to $\log_{10}$, there is an almost linear proportionality with H^+ concentration which is similar to gramicidin channels.

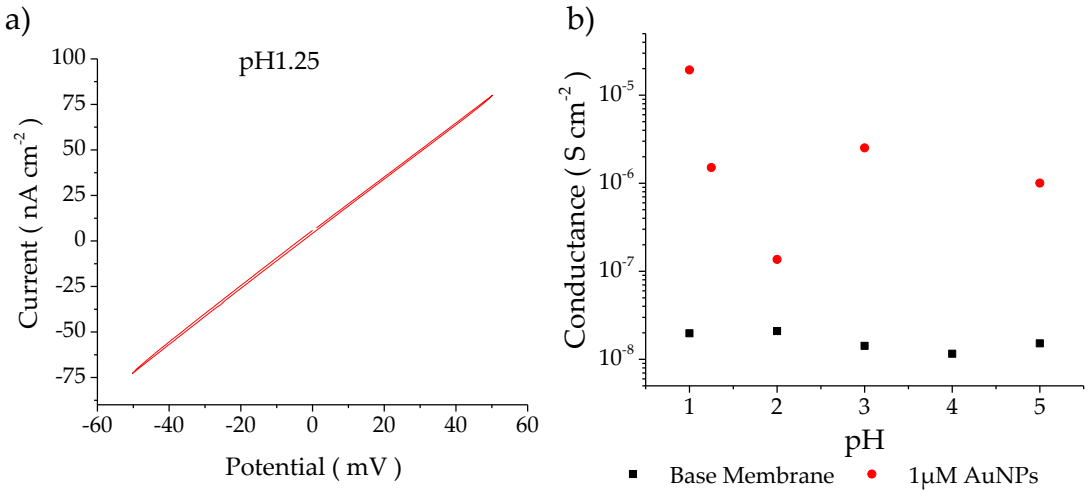

Figure 5. 4 – (a) CV of a pH1.25 membrane with 1 μM crown-AuNPs both sides of the membrane. (b) The conductance of the membranes at various pHs with (red) and without (black) 1 μM crown-AuNPs.

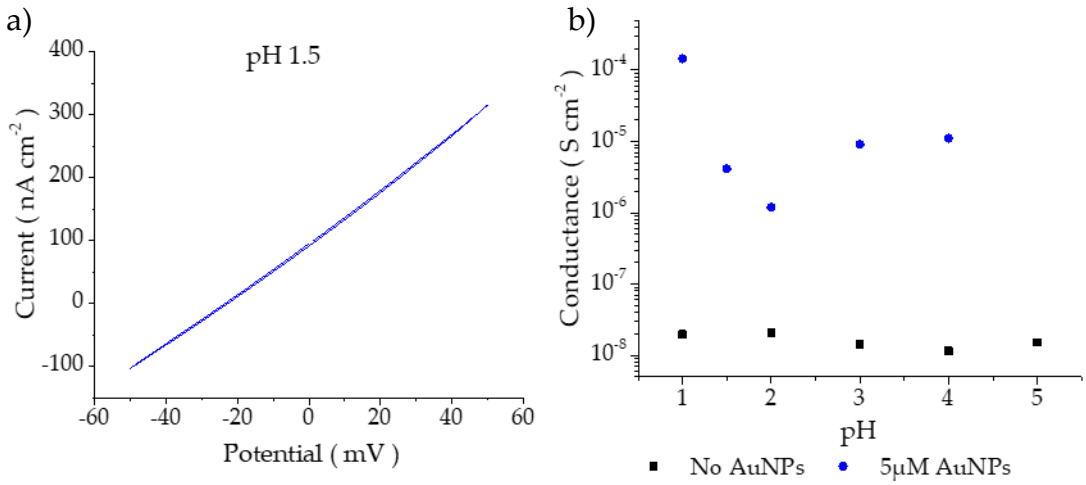

Figure 5. 5 – (a) CV of a pH1.5 membrane with 5 µM crown-AuNPs both sides of the membrane. (b) The conductance of the membranes at various pHs with (blue) and without (black) 5 µM crown-AuNPs.

For the 5 µM crown-AuNPs solutions, pH1.5 was studied, as it was the mean absolute pH value between pH1 and pH2 (Figure 5. 5). The conductance calculated for the pH1.5 membrane was 4.15 µScm^{-2} (3.s.f). Much like the 1 µM solution between these two pHs, the conductance increase was not linearly proportional to the square root of the H^+ concentration, but the logarithm of

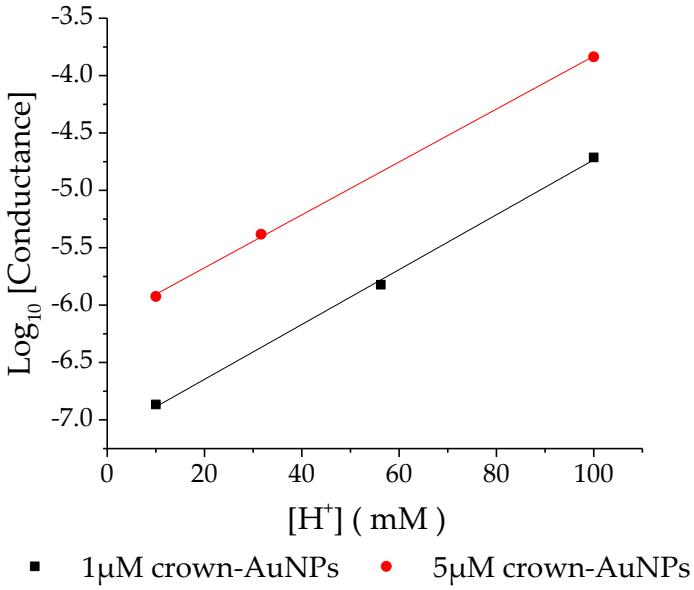

Figure 5. 6 – Plot showing the linear proportionality of Log_{10} [Conductance] vs H^+ concentration between pH1 and pH2 for both 1 µM (black) and 5 µM (red) crown-AuNP concentrations.

the conductance was linearly proportional to the H^+ concentration. The data was plotted, and the linear increase seen was the same for both 1 μM and 5 μM crown-AuNP solutions (Figure 5. 6). The difference in the intercept of the lines of best fit signalled that the increases in conductance were ten times higher for the 5 μM crown-AuNP solutions compared to the 1 μM crown-AuNP solutions. The linear relationship seen between the conductance and proton concentration observed between pH2 and pH1, at least, shows that the crown-AuNPs could be acting as a proton transporter.

5.2.1.4 – Comparison between 1 μM and 5 μM Crown-AuNP Solutions

All of the previous CV data was collected, calculating the conductance through the membrane and plotting conductance values against the pH (Figure 5. 7) to see if any trends could be identified. Firstly, the graph shows that increasing the crown-AuNP concentration in the electrolytes leads to an overall increase in conductance. Comparing the increase in conductance at pH levels of 1, 2, and 3, the average increase in conductance by increasing the crown-AuNP concentration 5-fold leads to a 6.61-fold increase, and whilst averaging only 3 data points is not ideal and the margin of error is large (±2.69), this never-the-less indicates that these crown-AuNPs are indeed the cause of the increase in conductance and that this increase is no artefact.

It is observed that for both sets of crown-AuNP concentration data, the pattern in conductance across the membrane at the different pHs is repeated. The difference between pH1 and pH2 for each set is similar: the pH1 membrane is 142 times more conductive than the pH2 membrane for 1 μM solutions, and it is 122 times more conductive for the 5 μM solutions.

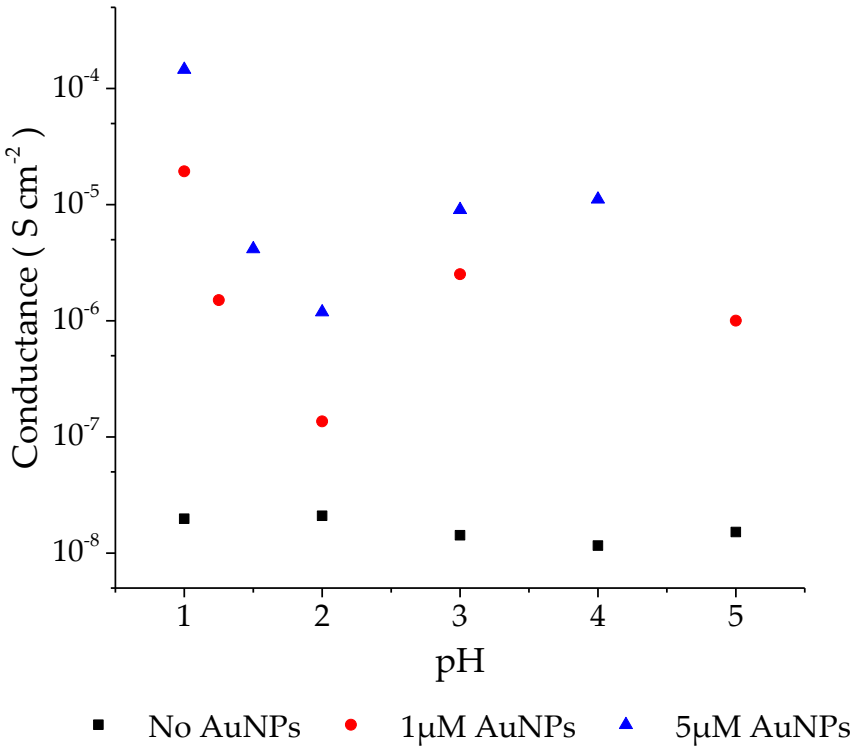

Figure 5. 7 – All conductance data for the membranes across pH 1 to 5 with crown-AuNPs both sides. The 5 μM crown-AuNP (blue) and 1 μM crown-AuNP solutions (red) both allow more current through than the standard membranes (black), with a similar profile across the different pHs.

5.2.2 – Crown-AuNPs on One Side Only

By running experiments with crown-AuNPs only on one side of the membrane, other insights into the process of the charge transfer could be gained. Firstly, to investigate whether the crown-AuNPs behave differently at different pHs. This may be seen through the possible movement of the CV, indicating a change in the zero-current potential across the membrane. Secondly, to discover whether only one of the polarisations of the R.E. 1, negative or positive, would see an increase in current, suggesting that the current may not be able to flow from the side that has no crown-AuNPs in the solution. The experiments were carried out on the two extremes of proton concentrations up to this point, pH1 and pH5, as the effect should be most pronounced when comparing the two extremes solutions (Figure 5. 8).

For pH1, the conductance of the system (calculated as the slope of the respective graphs) is lower when the crown AuNPs are only on one side of the membrane, having decreased from 1.94 μScm^{-2} with crown-AuNPs on both sides to 0.623 μScm^{-2}. For pH5, the conductance was also observed to decrease when crown-AuNPs were only on one side, from 1.00 μScm^{-2} to 0.310 μScm^{-2}, a similar decrease to a third. The conductance decrease is larger than expected given that the total crown-AuNPs at the membrane should have only decreased by half. The large decrease could be an indicator that there is a less energetic pathway for charge transport when there are crown-AuNPs in close proximity to one another on either side of the membrane. This could also explain why the conductance appeared to increase by more than five times, when the concentration of crown-AuNPs on both sides was five times higher in Section 5.2.1.4.

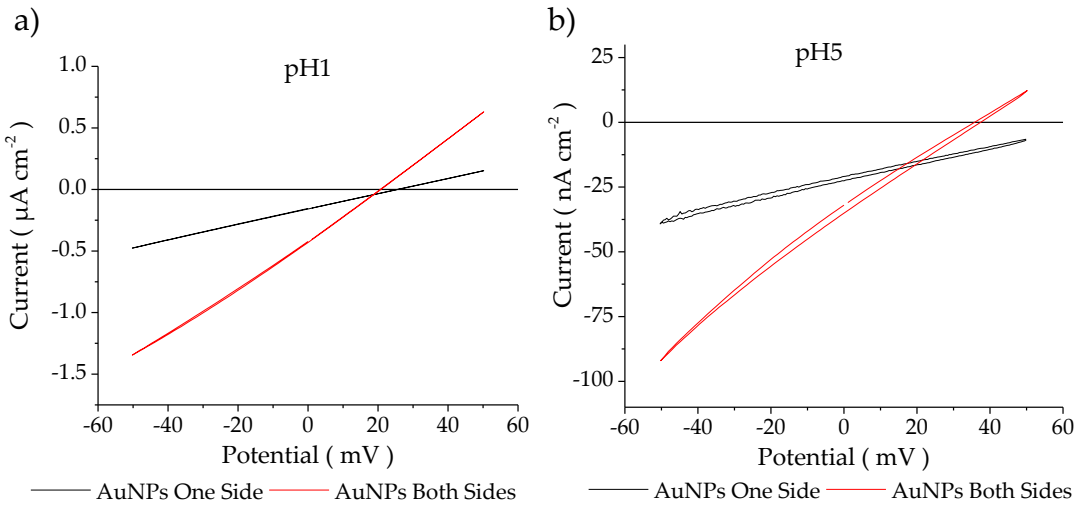

Figure 5. 8 – CVs comparing the current through a phospholipid membrane when crown-AuNPs are on one side of the membrane (black) or both sides (red) at (a) pH1 and (b) pH5. Y=0 has been added to help show the shift in the zero-current potential.

There is also a small shift in the zero-current potential of +4.5 mV for pH1 solutions. This can be explained in one of two opposing ways: the change in zero current potential is negligible since the charge on the crown-AuNPs is deemed to be close to zero, and it is not the partitioning of the crown-AuNPs that has caused this shift; it may well be experimental potential drift due to the relatively high currents flowing through the system beginning to affect the non-polarisable electrodes.

Alternatively, the crown-AuNPs could hold an extremely large negative charge. The Nernst-Donnan equation states that as the charge of a partitioning molecule increases, the potential shift decreases, and so the small change in the zero-current potential for the infinitely high ratio of AuNPs on one side compared to the other would mean the partitioning molecules must have a high charge. This explanation can be discounted given the expectation that the AuNPs will have more protons complexed at pH1 than at pH5, which will mean that they are more positively charged. Since highly negatively charged AuNPs should, also, not be able to pass through the hydrophobic region of the membrane, the possible explanation that the shift in zero-current potential

is due to the crown-AuNPs being highly negatively charged at pH1 seems unlikely.

For pH5 however, there is a large shift in the zero-current potential. Unfortunately, the potential window of ±50 mV that was studied did not cover the point at which the zero-current potential occurred, but by using a linear fit the potential value was calculated to be 72.5 mV, a shift of +35.5 mV from that measured for the same membrane with crown-AuNPs both sides. A positive shift with the crown-AuNPs on the working electrode side of the membrane, in the chamber solution, indicates that the crown-AuNPs should be negatively charged at pH5.

The CVs only show a shift in the potential, and the conductance is not dependent on the polarity of the membrane. This indicates that the crown-AuNPs are able to influence charge transport in both directions while only being present on one side of the membrane.

5.3 – Potential Measurements

5.3.1 – Differing crown-AuNP Concentration

It was observed that the zero-current potential differed when the crown-AuNPs were only on one side of membrane compared to when they were on both sides of the membrane. Therefore, it should be possible to calculate the charge on the crown-AuNPs by measuring the zero-current potentials for different ratios of crown-AuNP concentrations, and then using the Nernst-Donnan equation (Eq. 6) to calculate the charge on the crown-AuNPs, much as was done for gramicidin and the carb-AuNPs in Sections 3.3.3 and 4.3.1, respectively.

At pH2, the three concentrations of crown-AuNPs used were 10 μM, 1 μM and 0.1 μM, with the chamber solution (R.E. 1 side) remaining the same for

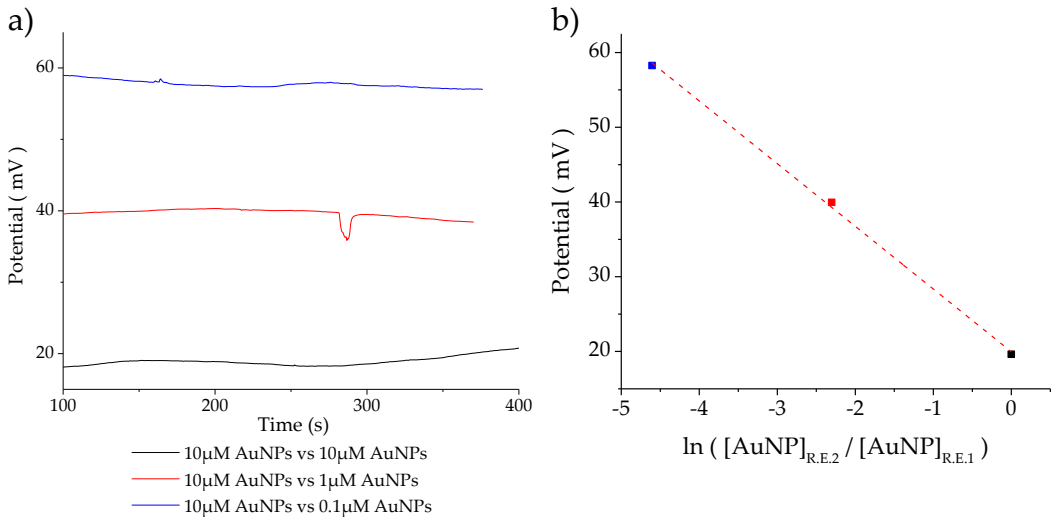

Figure 5. 9 – (a) Measurements of the zero-current potential using three different ratios of crown-AuNPs across the membrane. (b) The average potential measured from those experiments as a Nernst plot using crown-AuNPs as the partitioning species with a straight line fit to the data that was used to calculate the charge.

all solutions, at 10 μM, and the droplet solution being changed for each measurement. A Nernst plot using the average potential of the recordings was generated, and linear behaviour was seen (Figure 5. 9). The charge calculated for the crown-AuNPs at pH2 was -3.06. The crown-AuNPs are able to partition in a similar manner to the carb-AuNPs. The complexation seems to be more efficient though, as the charge of -3 was achieved at an electrolyte concentration of complexing ion ten times lower than the same charge for the carb-AuNPs in Section 4.3.1.1.

5.3.2 – Varying the pH

If and how the potential changed with different pHs was also investigated. Depending on how the potential changed, the results could give valuable information about how the crown-AuNPs interact with protons, and how the protons contribute to the currents seen in the CV measurements. If the charge calculated from the Nernst plot would be around +1, then it would be a clear sign that the protons are being transported by the crown-AuNPs across the membrane.

The potential measurements using pH2 to pH6 were used to produce a Nernst plot for H^+ (Figure 5. 10). The droplet solution was replaced whilst keeping the chamber solution constant at pH2. The Nernst plot did give a linear relationship, however, the charge associated with the potential changes was +2.18. As this does not correspond to the charge on the proton, other partitioning effects must be affecting the potential. This could be the chloride ions, but it may also be the crown-AuNPs themselves. These have already

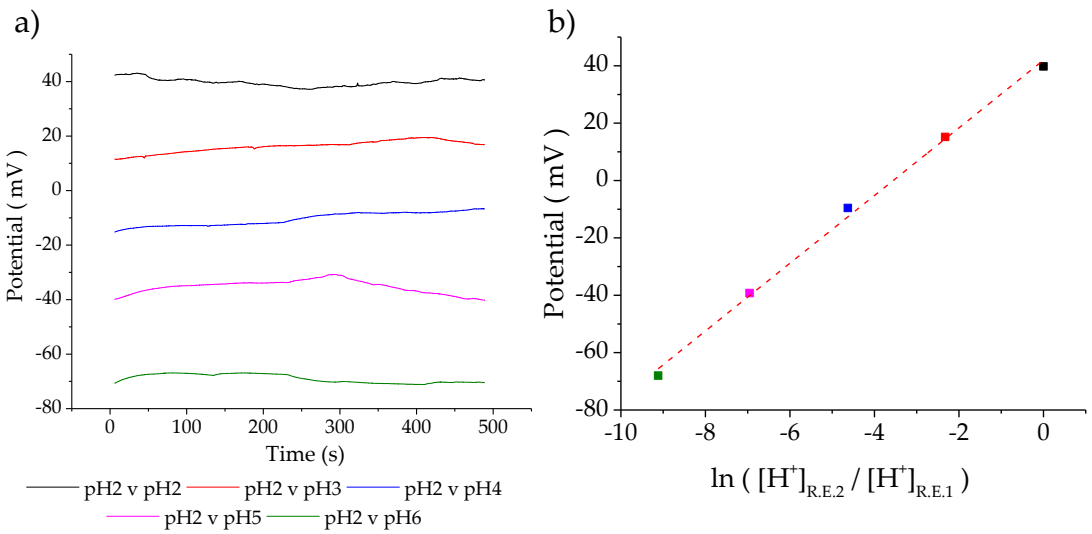

Figure 5. 10 – (a) Measurements of the zero-current potential when a pH gradient was present across the membrane. (b) Nernst plot for the corresponding average potentials with a straight line fit to the data that was used to calculate the charge.

been shown to be able to partition, and the charge may be influenced by the surrounding H^+ concentration.

5.4 – Zeta Potential Measurements

As previous experiments have shown, since the crown-AuNPs also seem to affect the membrane potential, creating a membrane potential of their own when the crown-AuNP concentration differs either side of the membrane, the charge on the crown-AuNPs carries its own importance. As trying to calculate the charges on the crown-AuNPs from the Nernst-Donnan plots would require a large number of membrane experiments for each concentration of protons, the ζ-potential of the crown-AuNPs was measured in different pHs as an indicator of the actual charge on the complex.

The data confirmed that the crown-AuNPs do have a charge associated with them, also confirming that should the crown-AuNP partition, a membrane potential would be expected if the concentrations differed across the divide. This corroborates the potentiometric measurements undertaken in Section 5.3.1.

The results also showed that the charge on the crown-AuNPs varied with the concentration of protons in solution (Figure 5. 11). The crown-AuNPs start as a highly negative charge in the low proton concentrations thought to be caused by the free valence electrons from the Au core of the NP. As the concentration is increased and more protons are complexed by the 12-crown-4 ligands, the charge on the whole crown-AuNP becomes more and more positive. The charge appears to linearly depend on the pH of the solutions, which suggests that it should be possible to reverse the polarity on the crown-AuNPs and make them significantly positively charged at high proton concentrations (~pH1). A linear fit of the pH data suggests that the crown-AuNPs have zero ζ-potential at ~pH2.2.

There is a known limitation of the zeta equipment, it being unable to calculate the ζ-potential of substances in highly conductive solutions, pH2 being on the cusp of being considered too conductive. Consequently, an increase in H^+ concentration meant that the equipment could not return a reliable measurement at pH1, and as a result, the ζ-potential of the crown-AuNPs at that point could not be ascertained.

The charge on the crown-AuNPs calculated from the potentiometry data does not agree with the data measured here, with the ζ-potential measured at pH2 to be +2.17, whereas the charge calculated from the slope of the Nernst-Donnan graph was -3.05. For the charges to be a different polarity is irregular. The accuracy of the results for values at pH2 may also be influenced by the conductance issues that affect the Zetasizer and may be in doubt.

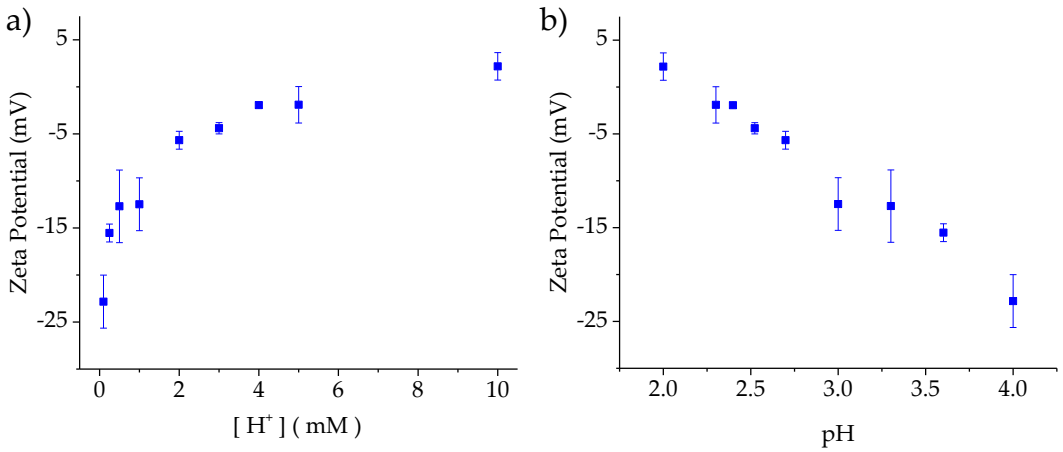

Figure 5. 11 – ζ-potential data of crown-AuNPs in different proton concentration environments. (a) ζ-potential as a function of proton concentration. (b) ζ-potential as a function of the pH of the solutions.

5.5 – First Hypothesis: Charged Carriers

The crown-AuNPs have been shown to increase the conductance through the membrane and to establish potentials across the membrane. Determining the mechanism for this was the next important process.

The current data suggests that the crown-AuNPs complex protons, where they are also themselves charged, penetrating and passing through the membrane, causing larger currents to flow through the membrane (Figure 5. 12). The charge on the crown-AuNP will change as the pH changes as seen from the ζ-potential experiments, where a higher absolute charge on the crown-AuNP should mean a higher possible current travelling through the membrane.

The current minimum seen at pH2, assuming that the crown-AuNPs continue to complex protons and the ligands have not yet become completely saturated at pH2, might be attributed to the particles being of near-zero charge in this environment. As such, they should be relatively unaffected by the potential bias applied across the membrane and so will not travel through it. As there is still an increase in current even at near-zero ζ-potential with the addition of crown-AuNPs to the solutions, it has been proposed that this corresponds to the small population of crown-AuNPs, assuming a Gaussian distribution, that are still charged enough to contribute to current flow through the membrane.

Decreasing the H^+ concentration from pH 2, the conductance increases, as the crown-AuNPs are in a state where they possess a negative charge that is small enough to allow them to penetrate through the membrane, but large enough to become a significant contributor to the current flowing through the membrane. The results show that pH4 produces a higher charge on the crown-AuNPs, and also a higher conductance through the membrane compared to pH3, which is in line with this thinking. pH5, however, is less conductive than

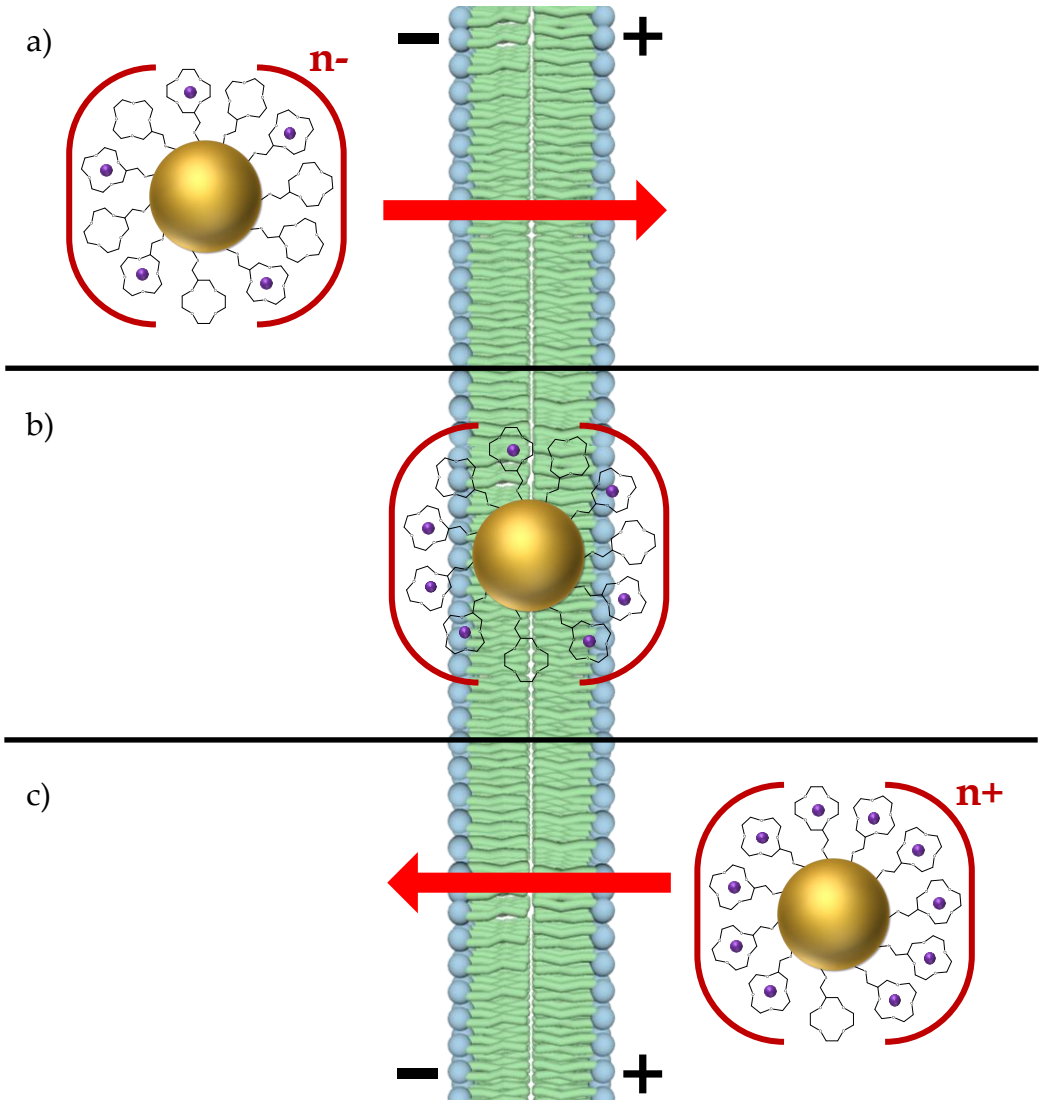

Figure 5. 12 – Proposed mechanism of charge transport through the membrane based on the first hypothesis. (a) At low H^+ concentrations (pH3, 4, and 5) the crown-AuNPs (gold circles) are not able to complex many H^+ ion (purple circles) and are negatively charged polyanions that are able to diffuse through the membrane and can contribute to current through the membrane under an applied potential. (b) At ~pH2, the crown-AuNPs hold enough protons and becomes neutral, and so are not affected by the applied potential and do not contribute to current passing through the membrane. (c) At higher H^+ concentrations (pH1) the crown-AuNPs are loaded with enough H+ ions so that they become positively charged, and so are affected by the applied potential and diffuse across the membrane.

pHs 4 and 3, even though it has a larger charge associated with it. Membranes are hydrophobic, and although many computational studies and experimental results conclude that small crown-AuNPs can travel through the membrane, it is likely that the larger the charge the crown-AuNPs exhibit, the less chance of them penetrating through the membrane. The decrease in conductance in pH5 solution is thought to be attributed to the charge of the crown-AuNPs becoming too large, and the possibility of translocation across the membrane becoming smaller, to the extent that the increase in charge on the crown-AuNPs does not compensate for the fall in the number of crown-AuNPs transferred, and so the overall increase in conductance decreases.

At pH1, the crown-AuNPs show an increase in conductance as they do at pH levels above 2, but instead of having a negative charge, it is thought that they have a positive charge, assuming the charge continues to follow the trend seen from the ζ-potential measurements. It would be expected to see a similar magnitude of charge at pH1 as that at pH3, which would then mean that the conductance should be also similar in magnitude. When looking at the deviation from the minimum conductance at pH2, there is an accelerated increase in conductance as the H^+ concentration is increased to pH1 compared to the gentler increase in conductance as the H^+ concentration is decreased to pH3. The phospholipids used in these membranes, asolectin, have negatively charged head groups, and so the positively charged particles at the lower pHs would be more electrostatically attracted to the membrane and be much more likely to go towards the membrane interface than a negatively charged crown-AuNP at the higher pHs. This increase in the population of crown-AuNPs at the interface would lead to an increase in the number of charge carriers participating in the current flow, increasing the conductance through the membrane.

The increase in conductance at pH1 could also be due to the positively charged crown-AuNPs causing pores to form in the membrane, which has been seen in other studies[118,119]. These pores would disrupt the membrane, allowing ions and water to flow through whilst the pore is open, increasing the conductance through the device. As the conductance through a pore would be proportional to the conductance of the solution, pH1 solutions would have a much higher conductance than pH3 solutions.

However, there are still things that this theory does not explain, such as why the potential shift with crown-AuNPs only one side of the membrane at pH1 is small and positive when it should be large and negative. To try and get a better understanding of how the crown-AuNPs behave at pH1 compared to the other proton concentrations, further investigation was warranted.

5.6 – Phase Transfer Experiments

To see whether the charge on the particles affected the propensity of the crown-AuNPs to go to the membrane, a small set of phase transfer experiments were undertaken. The hope being that the lower the charge a crown-AuNP carried, the more likely it would be to travel to the organic solvent or the phase boundary. Since the ζ-potential at pH1 could not be measured by the Zetasizer due to conductivity issues, this would also be useful to see whether the crown-AuNPs at pH1 behaved more like an uncharged crown-AuNP, as at pH2, or a charged crown-AuNP, as at pH3.

5.6.1 – Optical Experiments

When the solutions were first made, as noted in Section 2.4.3.1, observationally there was no difference between each solution, with the crown-AuNPs remaining in the aqueous phase and seemingly not interacting with the decane or the phase boundary (Figure 5. 13a). After three hours, the solutions were shaken manually to induce droplet formation, increasing the surface area of the phase boundary interface. It can be seen (Figure 5. 13b) that the colours of the pH1 and pH2 solutions are much lighter than before, meaning the crown-AuNPs must have either gone to the decane or the boundary interface. The top portion of the decane, however, shows little colouration and so it seems more likely that the crown-AuNPs have gone to the interface between the water and the decane, and a darker colour between

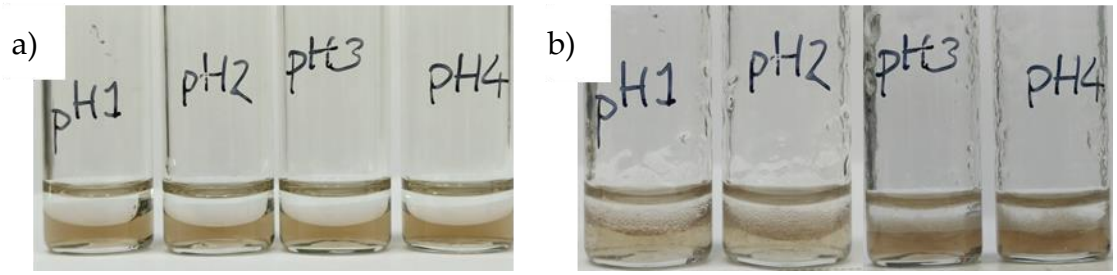

Figure 5. 13 – Photographs of the crown-AuNP solutions at different pHs with a layer of decane on the top of the solutions. (a) The solutions when they were first made, without any mixing. (b) The same crown-AuNP solutions that had been left for three hours and then shaken for 30 seconds.

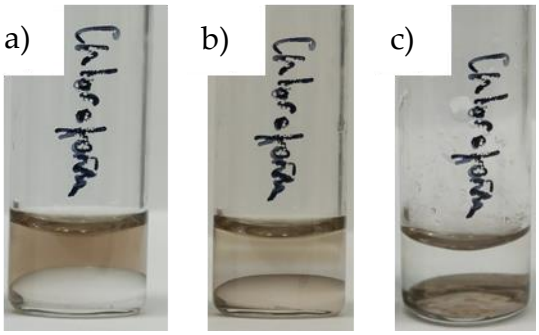

Figure 5. 14 – Crown-AuNP transfer from pH1 Milli-Q water (top phase) to chloroform (bottom phase). (a) The solution when it was first prepared. (b) One hour later, a depletion region can be seen above the phase separation. (c) One day later, the crown-AuNPs have completely transferred to the chloroform phase.

the two phases can be seen. As no crown-AuNPs go into the highly hydrophobic decane, it is unlikely that the crown-AuNPs will fully position themselves in a membrane's hydrophobic region.

The crown-AuNPs do however go into chloroform, an organic solvent less polar than water (Figure 5. 14), so it may be possible that the crown-AuNPs could partially interact with the hydrophobic regions.

The four decane solutions were checked again five days later to see whether the same behaviour occurred and to see whether the stability of the highly complexed crown-AuNPs in aqueous media had deteriorated enough for aggregation to occur. It can be seen that all of the droplets from the shaking have collapsed and that the decane phase is free from crown-AuNPs as it is

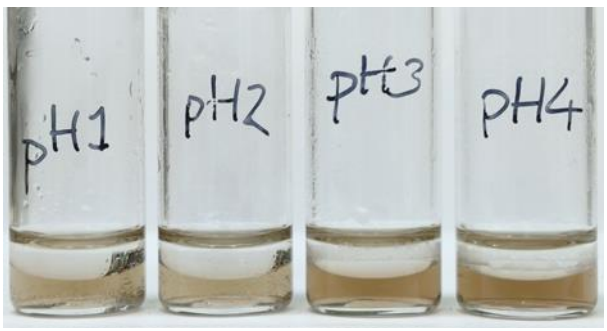

Figure 5. 15 – Photographs of the crown-AuNP solutions that have been left for 5 days. It can be seen that the decane phase is clear of crown-AuNPs

still colourless (Figure 5. 15). All the solutions remain the characteristic brown colour for AuNPs of 2-3 nm diameter size, and no red/blue colouration, which would be a sign that agglomeration/aggregation had happened, can be seen. There are no indications that the crown-AuNPs have aggregated and precipitated out of solution either, with no particulates at the bottom of the vial. The solutions for pH1 and pH2 are not as saturated as pH3 and pH4 as evidenced by the paler colour of the solution which means that some of the crown-AuNPs are still remaining at the interface, confirming that the crown-AuNPs of lower charge are more likely to migrate to the membrane.

The crown-AuNP solutions at pH1 did aggregate after a long period of time, as when the solutions were checked again after a few months, the solutions had become completely clear, and a purple residue was seen on the walls of the glass vial, indicating that the crown-AuNPs had accumulated there. This behaviour of sticking to the container walls has also been seen with larger, 7.5 nm 12-crown-4-functionalised AuNPs resulting in the coating of glass vials and plastic Eppendorfs[142]. It is thought that the 2-3 nm crown-AuNPs had become unstable due to increased hydrophobicity, agglomerated and then adhered to the surface of the container.

5.6.2 – UV-Vis

As was seen from the photographs above in Section 5.6.1, the intensity in the colour of the aqueous solutions decreased after the rapid shaking, with the crown-AuNPs presumably going to the aqueous-organic interface. It is also apparent that the colour of the pH1 and pH2 solutions is much less intense compared to the pH3 and pH4 solutions. To get a numerical measurement of this difference, UV-Vis spectra were run on both standard and latent solutions prepared in accordance with Section 2.4.3.2. The absorbance value at 400 nm was then used to compare the concentrations of crown-AuNPs in the solutions, compared with the same dilution of the stock solution using Milli-Q water.

The standard solutions of the crown-AuNPs all showed a small decrease in absorbance compared to the stock solution (Figure 5. 16). The decrease was greatest for pH1 and pH2 solutions. This may be an indication that as the

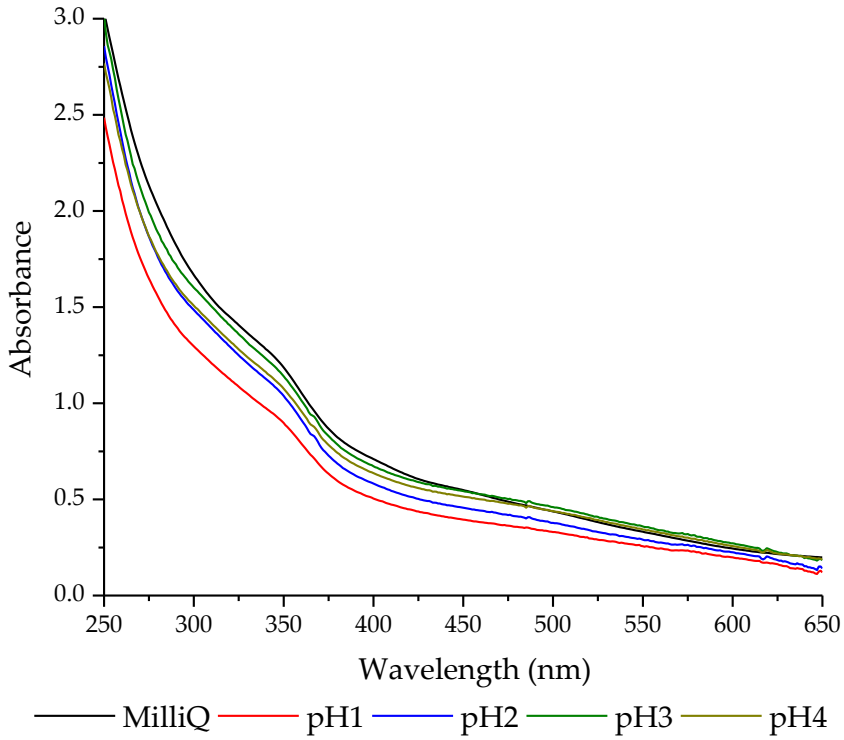

Figure 5. 16 – UV-Vis spectra of all "standard solutions", alongside the Milli-Q stock dilution (black).

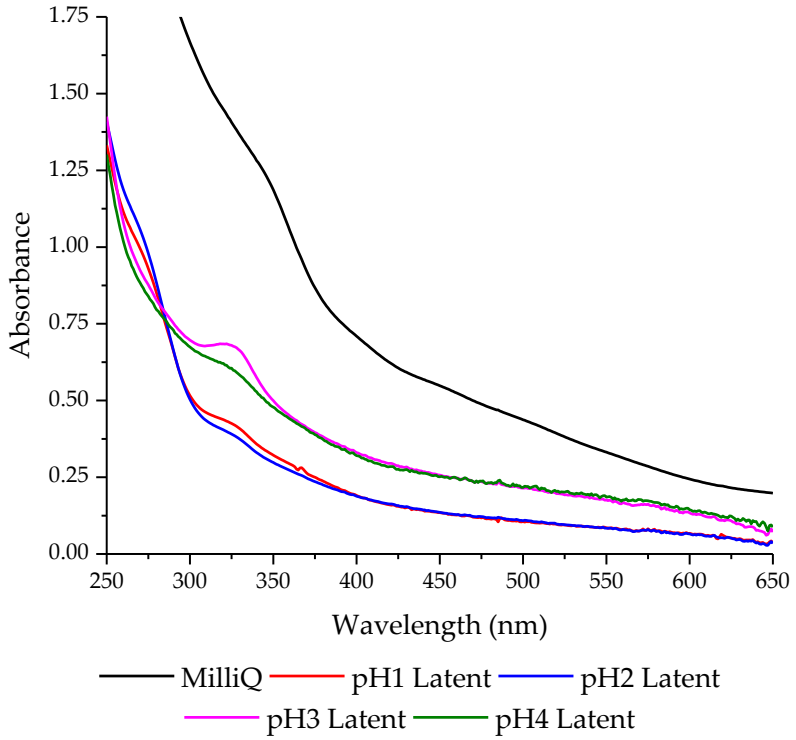

Figure 5. 17 – UV-Vis spectra of all of the latent crown-AuNP solutions and the Milli-Q stock dilution (black). For clarity of the latent solutions, absorbance of over 1.75 for the Milli-Q stock dilution is not shown.

charge on the crown-AuNPs tends to zero, the crown-AuNPs become hydrophobic and become less and less soluble in the Milli-Q water, leading to either particle aggregation, agglomeration, or a large number of crown-AuNPs situated at the water-air interface, removing themselves from solution. The overall shapes of the spectra do not change though, with the same slight rise at around 350 nm present in all crown-ether samples. It is not known exactly what causes this. The peak seems to be resolved much before the absorbance at 400 nm, and so it should not affect the calculations of the concentrations. As the rise is not affected by the pH, it does not seem to be a peak arising from proton complexation, and so will not be investigated further.

In comparison, the latent solutions of crown-AuNPs show significant changes compared to the stock solution (Figure 5. 17). They all show much lower

absorbance, indicative of a lower concentration of crown-AuNPs in the solution. The absorbance of pH1 and pH2, however, are markedly lower than those of both pH3 and pH4 for most of the plot. There seem to be two distinct regions, a clear change in behaviour for the crown-AuNPs at pH1 and pH2, compared to pH3 and pH4. This shows that at pH2 and higher H^+ concentrations, the crown-AuNPs exhibit more hydrophobic behaviour. It is interesting that for the latent solutions, no gradual change is seen in the propensity of the crown-AuNPs to position at the interface with increasing proton concentration. It is also surprising that when shaken, most of the AuNPs for both pH3 and pH4 are residing at the interface, even with the relatively high ζ-potential.

Although the cause of the peaks below 350 nm is unknown, it is interesting that the pH3 latent solution has a much more enhanced peak at ~325 nm, and that a second peak can be seen for both the pH1 and pH2 latent solutions at ~260 nm. The additional peak for pH1 and pH2 could be due to interactions with the oxygen atoms in the ether ring complexing protons which are known to be active around the ~290 nm region for 18-crown-6 systems[164]. However, it could also be due to rogue solvent droplet effects that have been accidentally transferred during pipetting. A more thorough study using UV-Vis methods as the primary analytical technique would be useful, but as these experiments were to focus on the change in concentrations of crown-AuNPs in the solutions, such a study was not carried out.

To calculate what percentage of crown-AuNPs remained in the solutions compared to the same dilution of Milli-Q water, the absorbance value at 450 nm for all solutions was compared to the absorbance value for the stock solution at the same dilution (Table 5. 3). It can be seen that for the standard solutions, the largest number of crown-AuNPs that have been removed from the solutions occurred at pH1, where 72.0 % of the crown-AuNPs were

Table 5. 3 – Calculated percentage values of crown-AuNPs in the standard and latent solutions (3.s.f.), compared to the same factor dilution of stock AuNPs.

	pH1	pH2	pH3	pH4
Standard Solution / % AuNPs	72.0	83.4	99.1	93.9
Latent Solution / % AuNPs	24.6	24.8	46.9	45.9

remaining in solution, with a significant loss of crown-AuNPs also at pH2, presumably to either aggregation of the crown-AuNPs (although no increase in red/blue absorbances is observed in the spectra), or the assembling of crown-AuNPs at the air-water interface. In comparison, pH3 and pH4 have not lost as many crown-AuNPs, with both retaining above 90 %. The latent solutions all have considerably fewer crown-AuNPs in solution, with pH1 and pH2 solutions losing over 75 % of the particles to the boundary interface, and the pH3 and pH4 solutions each losing around 50 %.

It is seen from the standard solutions that at pH1 and pH2, the crown-AuNPs start to passively settle at the water-decane interface, suggesting that they are becoming hydrophobic in these solutions. This supports the ζ-potential results, assuming maximum complexation occurs at ~pH2. Upon agitation, the crown-AuNPs in all of the HCl solutions partially collect at the interface, with the highest percentage losses occurring in the pH1 and pH2 solutions.

5.7 – Second Hypothesis: Switchable Mechanism

The phase transfer experiments show two distinct regimes for crown-AuNP behaviour, where pH1 and pH2 solutions lose 75 % of their crown-AuNPs to the phase boundary and so are predominately hydrophobic, and the pH3 and pH4 solutions lose around half. The current hypothesis that the crown-AuNPs are poly-ions that charged complex H^+ ions (Section 5.5) does not explain why the crown-AuNPs at pH1 do not behave as they do at pH3 in the phase

transfer experiments and the CVs where there are crown-AuNPs on only one side of the membrane. If the currents seen for the pH1 solutions were due to the crown-AuNPs being positively charged, then they could be expected to remain in the aqueous phase much like the negatively charged crown-AuNPs at pH3 and pH4. This does not seem to be the case, however, and at ≤pH2, whether it be due to increased instability in aqueous media leading to their agglomerating together, or saturation of the available complexation sites on the crown-AuNPs, they do not become positively charged, and instead self-assemble at the phase interface.

This poses the question – why do crown-AuNPs in pH1 produce significantly more current than pH2 in Section 5.2? The only difference is the proton concentration, and so rather than the current depending solely on the charge of the crown-AuNP, it is clearly also dependent on the proton concentration, meaning that the crown-AuNPs may be acting as H^+ transporters.

5.7.1 – pH0 vs pH1 Potential Measurement

One way to investigate whether the AuNPs had become H^+ transporters at high H^+ concentrations was to measure the membrane potential whilst in this behavioural regime i.e. using pH1 and pH0. A membrane with 1 μM crown-AuNPs at pH1 on both sides of the membrane was set up, and the potential across the membrane measured to calculate the baseline for the particular device. The droplet solution was then removed, and a droplet of 1 μM crown-AuNPs at pH0 was added in its place. The potential was then re-measured. The Nernst-Donnan equation calculates that for ideal solutions, a ratio of ten times higher concentration on either side of the membrane would lead to a potential measured of ~±60 mV depending on which side the working electrode was placed. As the droplet electrolyte was the higher concentration

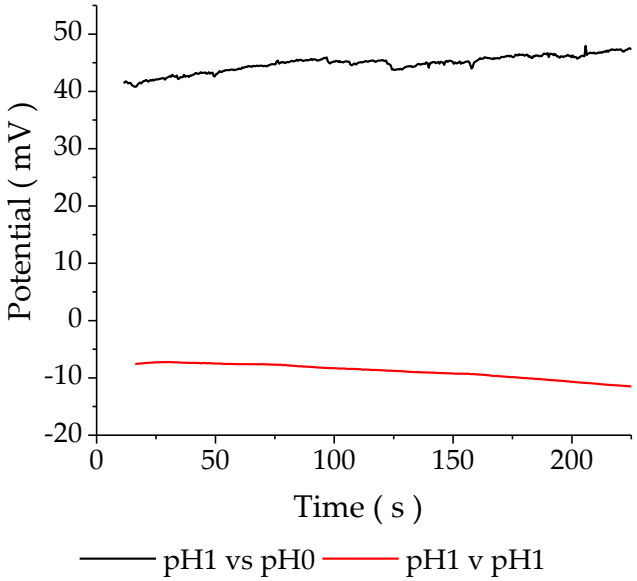

Figure 5. 18 – Potentiometry data measuring the membrane potential for the asymmetric pH1 vs pH0 (black) and symmetric pH1 (red) membranes.

of protons for the system being studied (the opposite side of the membrane to R.E. 1) a +60 mV potential change from the baseline would be expected.

The average potential was calculated for both membranes and a +53.8 mV shift in the potential was found, close to the expected result of +60 mV; much more in line with how a proton transporter would behave in the same situation (Figure 5. 18). The charge on the "proton" was calculated to be +1.10 (3.s.f), which is close to, but not equal to, the expected charge. It is thought that there are still some crown-AuNPs that are "counter-partitioning" and causing the potential of the membrane to not solely depend on the protons.

It is additionally thought that in keeping with the previous hypothesis, the crown-AuNPs act as a charged carrier at the low proton concentrations where they are negatively charged. However, when the crown-AuNPs become hydrophobic, the mechanism of charge transport changes. At ≤pH2, the increased complexation of positively charged protons cancels out the excess negative charge on the crown-AuNPs and they become hydrophobic, and so accumulate at the hydrophobic membrane. The 12-crown-4 ligands are then

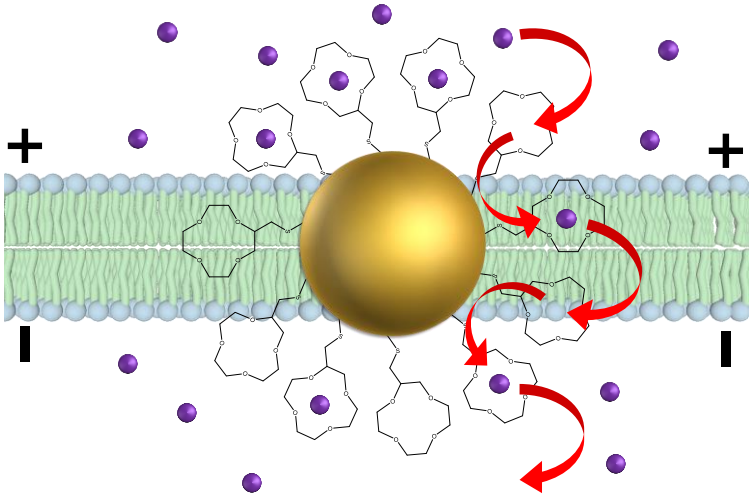

Figure 5. 19 – The alternative method of charge transport through the bilayer membrane via crown-AuNPs (gold circle). When the crown-AuNPs complex a sufficient number of H^+ ions (purple circles), they become hydrophobic and reside in the membrane. At this point, a pathway for the protons to travel across the membrane becomes available, hopping between the crown-ether ligands surrounding the Au core.

able to form a pathway for the protons to traverse and hop between each complexation site, travelling across the membrane in a similar way as how ions are transported through gramicidin channels (Figure 5. 19).

5.8 – Crown-AuNPs vs Gramicidin

Comparing the crown-AuNPs to gramicidin, it can be seen that the crown-AuNPs do not allow as much current through the membrane, but the current flow is still significant (Figure 5. 20). The large difference in mechanisms can also be appreciated by examining how they change in conductance with a change in proton concentration. Gramicidin, as discussed before, is a model channel ionophore: a protein that opens a pore in the membrane which allows monovalent cations and H_2O to travel through. The conductance through the membrane was proportional to the concentration of the ions in the solutions.

For the crown-AuNPs, the current is not proportional to the concentration of protons throughout. There is a local current minimum at pH2, where it is thought that the crown-AuNPs have a negligible charge, and so do not

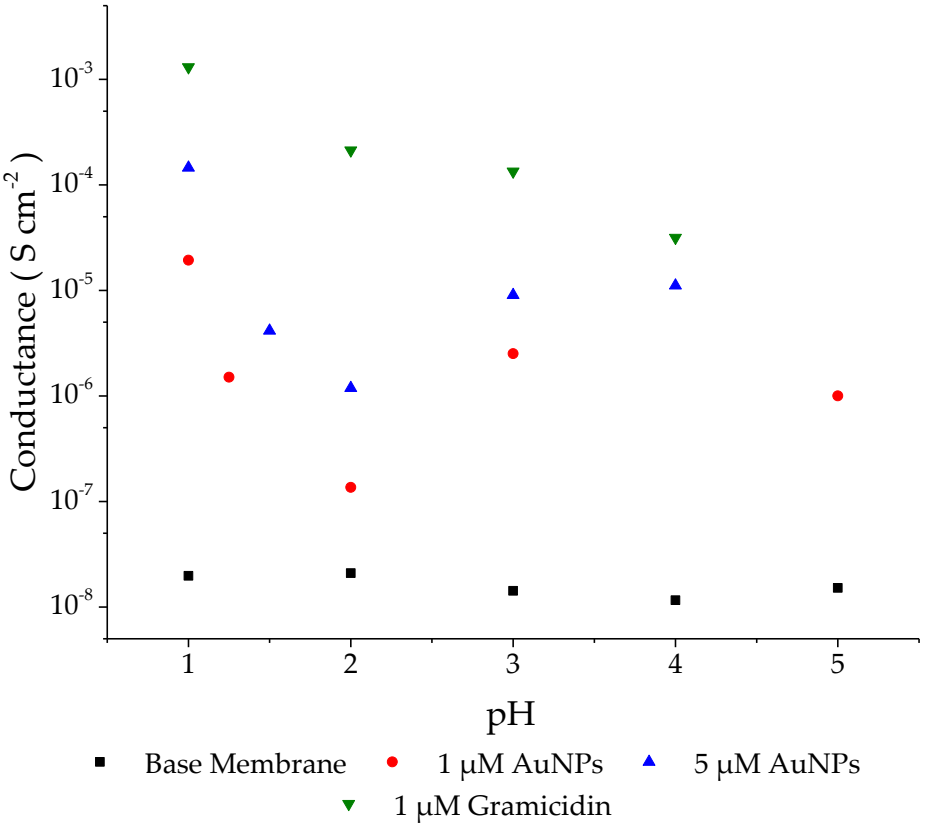

Figure 5. 20 – Comparison of the conductance per area through a membrane between the crown-AuNPs (red and blue) and gramicidin (green), as well as the un-modified membrane (black).

significantly contribute to the current, and the protons are not in a large enough concentration to give a high current.

The conductance of the membrane using 1 μM gramicidin is higher than that of the AuNPs across the range of pHs tested, even when using 5 μM crown-AuNPs. Whilst it is disappointing that the AuNPs do not behave as well as the natural ionophore, the conductance through the membrane due to the crown-AuNPs is still highly significant.

5.9 – Electron Transfer Study

Having obtained a general understanding of how the crown-AuNPs worked at the different pHs, an experiment that would test if the crown-AuNPs could act as a nanowire through the membrane and facilitate electron transfer across the membrane was attempted. For electron transfer to be viable, it was thought that the crown-AuNPs would need to be situated at or in the membrane, and so, the best solution would be to use the crown-AuNPs at pH2. At pH2, the crown-AuNPs are thought to become hydrophobic and go to the phase boundary interface, as seen from the UV-Vis experiments, but here they have also been shown to have the lowest ion/particle transfer. An increase in conductance through the membrane due to electron transfer would be easier to identify using the lowest conducting membrane. For these reasons, it was thought that using the crown-AuNPs at pH2 would lead to the best chance at seeing electron transfer across the membrane. The redox couple that was chosen to be the analyte was hexa-ammine ruthenium ($2^+/3^+$) chlorides. The ferro/ferri couple was not selected for use, as that couple was found to have an effect on the proton concentration of the solutions.

A simple way to establish whether electron transport occurs is to allow electrons to travel one in one direction only. This is done by separating the redox couple across the membrane. When Ru^{2+} is on one side and Ru^{3+} is on

the other, the redox reaction can only occur in the direction where the electron is transferring from Ru^{2+} to Ru^{3+} and not the other way around. This will mean that the current should be much higher when the electrodes are polarised in a way that facilitates the electron transfer, than when the polarity is the opposite and hinders it. Separate experiments with the Ru^{2+} on the chamber/R.E. 1 side of the membrane and the Ru^{3+} on the droplet/R.E. 2 side, and then vice versa, were then attempted.

It was seen that, for both experiments, there is an effect on the current measured with the addition of the ruthenium redox couple. The current when either redox couple is present is much lower than the currents seen when only H^+ was present, suggesting that the redox couple may either interfere with the membrane transfer process or interfere with the complexation of the protons with the crown-AuNPs. However, it was seen that when both redox ions were present, Ru^{2+} on the R.E.1 side and Ru^{3+} on the R.E.2 side, there is a shift

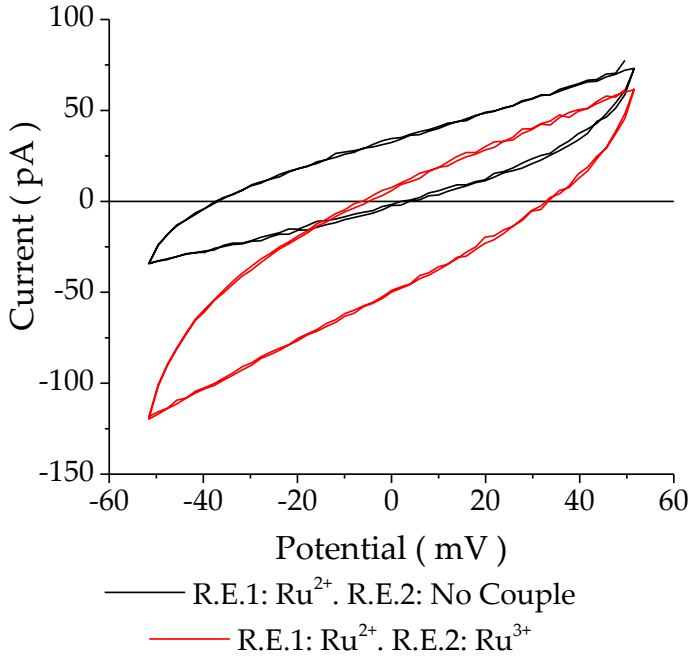

Figure 5. 21 – CVs comparing the current through a pH2 membrane with only Ru^{2+} on the R.E.1 side (black) against when Ru^{2+} is on the R.E. 1 side of the membrane and Ru^{3+} is on the R.E. 2 side (red), in the presence of 1 μM crown-AuNP on both sides of the membrane.

towards a positive potential (Figure 5. 21). This is the expected shift in potential for electrons transferring across the membrane from R.E. 1 to R.E. 2. However, whether this is electron transport or ion transport is hard to distinguish, as it could be an effect of the different interactions between the crown-AuNPs and each part of the redox couple.

The shifting of the zero-current potential and steady change in current seen when Ru^{2+} is on the R.E. 1 side suggest the crown-AuNPs act as an intermediary; a crown-AuNP getting reduced by the Ru^{2+} in the aqueous solution on one side of the membrane, transferring through the membrane and then reducing Ru^{3+} on the other side. There could be a problem if the reduced crown-AuNP is not able to pass through the membrane. However, since the crown-AuNPs appear to be able to cross the membrane for the large range of ζ-potentials across the pH range studied, this is not an issue here.

When the ruthenium complexes are reversed, the reverse effect on the CVs is not seen, which is surprising. Instead, there is an intriguing distortion when the applied potential would facilitate electron transfer in the appropriate direction, from the Ru^{2+} to the Ru^{3+} ions (Figure 5. 22).

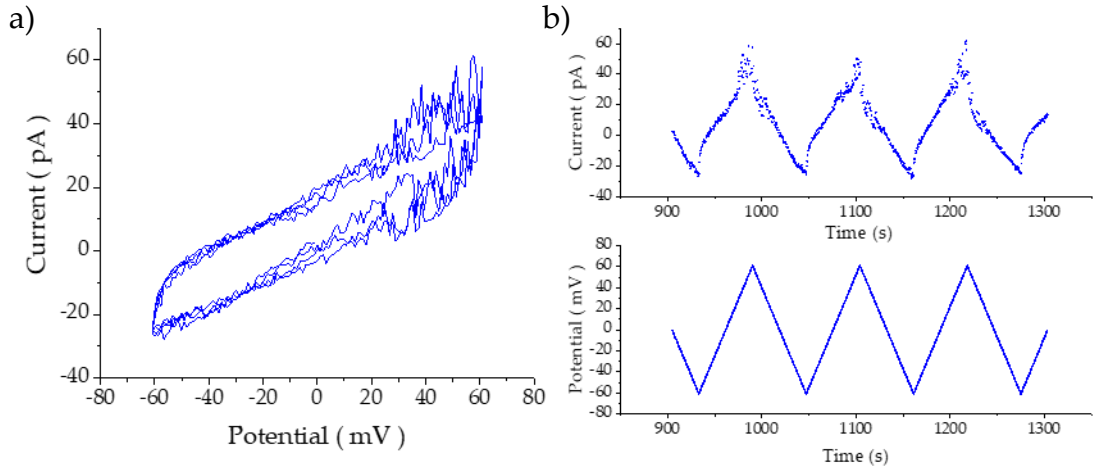

Figure 5. 22 – (a) CVs of a pH2 membrane with Ru^{3+} on the R.E. 1 side of the membrane and Ru^{2+} on the R.E. 2 side, (b) Top: The same CVs but as an I vs t plot. Bottom: The potential trace of the experiment to match the data above.

The sharp increases in current seen in the later measurement would imply an alternative mechanism – the crown-AuNPs may act as nano-wires for a brief period. When the crown-AuNPs are in the correct position inside the membrane, and a Ru^{2+} and a Ru^{3+} also position themselves in tunnelling range for an electron to pass to or from the crown-AuNP at the same time, a chain reaction might occur, and the electron would essentially pass from the Ru^{2+} to the Ru^{3+} without causing a reduction in the crown-AuNP. This would mean that the transfer of electrons would only be possible for a brief moment, which would lead to current spikes seen in the latter, rather than an increase in the continuous current which is seen in the former measurement.

A hypothesis as to why the two results are so different is that the two electrolyte solutions are not identical, as well as the solubility of the two ruthenium complexes also not being identical. The Ru (II) hexamine complex is only slightly soluble in H_2O, which may cause an issue when it is used as the droplet solution connected to R.E.2. The small volume of the droplet solution coupled with the slight solubility of Ru^{2+} may mean that an extremely small amount of Ru^{2+} is available to transfer the electrons and so the occurrence is rare, and spikes are seen. It would be interesting to see the results of these experiments using the aperture membrane formation method to identify whether the asymmetric solutions were the cause of the different CV profiles.

5.10 – Chapter 5 Conclusions

Proton transfer across membranes is of vital importance in biology and mimicking this process with a metallic crown-AuNP functionalised with a crown-ether ligand was attempted. What was found was that the crown-AuNPs did cause an increase in conductance through the membrane and that this conductance changed with the proton concentration in solution.

The crown-AuNPs were seen to be able to bind the protons, forming a crown-AuNP-proton complex; where the charge on the complex would change depending on the concentration of protons available in the surrounding medium. The crown-AuNP-proton complexes could then translocate across the membrane. This type of behaviour is similar to the carrier ionophore valinomycin, a potassium ion-selective transporter, but with the differences that there are multiple complexation sites on the crown-AuNPs, rather than the single guest-site for valinomycin, and the crown-AuNPs have an inherent charge associated with them, where they also are a contributor to the current through the membrane.

This was valid for the slightly acidic solutions, (pH3 and pH4) but when the proton concentrations were higher (pH1 and pH2), the mechanism seemed to change. The crown-AuNPs became hydrophobic at this complexation, where the positive charge on all the protons cancelled out the inherent negative charge on the crown-AuNPs. With the crown-AuNPs now hydrophobic, they were thought to be more attracted to the membrane than previously and would accumulate at the aqueous-membrane interface. It is unknown whether the crown-AuNPs could be situated in the hydrophobic part of the membrane for a long period of time. The large increase in the conductance through the membrane for pH1 vs pH2, even though the crown-AuNPs seemed to behave similarly in the phase transfer experiments, could indicate that the transport of an increased number of protons through the membrane was occurring.

Whilst this is not a standard type of proton transport seen with natural ionophores, the ability for the crown-AuNPs to complex protons and to move through membranes is clearly demonstrated.

Chapter 6 – Summary, Further Work and Conclusions

6.1 – Summary

Given that defective biological ionophores are the cause of multiple diseases, this research was undertaken in the hope that it would contribute to the development of artificial ion channels and carriers to mimic biological charge transport, providing new information to expedite possible treatment of such diseases.

As well-known facilitators of drug delivery via mediated endo- and exocytosis, AuNPs were selected for investigation since little is known about their ionophoric properties. The interactions between biological membranes and AuNPs is of high interest to multiple research disciplines and the presence of the metallic core may present a novel route for coupled electron-ion transfer in biological systems that is unique for metallic nanoparticles.

The first necessary objective was the preparation of a platform that could interrogate phospholipid bilayer membranes electrochemically. Two separate methods of membrane formation were used, the aperture-style method based around Montal and Mueller's work from the 1960 s, and the D.I.B. method popularised by Bayley *et al* more recently. The physical properties (resistance and capacitance) of the membranes were calculated using CVs and/or potential step experiments. They were found to be concordant with the surrounding literature. To verify that the membranes produced could be used for the forthcoming charge transport studies, the natural ionophore gramicidin was used as a model. When gramicidin was present, an increase in conductance was seen through the membranes. Blocking of the channel and Nernst-Donnan behaviour was observed using the Aperture and D.I.B. membranes, respectively.

Once the electrochemical platforms had been successfully verified, two types of functionalised 2-3nm AuNPs were tested. The first AuNPs analysed were functionalised with a mercapto-carborane ligand. These carb-AuNPs were known to trap ions within core-shell voids created by the packing around the AuNP of the spherical ligands. Using potential step experiments, it was found that the addition of carb-AuNPs to the electrolyte solutions increased the currents through the membrane. The increase in current measured was dependent on the identity of the ions present on either side of the membrane and the selectivity of the carb-AuNPs was calculated using the zero-current potentials. Currents through the membrane were much higher when an electrochemical gradient was present across the membrane. The charge of the carb-AuNPs was calculated in various ionic solutions assuming Nernst-Donnan behaviour. However, a linear relationship between potential and the logarithm of the carb-AuNP ratio was not observed for all systems, and results from that particular segment should be only used as a guideline.

The other type of AuNPs were examined as prospective H^+ carriers. Functionalised with 12-Crown-4-CH_2-SH, the cyclic voltammograms revealed an increase in conductance through the membrane when the crown-AuNPs were present. This increase in conductance was dependent on both the crown-AuNP and H^+ concentrations, with higher concentrations of each leading to larger increases in current passing through the membrane. The ability to change the ζ-potential of the crown-AuNPs in solutions at various H^+ concentrations was also identified. For high proton concentrations, the degree of complexation was enough that the crown-AuNPs exhibited a ζ-potential of zero. The mechanism of charge transport across the membrane was theorised using the CVs, potential measurements, UV-Vis and ζ-potential measurements. It is believed that at low H^+ concentrations, the crown-AuNP complexes are able to pass through the membrane when a potential is applied.

At high H^+ concentrations, they become hydrophobic and insert themselves into the membrane. The crown ether ligands are then in the correct position to form a channel to allow H^+ transport across the membrane. It was thought that these crown-AuNPs could still be electron active due to the small size of the 12-Crown-4 ligand. Electron transfer was attempted using the hexammineruthenium (II/III) redox couple at pH2, when the AuNPs were thought to be situated in the membrane. The results proved inconclusive. There was a change in the current response through the circuit when both of the redox complexes were present either side of the membrane which could indicate some form of electron transfer was occurring, however, when the solutions were reversed, the effect on the current was not.

Although not described in great detail, the 3D-printing within the project to create the electrochemical platforms provided additional challenges. Designing the electrochemical cells with the ability to test them immediately was of great use. The intrinsic limitations of the D.L.P. 3D printer caused periods of frustration at times and experimenting with the printing resolution and resins took more time than expected. However, using the modelling software Blender to design the electrochemical cells, whilst not the most important, was an unexpectedly enjoyable part of the project.

Difficulties were encountered in ensuring the homogeneity of test solutions being used and also in maintaining the structural integrity of the membranes under experimentation. However, there is reason to believe that further work will establish the suitability of AuNPs to provide another sought-after artificial route for electron transfer across biological membranes.

6.2 – Further Work

6.2.1 – Transport using Non-invasive Techniques

Techniques which do not employ an external applied force to probe the ability of the AuNPs to transfer charge would be able to provide complementary data to the findings seen in this thesis. Fluorescence spectroscopy could be used to monitor the potential of the membrane by utilising a potential-sensitive fluorescent dye, such as Safranin-O[165], and would allow more information to be obtained about the mechanism of transport at different H^+ concentrations. If the crown-AuNPs become hydrophobic at high H^+ concentrations and act as channels as hypothesised, ion transport down a concentration gradient should be feasible and could be identified by the polarisation of a membrane using the fluorescent dye. Equally, if this was not the case, information could still be collected. For example, if the AuNPs still acted as poly-anions that pass through the membranes themselves, spontaneous membrane crossing of a charged AuNP without an external driving force like the one created by the potentiostat may not occur. Consequently, a membrane potential would not be observed in that situation.

6.2.2 – Ion Specificity/UV-Vis Study

Having studied various ions using the carb-AuNPs and seen a variance in currents and potentials produced, it would be of interest to do the same with the crown-AuNPs, with special mention of using lithium, the more commonly known complexation molecule for the 12-Crown-4 ligand. This could be done in the same way as the carb-AuNPs, where each side of the membrane has a higher concentration of one ion than the other.

It may also be useful to attempt the UV-Vis study mentioned in Section 5.6.2, to discover whether the peaks could be assigned to complexation of protons.

A prominent peak was observed at ~325 nm in the UV-Vis spectra for the 12-crown-4 functionalised AuNPs when in the presence of HCl (Section 5.6.2). If the peak was due to some form of proton complexation, it may be interesting to study how the peak changed with proton concentration. The study could also be broadened to investigate whether different ions affected the peak which could then be used to identify relative complexation specificity. This could then be extended to other crown ether ligands, to see if it is possible to use crown ether-functionalised AuNPs as specific ion sensors.

6.2.3 – Anion Transport

Throughout the project, all ion transport was focused on cation transport, but anion transport would also be a valid method of transport to investigate. Many biological processes rely on the transport of anions across bilayers. However, if attempting to use the same methods as applied in this research, the complexation of anions would make the inherently negative AuNPs even more negatively charged. This would pose a challenge as the complexes would be unlikely to cross a membrane. It may be possible that a positively charged ligand could compensate for the extra negative charge.

6.2.4 – Ligand-Gated AuNP Ionophores

Preparing AuNPs that become hydrophobic in the presence of certain molecules could lead to gated ionophore analogues which could be created by coupling a complexing ligand. Switchable hydrophobicity has already been developed using dynamic covalent bond formations, and AuNPs could become active as ionophores due to *in situ* ligand exchange[166]. If the exchanges could be tailored to only occur when in a targeted region or cell, it could increase the therapeutic effectiveness, or reduce the toxicity of prospective biologically active AuNPs.

6.2.5 – Electron Transport

Although attempted briefly using crown-AuNPs without positive results, the possibility of electron transport across a phospholipid bilayer using metallic nanoparticles still exists. The degree of variation possible when using metallic nanoparticles is huge; properties including shape, size, composition, hydrophobicity, and co-ordinating ligand can be controlled, and a small modification in any of these could cause significant variance in performance. Whilst the 2-3 nm functionalised AuNPs used in this thesis have been shown to transport various ions, they were primarily chosen for their ability to permeate across the membrane and may not have been the optimal AuNPs for electron transport. There are inherent characteristics a single nanoparticle would need to possess to function as a nanowire.

To act in the envisioned way, they would need to reside in the membrane and consequently would need to be hydrophobic. To make an AuNP hydrophobic, organic ligands such as alkane-thiols or PEG are usually required to prevent the electron-rich gold core from interacting with the solution. This unfortunately usually results in blocking the electronic activity of the AuNP. Using an organic-soluble redox couple functionalised with a thiol to act as a ligand may be a potential solution, producing a hydrophobic AuNP whilst keeping the electronic activity of the metallic core available.

The AuNP would also need to be large enough to ensure an accessible electroactive site on either side of the membrane which could be influenced by the potential of the solutions on both sides of the membrane. With the phospholipid membrane thickness of around 4 nm, the AuNP core would have to be >4 nm to connect both solutions. A larger AuNP would also be more stable when separating solutions of differing potential with a larger distance between the two potential states.

To produce a single AuNP that would satisfy all the criteria with a single ligand may not be possible. It may therefore also be useful to look at particles using a combination of different ligands, each with a specific purpose. Janus particles have become a recent topic of interest in the nanoparticle community, creating particles with double functionalities (Figure 6. 1). If it were possible to create a half-hydrophobic, half-hydrophilic particle where the electronic activity of the metallic core was still accessible on the hydrophilic side of the AuNP and the other hydrophobic side situated in the membrane, this could resolve some of the problems that occur for organic-soluble nanoparticles. The transfer of electrons across the membrane would revolve around electron tunnelling across two particles, which, depending on the size of the hydrophobic ligand, could be a problem. It may even be possible to make bilayer membranes consisting solely of Janus particles. It would also be interesting to see whether a particle with three bands of hydrophobicity could be created, where the two "poles" of the particle were electronically active, but the equator would be positioned in the membrane.

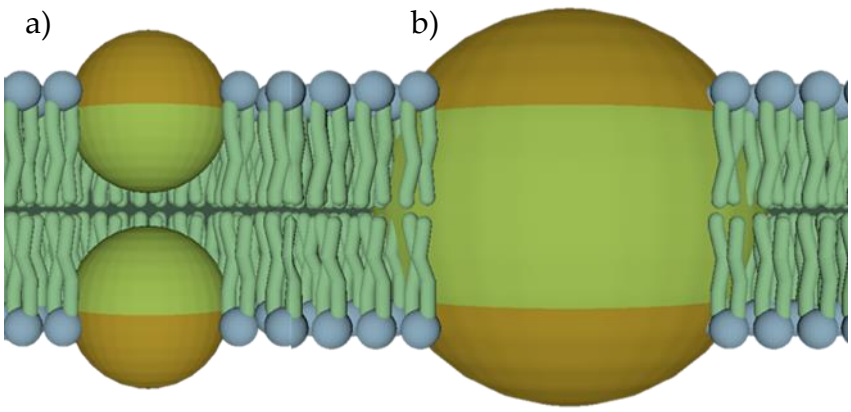

Figure 6. 1 – (a) Two Janus AuNPs positioned in the membrane that may allow electron tunnelling to occur. (b) A large AuNP that has a hydrophobic band while the two "poles" are still electronically active.

Rather than using one particle with many ligands, it could be also of interest to look at systems using more than one type of AuNP, each with its own unique ligand. Each AuNP would satisfy one of the criteria needed for an active nanowire to traverse the membrane. A system, perhaps, where one AuNP (the function of which would be to sit at or in the membrane) was joined or tethered to another AuNP which would function as the electro-active site (where a redox reaction could occur). The short distance between the particles, or the linking ligand used, could allow electrons to travel between the two particles. If this could be achieved on both sides of the membrane using two AuNPs in a "handcuff" style, or 3+ "chain" of AuNPs, electron transport across the membrane could be achieved, without having to compromise membrane structural integrity by using a large membrane-spanning nanoparticle (Figure 6. 2).

Whichever the case, be it finding an ideal ligand, using multiple ligands and controlling ligand placement on the AuNP, or by using a multi-AuNP system

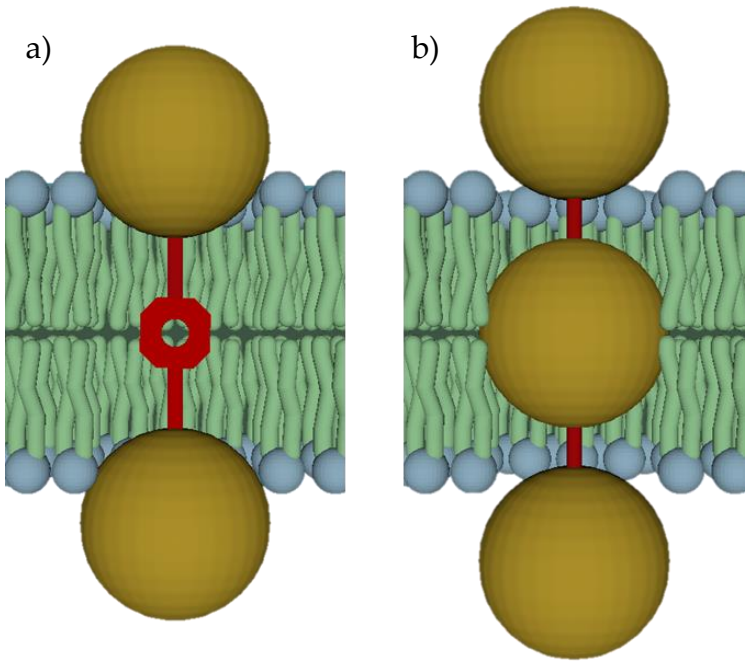

Figure 6. 2 – (a) "Handcuffed" and (b) "Chain" AuNPs could present possible routes towards electron transport though a membrane using metallic nanoparticles.

each performing a necessary function that together achieve the objective, the possibility of electron transfer across a biological membrane using metallic nanoparticles merits further investigation.

6.2.6 – Compartmentalised Energy Converting Systems

An exciting use for particles capable of transporting ions across membranes would be coupling the transport of ions to another process, analogous to the electron transport chain and ATP synthase. Converting the entropic energy gained by the transport of ions down a concentration gradient into other forms of energy to drive unfavourable processes, such as pumping ions against their concentration gradient and forming high-energy bonds would be a huge accomplishment. Or vice versa, utilising energy from a favourable process such as barium sulphate precipitation to pump ions up an electrochemical gradient or to force a redox reaction to occur. Work towards this aim has already begun.

6.3 – Final Conclusions

The primary thesis aim was the electrochemical analysis of prospective functionalised AuNPs with regard to facilitating charge transfer across phospholipid membranes. This was achieved using two phospholipid bilayer preparative methods, and two distinct functionalised AuNPs were analysed. The first AuNPs used mercapto-carborane and the second used 12-crown-4-CH2-SH as ligands, and they were found to transport ions and protons across model membranes, respectively.

Carb-AuNPs were found to increase the conductance of the bilayer membranes and are thought to be able to transport monovalent cations across the membranes via a shuttle mechanism. They exhibited selectivity with increased conductance and zero-current potential shifts for certain ions, and it is thought to be related to ionic size, both hydrated and non-hydrated. They also caused membrane potentials to form when the concentrations of differed either side of the membrane.

Crown-AuNPs were used to transport protons across the membrane and are currently believed to have a switchable transport mechanism. At low proton concentrations, they seem to act as water-soluble membrane penetrating ion carriers, and at high proton concentrations, they become hydrophobic and situate themselves in the membrane and form ion channels.

The results of the work carried out in this project were encouraging and provide additional evidence of the likelihood that AuNPs can be developed to mimic biological charge transport, with the potential to contribute to treatments for diseases where such mechanisms are compromised. The work in this thesis will hopefully pave the way for further analysis on metallic nanoparticle-based analogues of ionophores and give insights into possible methods for electron transporters. Although electron transport could not be

achieved conclusively, a cell-membrane nanowire has great implications within biological and electronic disciplines.

List of Figures

Chapter 1:

Chapter 2:

Chapter 3:

Chapter 4:

Chapter 5:

Chapter 6:

List of Tables

Chapter 1:

Chapter 3:

Chapter 4:

Chapter 5:

References

1. J. C. Freedman, *Cell Membranes*, Elsevier, 2012.
2. S. H. White and T. E. Thompson, *BBA - Biomembr.*, 1973, **323**, 7–22.
3. W. Stillwell, in *An Introduction to Biological Membranes*, Elsevier, 2016, 135–180.
4. H. T. Tien, *J. Mol. Biol.*, 1966, **16**, 577–580.
5. P. Sonksen and J. Sonksen, *Br. J. Anaesth.*, 2000, **85**, 69–79.
6. H. Schagger, W. A. Cramer and G. Vonjagow, *Anal. Biochem.*, 1994, **217**, 220–230.
7. B. M. Burkhart, R. M. Gassman, D. A. Langs, W. A. Pangborn, W. L. Duax and V. Pletnev, *Biopolym. - Pept. Sci. Sect.*, 1999, **51**, 129–144.
8. D. A. Kelkar and A. Chattopadhyay, *Biochim. Biophys. Acta - Biomembr.*, 2007, **1768**, 2011–2025.
9. J. Antoinette Killian, *Biochim. Biophys. Acta - Rev. Biomembr.*, 1992, **1113**, 391–425.
10. A. Finkelstein and O. S. Andersen, *J. Membr. Biol.*, 1981, **59**, 155–171.
11. W. K. Lee and P. C. Jordan, *Biophys. J.*, 1984, **46**, 805–819.
12. V. B. Myers and D. A. Haydon, *BBA - Biomembr.*, 1972, **274**, 313–322.
13. E. Bamberg and P. Läuger, *J. Membr. Biol.*, 1977, **35**, 351–375.
14. J. Sandblom, G. Eisenman and E. Neher, *J. Membr. Biol.*, 1977, **31**, 383–417.
15. Y. Marcus, *Chem. Rev.*, 1988, **88**, 1475–1498.
16. D. W. Smith, *J. Chem. Educ.*, 1977, **54**, 540–542.
17. R. D. Shannon, *Acta Crystallogr.*, 1976, **A32**, 751.
18. G. Eisenman, J. Sandblom and E. Neher, *Biophys. J.*, 1978, **22**, 307–340.
19. N. Agmon, *Chem. Phys. Lett.*, 1995, **244**, 456–462.
20. G. Stark, B. Ketterer, R. Benz and P. Läuger, *Biophys. J.*, 1971, **11**, 981–994.
21. A. E. Vallejo and C. A. Gervasi, *J. Electroanal. Chem.*, 2007, **603**, 51–58.
22. O. Shirai, H. Yamana, T. Ohnuki, Y. Yoshida and S. Kihara, *J. Electroanal. Chem.*, 2004, **570**, 219–226.
23. Z. F. Su, X. Q. Ran, J. J. Leitch, A. L. Schwan, R. Faragher and J. Lipkowski, *Langmuir*, 2019, **35**, 16935–16943.
24. P. L. Yeagle, *Struct. Biol. Membr. Third Ed.*, 2011, 7–12.
25. U. Brandt, *Annu. Rev. Biochem.*, 2006, **75**, 69–92.
26. B. P. O. Sullivan and S. D. Freedman, *Lancet*, 2009, **373**, 1891–1904.
27. X. Ma and Y. Zhao, *Chem. Rev.*, 2015, **115**, 7794–7839.
28. S. Negin, B. A. Smith, A. Unger, W. M. Leevy and G. W. Gokel, *Int. J. Biomed. Imaging*, 2013, **2013**, 1–11.
29. H. Valkenier, C. M. Dias, C. P. Butts and A. P. Davis, *Tetrahedron*, 2017,

73, 4955–4962.
30. J.-M. Lehn, *Angew. Chemie Int. Ed. English*, 1988, **27**, 89–112.
31. S. Erbas-Cakmak, D. A. Leigh, C. T. McTernan and A. L. Nussbaumer, *Chem. Rev.*, 2015, **115**, 10081–10206.
32. N. Sakai and S. Matile, *Langmuir*, 2013, **29**, 9031–9040.
33. I. Tabushi, Y. Kuroda and K. Yokota, *Tetrahedron Lett.*, 1982, **23**, 4601–4604.
34. N. T. Lin, C. Y. Xie, S. L. Huang, C. H. Chen and T. Y. Luh, *Chem. - An Asian J.*, 2013, **8**, 1436–1440.
35. D. Montesarchio, C. Coppola, M. Boccalon and P. Tecilla, *Carbohydr. Res.*, 2012, **356**, 62–74.
36. W. Si, Z.-T. Li and J.-L. Hou, *Angew. Chemie Int. Ed.*, 2014, **53**, 4578–4581.
37. L. Chen, W. Si, L. Zhang, G. Tang, Z.-T. Li and J.-L. Hou, *J. Am. Chem. Soc.*, 2013, **135**, 2152–2155.
38. W.-X. Feng, Z. Sun and M. Barboiu, *Isr. J. Chem.*, 2018, **58**, 1209–1218.
39. W. X. Feng, Z. Sun, Y. Zhang, Y. M. Legrand, E. Petit, C. Y. Su and M. Barboiu, *Org. Lett.*, 2017, **19**, 1438–1441.
40. W. X. Feng, Z. Sun and M. Barboiu, *Isr. J. Chem.*, 2018, **58**, 1173–1182.
41. J. Y. Chen and J. L. Hou, *Org. Chem. Front.*, 2018, **5**, 1728–1736.
42. T. Ogoshi, N. Ueshima, F. Sakakibara, T. A. Yamagishi and T. Haino, *Org. Lett.*, 2014, **16**, 2896–2899.
43. P. Xin, H. Kong, Y. Sun, L. Zhao, H. Fang, H. Zhu, T. Jiang, J. Guo, Q. Zhang, W. Dong and C. Chen, *Angew. Chemie Int. Ed.*, 2019, **58**, 2779–2784.
44. I. Tabushi, Y. Kuroda and K. Yokota, *Tetrahedron Lett.*, 1982, **23**, 4601–4604.
45. M. J. Pregel, L. Jullien and J.-M. Lehn, *Angew. Chemie Int. Ed. English*, 1992, **31**, 1637–1640.
46. N. Madhavan, E. C. Robert and M. S. Gin, *Angew. Chemie Int. Ed.*, 2005, **44**, 7584–7587.
47. H. Mamad-Hemouch, L. Bacri, C. Huin, C. Przybylski, B. Thiébot, G. Patriarche, N. Jarroux and J. Pelta, *Nanoscale*, 2018, **10**, 15303–15316.
48. F. Ugozzoli, A. Casnati, A. Pochini, R. Ungaro, F. Arnaud, S. Fanni, M. J. Schwing, R. J. M. Egberink, F. de Jong and D. N. Reinhoudt, *J. Am. Chem. Soc.*, 1995, **117**, 2767–2777.
49. W. F. Nijenhuis, E. G. Buitenhuis, F. de Jong, D. N. Reinhoudt and E. J. R. Sudholter, *J. Am. Chem. Soc.*, 1991, **113**, 7963–7968.
50. Y. Okada, M. Mizutani and J. Nishimura, *Tetrahedron Lett.*, 1998, **39**, 8467–8470.
51. O. A. Okunola, J. L. Seganish, K. J. Salimian, P. Y. Zavalij and J. T. Davis, *Tetrahedron*, 2007, **63**, 10743–10750.
52. J. L. Seganish, J. C. Fettinger and J. T. Davis, *Supramolecular Chemistry*,

Taylor & Francis Group, 2006, **18**, 257–264.
53. S. Licen, V. Bagnacani, L. Baldini, A. Casnati, F. Sansone, M. Giannetto, P. Pengo and P. Tecilla, *Supramol. Chem.*, 2013, **25**, 631–640.
54. M. Shamsipur and M. Asgari, *Sensors Actuators B: Chemical*, 2015, **209**, 9-14
55. S. Howorka, *Nat. Nanotechnol.*, 2017, **12**, 619–630.
56. A. Alexeev, W. E. Uspal and A. C. Balazs, *ACS Nano*, 2008, **2**, 1117–1122.
57. V. Maingi, J. R. Burns, J. J. Uusitalo, S. Howorka, S. J. Marrink and M. S. P. Sansom, *Nat. Commun.*, 2017, **8**, 14784.
58. J. R. Burns, A. Seifert, N. Fertig and S. Howorka, *Nat. Nanotechnol.*, 2016, **11**, 152–156.
59. S. Howorka and Z. Siwy, *Chem. Soc. Rev.*, 2009, **38**, 2360–2384.
60. P. Li, G. Xie, X.-Y. Kong, Z. Zhang, K. Xiao, L. Wen and L. Jiang, *Angew. Chemie Int. Ed.*, 2016, **55**, 15637–15641.
61. G. W. Gokel and H. D. Durst, *Synthesis (Stuttg).*, 1976, **1976**, 168–184.
62. G. Wipff, P. Weiner and P. Kollman, *J. Am. Chem. Soc.*, 1982, **104**, 3249–3258.
63. G. W. Gokel, W. M. Leevy and M. E. Weber, *Chem. Rev.*, 2004, **104**, 2723–2750.
64. H. Sato, H. Hakamada, Y. Yamazaki, M. Uto, M. Sugawara and Y. Umezawa, *Biosens. Bioelectron.*, 1998, **13**, 1035–1046.
65. K. H. Wong, K. Yagi and J. Smid, *J. Membr. Biol.*, 1974, **18**, 379–397.
66. Q. Xie, Y. Li, G. Gokel, J. Hernández and L. Echegoyen, *J. Am. Chem. Soc.*, 1994, **116**, 690–696.
67. B. Dietrich, J. M. Lehn, J. P. Sauvage and J. Blanzat, *Tetrahedron*, 1973, **29**, 1629–1645.
68. J. H. Lee, J. H. Lee, Y. R. Choi, P. Kang, M. G. Choi and K. S. Jeong, *J. Org. Chem.*, 2014, **79**, 6403–6409.
69. J. García-Calvo, T. Torroba, V. Brañas-Fresnillo, G. Perdomo, I. Cózar-Castellano, Y. H. Li, Y. M. Legrand and M. Barboiu, *Chem. - A Eur. J.*, 2019, **25**, 9287–9294.
70. V. V. Teplova, R. Mikkola, A. A. Tonshin, N. E. L. Saris and M. S. Salkinoja-Salonen, *Toxicol. Appl. Pharmacol.*, 2006, **210**, 39–46.
71. B. Limburg, E. Bouwman and S. Bonnet, *Chem. Commun.*, 2015, **51**, 17128–17131.
72. G. Steinberg-Yfrach, P. A. Liddell, S. C. Hung, A. L. Moore, D. Gust and T. A. Moore, *Nature*, 1997, **385**, 239–241.
73. H. Imahori and Y. Sakata, *Eur. J. Org. Chem*, 1999, **1999**, 2445–2457.
74. M. Komatsu, T. Sagara and N. Nakashima, *J. Electrochem. Soc.*, 2002, **149**, 227–232.
75. K. M. Kadish and M. M. Morrison, *J. Am. Chem. Soc.*, 1976, **98**, 3326–3328.
76. J. N. Robinson and D. J. Cole-Hamilton, *Chem. Soc. Rev.*, 1991, **20**, 49.

77. P. Ghosh, G. Han, M. De, C. K. Kim and V. M. Rotello, *Adv. Drug Deliv. Rev.*, 2008, **60**, 1307–1315.
78. K. K. Sandhu, C. M. McIntosh, J. M. Simard, S. W. Smith and V. M. Rotello, *Bioconjug. Chem.*, 2002, **13**, 3–6.
79. M. De, P. S. Ghosh and V. M. Rotello, *Adv. Mater.*, 2008, **20**, 4225–4241.
80. M. Vert, Y. Doi, K. H. Hellwich, M. Hess, P. Hodge, P. Kubisa, M. Rinaudo and F. Schué, *Pure Appl. Chem.*, 2012, **84**, 377–410.
81. G. Li and R. Jin, *Acc. Chem. Res.*, 2013, **46**, 1749–1758.
82. S. Schlücker, *Angew. Chemie Int. Ed.*, 2014, **53**, 4756–4795.
83. I. Ojea-Jiménez and J. M. Campanera, *J. Phys. Chem. C*, 2012, **116**, 23682–23691.
84. P. Thoniyot, M. J. Tan, A. A. Karim, D. J. Young and X. J. Loh, *Adv. Sci.*, 2015, **2**, 1400010.
85. R. B. Grubbs, *Polym. Rev.*, 2007, **47**, 197–215.
86. E. Pensa, E. Cortés, G. Corthey, P. Carro, C. Vericat, M. H. Fonticelli, G. Benítez, A. A. Rubert and R. C. Salvarezza, *Acc. Chem. Res.*, 2012, **45**, 1183–1192.
87. J. C. Love, L. A. Estroff, J. K. Kriebel, R. G. Nuzzo and G. M. Whitesides, *Chem. Rev.*, 2005, **105**, 1103–1169.
88. A. Z. Wilczewska, K. Niemirowicz and K. H. Markiewicz, 2012, **64**, 1020–1037.
89. X. Liu, N. Huang, H. Li, Q. Jin and J. Ji, *Langmuir*, 2013, **29**, 9138–9148.
90. A. Albanese, P. S. Tang and W. C. W. Chan, *Annu. Rev. Biomed. Eng.*, 2012, **14**, 1–16.
91. S. Salatin, S. Maleki Dizaj and A. Yari Khosroushahi, *Cell Biol. Int.*, 2015, **39**, 881–890.
92. R. Gupta and B. Rai, *Sci. Rep.*, 2017, **7**, 45292.
93. Y. Li, X. Li, Z. Li and H. Gao, *Nanoscale*, 2012, **4**, 3768–3775.
94. J. Turkevich, P. C. Stevenson and J. Hillier, *J. Phys. Chem.*, 1953, **57**, 670–673.
95. R. P. Richter, R. Bérat and A. R. Brisson, *Langmuir*, 2006, **22**, 3497–3505.
96. J. Piella, N. G. Bastús and V. Puntes, *Chem. Mater.*, 2016, **28**, 1066–1075.
97. M. Brust, M. Walker, D. Bethell, D. J. Schiffrin and R. Whyman, *J. Chem. Soc., Chem. Commun.*, 1994, 801–802.
98. C. L. Lu, K. S. Prasad, H. L. Wu, J. A. A. Ho and M. H. Huang, *J. Am. Chem. Soc.*, 2010, **132**, 14546–14553.
99. I. Fratoddi, *Nanomaterials*, 2017, **8**, 11.
100. B. Nikoobakht and M. A. El-Sayed, *Chem. Mater.*, 2003, **15**, 1957–1962.
101. X. Huang, S. Neretina and M. A. El-Sayed, *Adv. Mater.*, 2009, **21**, 4880–4910.
102. P. Senthil Kumar, I. Pastoriza-Santos, B. Rodríguez-González, F. Javier García De Abajo and L. M. Liz-Marzán, *Nanotechnology*, 2008, **19**,

015606.
103. C. G. Khoury and T. Vo-Dinh, *J. Phys. Chem. C*, 2008, **112**, 18849–18859.
104. S. Huo, S. Jin, X. Ma, X. Xue, K. Yang, A. Kumar, P. C. Wang, J. Zhang, Z. Hu and X. J. Liang, *ACS Nano*, 2014, **8**, 5852–5862.
105. N. Li, P. Zhao and D. Astruc, *Angew. Chemie - Int. Ed.*, 2014, **53**, 1756–1789.
106. F. Della Sala and E. R. Kay, *Angew. Chemie - Int. Ed.*, 2015, **54**, 4187–4191.
107. S. Borsley and E. R. Kay, *Chem. Commun.*, 2016, **52**, 9117–9120.
108. M. I. Bodnarchuk, S. Yakunin, L. Piveteau and M. V. Kovalenko, *Nat. Commun.*, 2015, **6**, 1–8.
109. I. H. El-Sayed, X. Huang and M. A. El-Sayed, *Cancer Lett.*, 2006, **239**, 129–135.
110. J. Zhou, L. Du, L. Zou, Y. Zou, N. Hu and P. Wang, *Sensors Actuators B Chem.*, 2014, **197**, 220–227.
111. I. Canton and G. Battaglia, *Chem. Soc. Rev.*, 2012, **41**, 2718–2739.
112. E. Fröhlich, *Int. J. Nanomedicine*, 2012, **7**, 5577-5591.
113. G. J. Gordillo, Ž. Krpetić and M. Brust, *ACS Nano*, 2014, **8**, 6074–6080.
114. L. A. Dykman and N. G. Khlebtsov, *Chem. Rev.*, 2014, **114**, 1258–1288.
115. B. D. Chithrani, A. A. Ghazani and W. C. W. Chan, *Nano Lett.*, 2006, **6**, 662–668.
116. A. R. Mhashal and S. Roy, *PLoS One*, 2014, **9** (12), e114152.
117. C. M. Goodman, C. D. McCusker, T. Yilmaz and V. M. Rotello, *Bioconjug. Chem.*, 2004, **15**, 897–900.
118. P. R. Leroueil, S. A. Berry, K. Duthie, G. Han, V. M. Rotello, D. Q. McNerny, J. R. Baker, B. G. Orr and M. M. B. Holl, *Nano Lett.*, 2008, **8**, 420–424.
119. B. Lu, T. Smith and J. J. Schmidt, *Nanoscale*, 2015, **7**, 7858–7866.
120. O. P. Hamill, A. Marty, E. Neher, B. Sakmann and F. J. Sigworth, *Pflügers Arch. Eur. J. Physiol.*, 1981, **391**, 85–100.
121. M. R. Rasch, E. Rossinyol, J. L. Hueso, B. W. Goodfellow, J. Arbiol and B. A. Korgel, *Nano Lett.*, 2010, **10**, 3733–3739.
122. P. Mueller, D. O. Rudin, H. T. Tien and W. C. Wescott, *Nature*, 1962, **194**, 979–980.
123. M. Montal and P. Mueller, *Proc. Natl. Acad. Sci. U. S. A.*, 1972, **69**, 3561–3566.
124. R. Benz, O. Fröhlich, P. Läuger and M. Montal, *BBA - Biomembr.*, 1975, **394**, 323–334.
125. H. Sato, H. Hakamada, Y. Yamazaki and M. Uto, 1998, **13**, 1035–1046.
126. H. Suzuki, K. V. Tabata, H. Noji and S. Takeuchi, *Langmuir*, 2006, **22**, 1937–1942.
127. E. L. Florin and H. E. Gaub, *Biophys. J.*, 1993, **64**, 375–83.
128. H. Bayley, B. Cronin, A. Heron, M. A. Holden, W. L. Hwang, R. Syeda,

J. Thompson and M. Wallace, *Mol. Biosyst.*, 2008, **4**, 1191–1208.
129. S. Leptihn, O. K. Castell, B. Cronin, E.-H. Lee, L. C. M. Gross, D. P. Marshall, J. R. Thompson, M. Holden and M. I. Wallace, *Nat. Protoc.*, 2013, **8**, 1048–57.
130. W. L. Hwang, M. Chen, B. Cronin, M. A. Holden and H. Bayley, *J. Am. Chem. Soc.*, 2008, **130**, 5878–5879.
131. W. L. Hwang, M. A. Holden, S. White and H. Bayley, *J. Am. Chem. Soc.*, 2007, **129**, 11854–11864.
132. M. A. Holden, D. Needham and H. Bayley, *J. Am. Chem. Soc.*, 2007, **129**, 8650–8655.
133. P. H. King, G. Jones, H. Morgan, M. R. R. De Planque and K. P. Zauner, *Lab Chip*, 2014, **14**, 722–729.
134. L. K. Tamm and H. M. McConnell, *Biophys. J.*, 1985, **47**, 105–13.
135. W. Hoiles, V. Krishnamurthy and B. Cornell, *IEEE Trans. Biomed. Circuits Syst.*, 2015, **9**, 321–333.
136. S. Rebaud, O. Maniti and A. P. Girard-Egrot, *Biochimie*, 2014, **107**, 135–142.
137. G. J. Taylor, G. A. Venkatesan, C. P. Collier and S. A. Sarles, *Soft Matter*, 2015, **11**, 7592–7605.
138. P. Läuger, W. Lesslauer, E. Marti and J. Richter, *Biochim. Biophys. Acta*, 1966, **135**, 20–32.
139. S. H. White, *BBA - Biomembr.*, 1974, **356**, 8–16.
140. S. Bhattacharjee, *J. Control. Release*, 2016, **235**, 337–351.
141. W. Haiss, N. T. K. Thanh, J. Aveyard and D. G. Fernig, *Anal. Chem.*, 2007, **79**, 4215–4221.
142. A. P. Hill, PhD Thesis, University of Liverpool, 2018.
143. J. L. Erkal, A. Selimovic, B. C. Gross, S. Y. Lockwood, E. L. Walton, S. McNamara, R. S. Martin and D. M. Spence, *Lab Chip*, 2014, **14**, 2023–2032.
144. P. H. King, G. Jones, H. Morgan, M. R. R. De Planque and K. P. Zauner, *Lab Chip*, 2014, **14**, 722–729.
145. Y. He, Y. Wu, J. Z. Fu, Q. Gao and J. J. Qiu, *Electroanalysis*, 2016, **28**, 1658–1678.
146. C. Vinas, R. Benakki, F. Teixidor and J. Casabo, *Inorg. Chem.*, 1995, **34**, 3844–3845.
147. C. Kiely, D. J. Schiffrin, M. Brust, J. Fink and D. Bethell, *J. Chem. Soc. Chem. Commun.*, 2004, 1655.
148. A. M. Cioran, A. D. Musteti, F. Teixidor, Željka Krpetić, I. A. Prior, Q. He, C. J. Kiely, M. Brust and C. Viñas, *J. Am. Chem. Soc.*, 2012, **134**, 212–221.
149. H. Suzuki, K. V. Tabata, H. Noji and S. Takeuchi, *Biosens. Bioelectron.*, 2007, **22**, 1111–1115.

150. J. K. W. Chui and T. M. Fyles, *Chem. Soc. Rev.*, 2012, **41**, 148–175.
151. L. Bacri, H. Mamad-Hemouch, C. Przybylski, B. Thiébot, G. Patriarche, N. Jarroux and J. Pelta, *Faraday Discuss.*, 2018, **210**, 41–54.
152. S. H. White, *Biophys. J.*, 1972, **12**, 432–445.
153. S. Michielsen and R. Pecora, *Biochemistry*, 1981, **20**, 6994–6997.
154. L. M. Tsofina, E. A. Liberman and A. V. Babakov, *Nature*, 1966, **212**, 681–683.
155. L. Onsager and R. M. Fuoss, *J. Phys. Chem.*, 1932, **36**, 2689–2778.
156. T. E. Andreoli, *J. Gen. Physiol.*, 2004, **50**, 2527–2545.
157. L. Ding, J. Li, S. Dong and E. Wang, *J. Electroanal. Chem.*, 1996, **416**, 105–112.
158. M. P. Grzelczak, S. P. Danks, R. C. Klipp, D. Belic, A. Zaulet, C. Kunstmann-Olsen, D. F. Bradley, T. Tsukuda, C. Viñas, F. Teixidor, J. J. Abramson and M. Brust, *ACS Nano*, 2017, **11**, 12492–12499.
159. A. L. Hodgkin and B. Katz, *J. Physiol.*, 1949, **108**, 37–77.
160. D. E. Goldman, *J. Gen. Physiol.*, 1943, **27**, 37–60.
161. P. Hurtado, F. Gámez, S. Hamad, B. Martínez-Haya, J. D. Steill and J. Oomens, *J. Phys. Chem. A*, 2011, **115**, 7275–7282.
162. Z. X. Shu, *J. Electrochem. Soc.*, 1993, **140**, 922.
163. P. P. Power, *Acc. Chem. Res.*, 1988, **21**, 147–153.
164. D. K. Sarfo, A. Sivanesan, E. L. Izake and G. A. Ayoko, *RSC Adv.*, 2017, **7**, 21567–21575.
165. G. A. Woolley, M. K. Kapral and C. M. Deber, *FEBS Lett.*, 1987, **224**, 337–342.
166. E. R. Kay, *Chem. - A Eur. J.*, 2016, **22**, 10706–10716.

Publications and Presentations

Publications

M. P. Grzelczak, **S. P. Danks**, R. C. Klipp, D. Belic, A. Zaulet, C. Kunstmann-Olsen, D. F. Bradley, T. Tsukuda, C. Viñas, F. Teixidor, J. J. Abramson and M. Brust - *Ion Transport across Biological Membranes by Carborane-Capped Gold Nanoparticles* - ACS Nano, 2017, **11**, 12, 12492–12499.

Presentations

Ion Transport across Phospholipid Bilayer Membranes via Functionalised Gold Nanoparticles. – Poster presentation at the ECS Student Conference – June 2017